Spin foam models for 3D quantum geometry

R. J. Dowdall, MMathPhys.

Thesis submitted to The University of Nottingham
for the degree of Doctor of Philosophy

March 2010

Abstract

Various aspects of three-dimensional spin foam models for quantum gravity are discussed. Spin foam models and graphical calculus are introduced via the Ponzano-Regge model for 3d gravity and some important properties of this model are described. The asymptotic formula for the 6j symbol found by Ponzano and Regge is generalised to include the Ponzano-Regge amplitude for triangulations of handlebodies. Some simple observables are computed in a model for fermions coupled to 3d gravity. The result is a sum over spin foam models with certain vertex amplitudes which are described. An explicit example is given and the vertex amplitudes expressed in terms of 6j symbols. Finally, a group field theory for this spin foam model is described.

Foreword

This thesis discusses various aspects of the spin foam approach to quantum gravity.

Quantum gravity has become a large branch of theoretical physics with a number of interesting approaches. While this work will focus entirely on the spin foam approach this is not intended to suggest that these models are the "correct" theory of quantum gravity. A number of important and difficult questions remain open in the field and some of these will be mentioned if they are relevant in the text. One of the most compelling reasons to consider spin foam models is the number of different paths that seem to lead there. They give a concrete realisation of Penrose's ideas about spacetime and representation theory; they can be described from the point of view of topological quantum field theories and some models can be related to Chern-Simons functional integrals; recently the boundary spaces of some 4d spin foam models have been connected with the kinematical Hilbert spaces of loop quantum gravity; finally, although by a less direct route, the group field theory approach that provides a sum over spin foams has been related to dynamical triangulations.

Not all of the research contained within this thesis is my own work. I was fortunate to have a number of other people at the University of Nottingham who were interested in spin foam models and much of my work was carried out in collaboration with them and my supervisor. The research in chapter 2 and some of the end of Chapter 1 was carried out with Frank Hellmann and Henrique Gomes and resulted in the paper [C] below. Chapter 3 was research done with Winston Fairbairn. Chapter 4 is my own work.

The research in the thesis has been published in the following papers and preprints:

[A] J. W. Barrett, R. J. Dowdall, W. J. Fairbairn, H. Gomes, and F. Hellmann, "Asymptotic analysis of the EPRL four-simplex amplitude," J.Math.Phys.50:112504, 2009, arXiv:0902.1170.

[B] J. W. Barrett, R. J. Dowdall, W. J. Fairbairn, F. Hellmann, and R. Pereira, "Lorentzian spin foam amplitudes: graphical calculus and asymptotics," 2009, arXiv:0907.2440, *Class.Quant.Grav.*27:165009,2010

[C] R. J. Dowdall, H. Gomes, and F. Hellmann, "Asymptotic analysis of the Ponzano-Regge model for handlebodies," *J. Phys. A: Math. Theor.* 43 115203, 2010, arXiv:0909.2027.

[D] R. J. Dowdall and W. J. Fairbairn, "Observables in 3d spinfoam quantum gravity with fermions," *Gen. Rel. Grav.*, DOI: 10.1007/s10714-010-1107-0, arXiv:1003.1847.

[E] R. J. Dowdall, "Wilson loops, geometric operators and fermions in 3d group field theory," *Cent. Eur. J. Phys.*, DOI: 10.2478/s11534-010-0137-2, arXiv:0911.2391.

These may be referred to throughout the text.

The work from [A] and [B] is not included although similar methods are used in Chapter 2 and they may be referred to. The organisation of the thesis can be summarised as follows: Chapter 1 gives an introduction to spin foam models from the lattice BF theory approach. There are a number of different ways to motivate the construction of the models but I chose this method because it will be used in later chapters. A number of important aspects are discussed for use in later chapters such as graphical calculus and regularisation. Chapter 2 generalises a well known result on the asymptotic properties of spin networks. In Chapter 3, I describe a way of coupling fermionic matter to 3d spin foam models and compute some observables. Finally, Chapter 4 discusses a way of resolving the triangulation dependence of the spin foam model coupled to fermions by describing a group field theory to sum over triangulations.

Acknowledgements

I would like to acknowledge the support of everyone in the quantum gravity group at Nottingham, in particular my supervisor John Barrett. I would also like to thank my partner Catherine for putting up with the unusual working hours of a graduate student.

Contents

Chapter 1

3d quantum gravity, the 6j symbol and the Ponzano-Regge model

1.1 Introduction

The first two chapters of this thesis will discuss three dimensional spin foam quantum gravity and its semiclassical limit. Spin foam quantum gravity is an attempt at a covariant path integral quantisation in which the problem is to make sense of the integral

$$Z = \int_{\text{METRICS}} \exp iS_{\text{GR}}, \tag{1.1.1}$$

where we are formally writing the partition function for quantum gravity by integrating over all metrics on a spacetime manifold. We may also wish to introduce some boundary conditions in order to define transition amplitudes between 3-geometries. Spin foam models provide a possible way to define this integral and demonstrate another important connection between fundamental physics and the representation theory of groups.

Although it did not receive much attention at first, the first spin foam model was written by Ponzano and Regge [1]. They wrote an asymptotic formula for the 6j symbol appearing in quantum mechanical angular momentum calculations which contained the Regge action of discrete 3d gravity for a tetrahedron with edge lengths related to the spin labels of the 6j. With this motivation, they constructed a discrete theory of 3d quantum gravity based on the 6j symbol. Summarising the construction of this model and its relation to 3d gravity and BF theory will be the subject of this chapter. We will not take a historical approach but, to allow generalisations in later chapters, we will start by writing a discretised BF theory path integral and show that this is equivalent to the Ponzano-Regge model. We will then mention some of the important features that we will use in later sections. Perhaps surprisingly, the asymptotic formula for the Ponzano-Regge model was not generalised to triangulations larger than a single tetrahedron. This will be the subject of the second

chapter where we will extend the 6j formula to cover triangulations of handlebodies.

1.2 3d gravity as a BF theory

We begin by recalling the first order formalism for 3d gravity [2–4]. This is useful as it allows the coupling of fermions and we can construct a simple discretisation which we will use in later sections.

The first of the two independent fields is the frame field which is an $\mathfrak{su}(2)$ valued one form $e = e^i_\mu dx^\mu \tau^i$, where $\tau^j = \frac{i}{2}\sigma$ are the $\mathfrak{su}(2)$ generators. The frame field is related to the metric in the usual way $g_{\mu\nu} = \eta_{ij} e^i_\mu e^j_\nu$. The internal indices are contracted using the metric $\eta = \mathrm{Diag}(1,1,1)$. The second field is an $\mathfrak{su}(2)$ valued connection one-form $w = w^i_\mu dx^\mu \tau^i$. We can write the curvature of this connection as $F(w) = dw + w \wedge w$ and we can write the action for 3d gravity on a spacetime manifold M as

$$S[e,w] = \frac{1}{\kappa}\int_M \mathrm{tr}\left(e \wedge F(w)\right), \tag{1.2.1}$$

with the trace in the spinor representation. Varying the connection gives the equation of motion

$$d_w e = 0 \tag{1.2.2}$$

so that the frame field must be compatible with the connection. Varying e gives

$$F(w) = 0. \tag{1.2.3}$$

So in 3d, we only have to deal with flat geometries. This makes the quantum theory much easier to deal with. For this to be equivalent to gravity, we need the additional constraint that the frame field be non-degenerate. Without this restriction the above action describes 3d SU(2) BF theory [5] so we see that in 3d, BF theory and gravity are very similar theories. The classical theories both do not possess local degrees of freedom. In 4d, gravity is not a BF theory but BF theory will be a useful starting point for constructing quantum theories of gravity.

The action also has the following symmetries, the SU(2) (rotational) gauge symmetry

$$\begin{aligned} e &\rightarrow geg^{-1} \\ w &\rightarrow gwg^{-1} + (dg)g^{-1} \end{aligned} \tag{1.2.4}$$

for $g \in \mathrm{SU}(2)$ and a translation symmetry

$$\begin{aligned} e &\rightarrow e + d_w\phi \\ w &\rightarrow w \end{aligned} \tag{1.2.5}$$

with $\phi \in \mathfrak{su}(2)$. We will find analogues of these symmetries when we attempt to discretise the theory which must be fixed in order to avoid divergences.

1.3 More on 3d gravity

One can gain further insight into the nature of 3d general relativity by considering the Hamiltonian formulation [6, 7]. Since this will not be used in later chapters, only a brief summary will be given here.

The Hamiltonian form of 3d GR is given by splitting the spacetime into a set of spacelike hypersurfaces, e.g. the manifold is of the form $\Sigma \times \mathbb{R}$. Each hypersurface has a spatial metric h_{ab}, which in 3d has 3 indpendent components and $a, b = 1, 2$, this is the configuration space. The unit normal to the hypersurface is denoted n_a and we have the lapse N and the shift N_a which together describe the steps between adjacent hypersurfaces. The extrinsic curvature is given by the covariant derivative of n_a, i.e. $K_{ab} = h_a{}^c \nabla_c n_b$ which allows us to write the momentum conjugate to the spatial metric as

$$p^{ab} = h^{1/2}(Kh^{ab} - K^{ab})$$

where $h = \det h_{ab}$ and K is just the contraction of the extrinsic curvature. The Lagrangian (or Hamiltonian) can be re-expressed in terms of these new variables and one finds that the lapse and shift act as Lagrange multipliers (they have vanishing conjugate momenta) for some constraints H, H_a

$$\begin{aligned} H &= 2\kappa h^{-1/2}\left(p_{ab}p^{ab} - p^2\right) - \frac{1}{2\kappa}h^{-1/2}{}^{(2)}R = 0 \\ H_a &= -2^{(2)}\nabla_b p_a^b = 0 \end{aligned}$$

${}^{(2)}R$ is the Ricci scalar for the spatial metric and ${}^{(2)}\nabla_b$ is the covariant derivative compatible with the spatial metric. With the Hamiltonian one can also write evolution equations for h_{ab}, p_{ab}.

We can now state that the un-reduced phase space for 3d GR is six dimensional since h_{ab}, p_{ab} have 3 components each. However, the freedom to choose a hypersurface and coordinates on that hypersurface removes three of these. We also have the three constraints H, H_a so this leaves zero local dynamical degrees of freedom. So even once matter is added to the theory, spacetime outside the matter is still flat. There are no gravitational waves in 3d GR and Newton's law is not obtained in any limit. Although matter cannot have any effect locally, it can still cause global effects, for this reason one says that 3d gravity is a "topological" theory. In contrast, the spatial metric in 4d GR has 6 components, and so the phase space without the constraints is 12 dimensional. Four of these are removed by

choice of coordinates and 4 by the constraints H, H_a (since now $a = 1, 2, 3$.) This leaves a four-dimensional reduced phase space, and we say that 4d GR has 2 local degrees of freedom.

Since 3d GR is simpler in this respect, it will be easier to construct and study the corresponding quantum theory. Obviously there will be additional complications when one considers the 4d case, but by studying 3d we hope to gain some insight into how to tackle this harder problem.

1.4 A path integral for discrete BF theory

As mentioned in the introduction, the Ponzano-Regge model for 3d gravity can be constructed by starting from a discretised version of BF theory that is similar to standard lattice gauge theories used in particle physics. Let us assume we have an orientable, compact, 3-manifold M that is our spacetime. It may have boundary ∂M. To discretise the BF theory, we must first choose an appropriate structure on which to discretise it. We pick a triangulation Δ of the spacetime manifold M and label the vertices, edges and triangles by V, E and T respectively. We also choose an arbitrary orientation for Δ. In later chapters we will use a more refined discretisation of the spacetime into wedges, however the triangulation will be sufficient here. We can discretise the frame fields by integrating them along the edges of the triangulation. This assigns an SU(2) Lie algebra element e_E to each edge by

$$e_E = \int_{\text{edge } E} e_\mu dx^\mu. \tag{1.4.1}$$

To discretise the connection, we consider the dual triangulation Δ^* with nodes, edges and faces v, e and f. To each dual edge e, assign the holonomy of the connection w_e. This gives an SU(2) element which we denote g_e.

$$g_e = \exp \int_{\text{dual edge } e} w_e. \tag{1.4.2}$$

To construct the discrete action, we take the path ordered product of group elements around a dual face f, denoted

$$G_f = G_E = \overrightarrow{\prod_{e \subset f}} g_e. \tag{1.4.3}$$

Choosing an arbitrary dual vertex u as the starting point of the holonomy, we then take as our starting point, the action

$$S_{\text{GR}} = \sum_E \text{tr}\left(e_E G_E\right) \tag{1.4.4}$$

The labels E and f are interchangeable as they refer to the same objects topologically. We will briefly mention an important symmetry of the action that will be necessary for

later chapters. In a similar way to the continuum BF theory, the action is invariant under SU(2) gauge transformations at each dual vertex

$$\begin{aligned} e_E &\mapsto k_u^{-1} e_E k_u \\ G_E &\mapsto k_u^{-1} G_E k_u \end{aligned} \tag{1.4.5}$$

where $k_v \in \mathrm{SU}(2)$ is a group element associated to each vertex v. The action also admits a translation symmetry as in the continuum [2]

We can now write the partition function for this discrete BF theory, which reads

$$\mathcal{Z}_{\mathrm{GR}} = \left(\prod_E \int_{\mathfrak{su}(2)} de_E \right) \left(\prod_{\overline{e}} \int_{\mathrm{SU}(2)} dg_{\overline{e}} \right) \, e^{iS_{\mathrm{GR}}}. \tag{1.4.6}$$

The integrals are performed using the normalised SU(2) Haar measure dg, and the usual measure de on $\mathbb{R}^3$. While this path integral has clear links to a quantisation of GR, it is difficult to extract numbers in this form.

To make it easier to compute the partition function, and to recover the original form of the Ponzano-Regge model, one must perform the integral over the discretised frame fields and then a Fourier transform on the group variables to transfer the variables to the half integer spin labels appearing in the 6j symbol. In its current form, equation 1.4.6 will not give the true Ponzano-Regge formula but a very similar model based on only the integer spin labels. The key to this difference is the following formula [2]

$$\frac{1}{4\pi} \int d^3x \exp i \operatorname{tr}(Xg) = \delta(g) + \delta(-g) \tag{1.4.7}$$

for a Lie algebra element $X = x^i \tau^i$ and an SU(2) element g, the delta function is on SU(2). Using this, we see that the integral over the e_E in equation (1.4.6) gives a delta function on SO(3), i.e. it is peaked on both G_E and $-G_E$ reflecting the 2-1 homomorphism between SU(2) and SO(3). Whilst the path integral above seems perfectly valid, we would like to recover the Ponzano-Regge model so we use the trick from [8] and insert the observable

$$\frac{1}{2} \left(1 + \frac{1}{2} \operatorname{tr} G_E \right) \tag{1.4.8}$$

into the partition function. This observable is equal to one when G_E is the identity and zero when it is minus the identity. Hence

$$\begin{aligned} \mathcal{Z}_{\mathrm{GR}} &= \left(\prod_E \int_{\mathfrak{su}(2)} de_E \right) \left(\prod_{\overline{e}} \int_{\mathrm{SU}(2)} dg_{\overline{e}} \right) \, \frac{1}{2} \left(1 + \frac{1}{2} \operatorname{tr} G_E \right) e^{iS_{\mathrm{GR}}} \\ &= \left(\prod_{\overline{e}} \int_{\mathrm{SU}(2)} dg_{\overline{e}} \right) \, \prod_E \delta\left(G_E\right) \end{aligned} \tag{1.4.9}$$

So we see that, as expected from the equations of motion, the effect of the e field is to act as a Lagrange multiplier which enforces that the integration is only over flat SU(2)

connections. So the partition function can be interpreted as an integral over the space of flat SU(2) connections. We also see in this form that the partition function can easily be divergent as if there are not enough group integrals, we will be left with delta functions evaluated at the identity.

The next step in the derivation involves using harmonic analysis on SU(2), in particular the Peter-Weyl theorem. The Peter-Weyl theorem provides a way to express functions of group variables by Fourier decomposing over the irreducible, unitary representations of the group. The formula that we will need is

$$\delta(g) = \sum_{j \in \frac{\mathbb{N}}{2}} d_j \chi_j(g) \tag{1.4.10}$$

$\chi_j(g)$ is the trace of the representation matrix of g in the j representation, i.e. $\chi_j(g) = \operatorname{tr} D^j(g)$, $d_j = \dim j = 2j + 1$ is the dimension of that representation. This is derived in appendix A along with a brief description of the Peter-Weyl theorem. Fourier transforming the delta functions corresponding to each edge and labelling the irreducible representations in the decomposition by j_E for edge E, we get

$$\mathcal{Z}_{\mathrm{GR}} = \sum_{j_E} \left(\prod_{\overline{e}} \int_{\mathrm{SU}(2)} dg_{\overline{e}} \right) \prod_E d_{j_E} \chi_{j_E}(G_E) \tag{1.4.11}$$

This is a good point to introduce graphical calculus in order to complete the derivation of the Ponzano-Regge model. The graphical calculus allows one to compute complicated expressions involving representations of group variables very easily and, although the case here is quite simple, later chapters will require the computation of more complicated expressions.

1.5 Graphical calculus and spin networks

The purpose of graphical calculus is to be able to manipulate representation theoretic expressions using a selection of diagrammatic identities. This was used in quantum mechanical angular momentum calculations, i.e. representations of SU(2) before its use in quantum gravity. The formalism can also be extended to quantum groups but, since we only need the simpler case here, we will concentrate on SU(2). There are various different conventions used for spin networks, each having advantages and disadvantages. Unfortunately we will need to consider two differing conventions in different chapters of this thesis which we will refer to as Kauffman and Lins spin networks [9] and angular momentum diagrams [10]. The Kauffman-Lins networks have the advantage that they are invariant under Reidemeister moves in the plane but in the angular momentum diagrams it is easier to deal with phases that occur in integrals over tensor products of group elements.

1.5.1 Kauffman-Lins spin networks

We use the binor calculus [11, 12], this corresponds to a choice of Kauffman parameter $A = -1$ and the association of a minus sign to every crossing. A Kauffman-Lins spin network diagram is constructed from SU(2) invariant objects, called intertwiners. The most elementary object is the identity operator which is drawn as a vertical line

(1.5.1)

In the fundamental representation, this corresponds to δ^a_b. If we denote the spin j representation space as V_j, then higher spin representations of SU(2) are obtained by taking $2j$ symmetrised tensor products of the fundamental representation. To accomplish this, we must antisymmetrize the lines in the diagram because of the minus sign associated to each crossing.

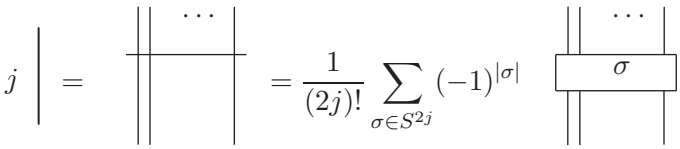

(1.5.2)

I.e., we sum over permutations σ, in the permutation group on $2j$ elements, of the lines in the fundamental representation. $|\sigma|$ is the minimum number of crossings needed to obtain the permutation. This antisymmetrisation combined with the minus sign will symmetrise the indices of the associated tensor. Note for later use that this projector onto the symmetric subspace is idempotent

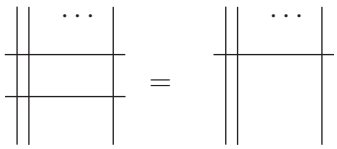

(1.5.3)

The open ends of the diagram are fixed, lines at the top of the diagram correspond to the vector spaces V_j of the appropriate representation and lines at the bottom correspond to V_j^*. Two other important diagrams are the cup diagram

(1.5.4)

corresponding to the tensor $i\epsilon_{ab}$, i.e. a map in $\mathrm{Hom}(V_{\frac{1}{2}} \otimes V_{\frac{1}{2}}, \mathbb{C})$, and the cap diagram

(1.5.5)

corresponding to the dual $i\epsilon^{ab}$ tensor. Again, the higher spin versions $\epsilon_j \in \mathrm{Hom}(V_j \otimes V_j, \mathbb{C})$ and $\epsilon^j \in \mathrm{Hom}(\mathbb{C}, V_j^* \otimes V_j^*)$ are given by the symmetrised tensor products and are drawn as cup and cap diagrams with a j label on the line.

(1.5.6)

These cup and cap diagrams can be used to change the vector space corresponding to an open end of a diagram to its dual. The cap diagram also gives a bilinear inner product between two states in V_j. Using the cup, cap and identity diagrams, we can write the binor identity. Starting from

$$\epsilon^{ab}\epsilon_{cd} = \delta^a_c\delta^b_d - \delta^a_d\delta^b_c \tag{1.5.7}$$

and using cup$= i\epsilon^{ab}$, cap$= i\epsilon_{ab}$ and associating the minus sign to the crossing from the final pair of deltas gives

(1.5.8)

Finally, there is a diagram for three lines meeting at a point with different spin labels.

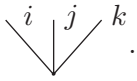

. (1.5.9)

This is an element of $\mathrm{Inv}_{\mathrm{SU}(2)}(V_i \otimes V_j \otimes V_k, \mathbb{C})$, and is also constructed from symmetrised products of fundamental lines. The spin labels must satisfy the admissibility conditions $i + j \geq k, k + i \geq j, j + k \geq i$ and $i + j + k \in \mathbb{N}$. The intertwiner is constructed in a canonical way with no crossings, for example

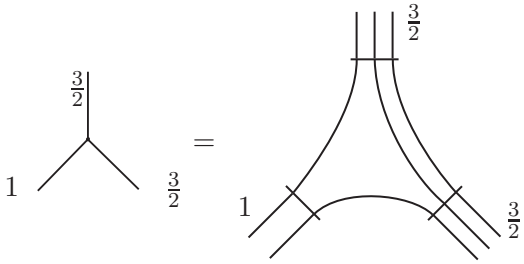

(1.5.10)

This generalises to higher valence intertwiners

$$\iota \in \mathrm{Hom}(V_{j_1} \otimes ... \otimes V_{j_n}, \mathbb{C}),$$

by choosing a decomposition into 3-valent intertwiners. These are given by a vertex with n ingoing lines:

(1.5.11)

The dual map $\iota^* \in \mathrm{Hom}(\mathbb{C}, V_{j_1} \otimes ... \otimes V_{j_n})$ is drawn as the inverse of this diagram

(1.5.12)

Twisting two of the three lines in a three-valent vertex results in a minus sign

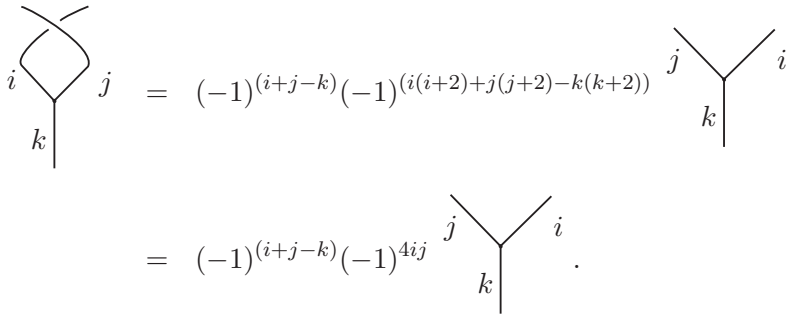

(1.5.13)

The normalisation of the spin network vertices is an important and often confusing issue. The Kauffman-Lins 3-valent intertwiners are not normalised. The norm of a 3-valent intertwiner is given by

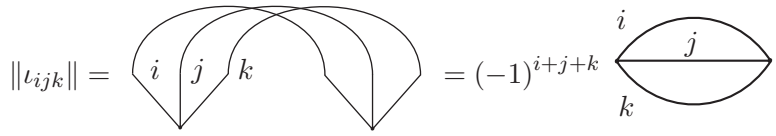

(1.5.14)

The value of this spin network is computed in [9]

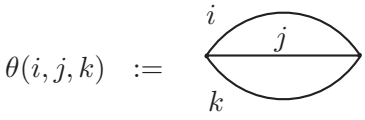

$$= \frac{(-1)^{i+j+k}(i+j+k+1)!(i+j-k)!(j+k-i)!(k+i-j)!}{i!j!k!} \quad (1.5.15)$$

It is possible to work with intertwiners that are normalised

(1.5.16)

so that the norm of the intertwiner $\|\Upsilon_{ijk}\| = (\Upsilon_{ijk})_{abc}(\Upsilon_{ijk})_{a'b'c'}\epsilon^{aa'}\epsilon^{bb'}\epsilon^{cc'} = 1$. Diagramatically this is

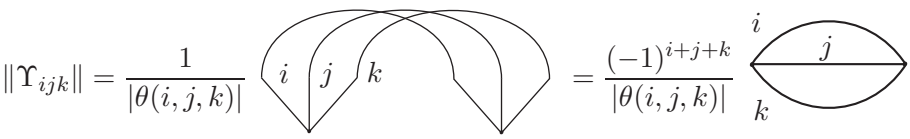

(1.5.17)

Since the $(-1)^{i+j+k}$ cancels the sign in the theta network.

Tensor products are expressed by drawing diagrams adjacent to each other, e.g.

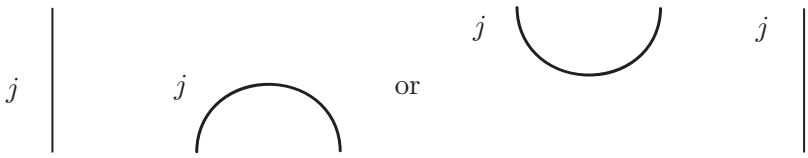

(1.5.18)

and composing diagrams is done by drawing them one on top of the other and connecting the lines.

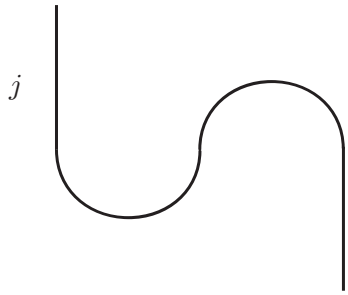

(1.5.19)

One of the useful properties of this formalism is that the expressions corresponding to the diagrams (sometimes referred to simply as the diagrams) are invariant under Reidemeister moves in the plane that leave the external edges of the diagram fixed

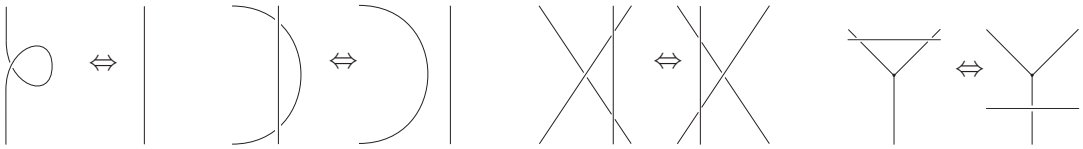

with the addition of another move that moves a line over a vertex. A closed diagram with no external edges is a map from $\mathbb{C}$ to itself and so is a complex number, we often refer to this as the value of the spin network.

A number of useful expressions can be put into diagrammatical notation. A closed loop gives the dimension of the representation with additional minus signs

$$= (-1)^{2j}(2j+1). \tag{1.5.20}$$

Schur's lemma is the following

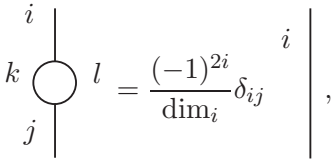

$$= \frac{(-1)^{2i}}{\dim_i}\delta_{ij}, \tag{1.5.21}$$

and we have the important recoupling identity

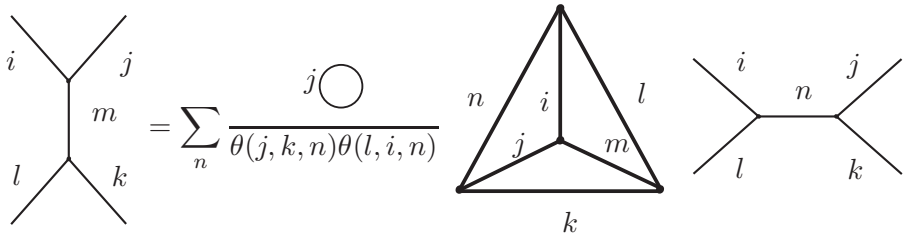

(1.5.22)

Kauffman and Lins define the recoupling coefficient as the following

$$\left\{ \begin{array}{ccc} a & b & c \\ d & e & f \end{array} \right\}_{KL} = \frac{f\bigcirc}{\theta(f,a,e)\theta(f,b,d)} \quad \begin{array}{ccccc} & & f & & e \\ & & a & & \\ & & b & & c \\ & & & & \\ & & d & & \end{array} \tag{1.5.23}$$

This is different to the 6j symbol found in angular momentum recoupling computations and does not have the usual tetrahedral symmetry of the 6j. Comparing the analytical formulae for the different conventions shows that the following definition for the 6j symbol agrees with that of Wigner [13]

$$\begin{aligned} \left\{ \begin{array}{ccc} i & j & m \\ k & l & n \end{array} \right\} &= \frac{1}{\sqrt{|\theta(i,j,m)\theta(k,l,m)\theta(i,n,l)\theta(j,k,n)|}} \quad \begin{array}{ccccc} & & & & \\ n & & i & & l \\ & & j & & m \\ & & & & \\ & & k & & \end{array} \\ &= \Delta(i,j,m)\Delta(k,l,m)\Delta(i,n,l)\Delta(j,k,n) \\ &\quad \times \sum_t (-1)^t (t+1)! \left[(t-i-j-m)!(t-k-l-m)! \right. \\ &\quad \times (t-i-n-l)!(t-j-k-n)!(i+j+k+l-t)! \\ &\quad \left. \times (i+m+k+n-t)!(j+m+l+n-t)! \right]^{-1} \end{aligned} \tag{1.5.24}$$

Where

$$\Delta(a,b,c) = \left[\frac{(a+b-c)!(b+c-a)!(c+a-b)!}{(a+b+c+1)!} \right]^{1/2}. \tag{1.5.25}$$

With these normalised intertwiners, the recoupling identity reads

$$\frac{1}{\sqrt{|\theta(i,j,m)\theta(k,l,m)|}} \quad \begin{array}{ccccc} i & & & & j \\ & & m & & \\ l & & & & k \end{array}$$

$$= \sum_n \dim n (-1)^{i+j+k+l} \left\{ \begin{array}{ccc} i & j & m \\ k & l & n \end{array} \right\} \frac{1}{\sqrt{|\theta(i,l,n)\theta(j,k,n)|}} \quad \begin{array}{ccccc} i & & & & j \\ & & n & & \\ l & & & & k \end{array} \tag{1.5.26}$$

A consequence of this is the following move (the Wigner-Eckart identity)

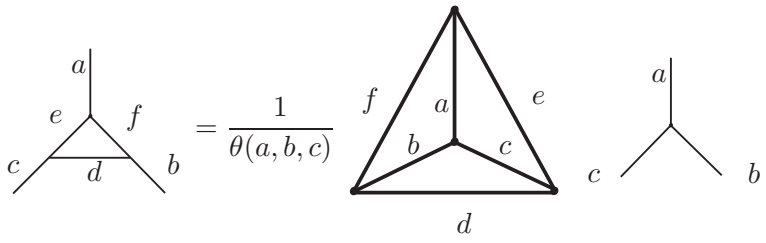

(1.5.27)

Semisimplicity of SU(2) is expressed by the following diagram

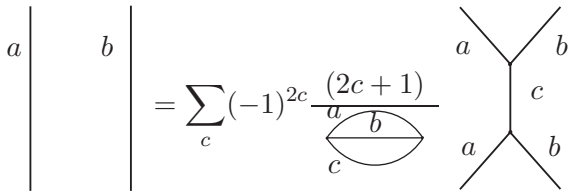

(1.5.28)

These identities will be used to evaluate spin network diagrams in later chapters.

1.5.2 Kauffman and Lins cable diagrams

The term *cable diagram* is used to refer to diagrams that contain representations of group variables. This will include a simple diagrammatic way of integrating over tensor products of group elements. A group element g in the spin j representation is depicted by

The character of a group element $\chi_j(g)$ is thus drawn as

$\chi_j(g) = (-1)^{2j}$ 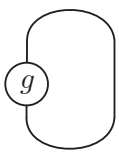

. (1.5.29)

A Haar integral over the tensor product of n representations of a group element is represented by a box over the n lines

$\int_{SU(2)} dg\ D^{j_1}(g) \otimes ... \otimes D^{j_n}(g) =$ 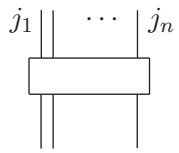

(1.5.30)

For three representations, the integral gives

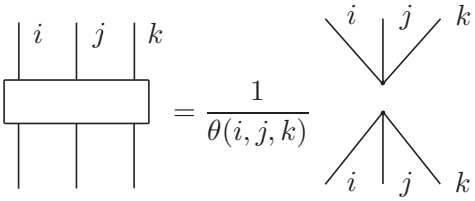

(1.5.31)

In later chapters, we will generalise this to include the tensor product of four or more representations. We also have [14]

$$\sum_{j_0}(-1)^{2j_0}(2j_0+1)$$

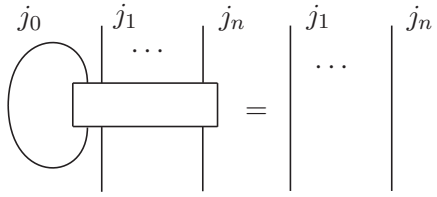

(1.5.32)

There are many other useful identities and operations that can be performed with spin network and cable diagrams, these are just the minimum set that will be used in later chapters.

1.5.3 Angular momentum diagrams

Various different graphical methods exist for angular momentum recoupling, each with advantages and disadvantages. A method rather different to the Kauffmann-Lins diagrams will now be described. This convention is closer to that found in original physics literature, the main practical difference from the Kauffman-Lins diagrams is the need to orient the lines and the vertices.

The next section is based on [10, 13], similar descriptions can also be found in the spin foam literature in e.g. [15, 16]. We first note the existence of the epsilon map $\epsilon^j : V_j \to V_j^*$ between the jth representation space and its dual. Its components in the standard basis $e^j_m = |j, m\rangle$, $m = -j, ..., j$ are given by the Wigner $1j$ symbol

$$\epsilon^j_{\alpha\beta} = \epsilon^{j\,\alpha\beta} = (-1)^{j-\beta}\delta_{\alpha,-\beta}.$$

This map satisfies the properties

$$\epsilon^j_{\beta\alpha} = (-1)^{2j}\epsilon^j_{\alpha\beta} = (-1)^{j+\beta}\delta_{\beta,-\alpha}, \quad \text{and} \quad \epsilon^j_{\alpha\beta}\epsilon^{j\,\beta\gamma} = (-1)^{2j}\delta^\gamma_\alpha.$$

For all triples of unitary, irreducible representations π^i, π^j, π^k of SU(2), let

$$C^k_{ij} : V_i \otimes V_j \to V_k, \quad \text{and} \quad C^{ij}_k : V_k \to V_i \otimes V_j, \tag{1.5.33}$$

denote the Clebsch-Gordan intertwining operators whose coefficients

$$C^{ij}_{\ k}(e^k_\gamma) = \sum_{\alpha,\beta} \left(\begin{array}{cc|c} \alpha & \beta & k \\ i & j & \gamma \end{array} \right) e^i_\alpha \otimes e^j_\beta, \quad \text{and} \quad C^k_{ij}(e^i_\alpha \otimes e^j_\beta) = \sum_\gamma \left(\begin{array}{c|cc} \gamma & i & j \\ k & \alpha & \beta \end{array} \right) e^k_\gamma, \tag{1.5.34}$$

can be found in [13]. These intertwiners are unique up to normalisation because the space of three-valent intertwiners is a vector space of dimension one. This fact does not completely specify the phase of the intertwiners which must be done more carefuly, see [10]. The tensor product of two representations is given by the following standard formula

$$V_i \otimes V_j \cong \bigoplus_{k=|i-j|}^{i+j} V_k,$$

which gives $\pi^i \otimes \pi^j = \sum_k C^k_{\ ij}\, \pi^k\, C^{ij}_{\ k}$. Relative to the chosen bases, this yields

$$\pi^{i\,\alpha}_{\ \ \beta}\, \pi^{j\,\gamma}_{\ \ \delta} = \sum_{k,\epsilon,\zeta} \left(\begin{array}{cc|c} \alpha & \gamma & k \\ i & j & \zeta \end{array} \right) \pi^{k\,\zeta}_{\ \ \epsilon} \left(\begin{array}{c|cc} \epsilon & i & j \\ k & \beta & \delta \end{array} \right). \tag{1.5.35}$$

A more symmetric intertwining operator called a $3j$ symbol can be constructed from the Clebsch-Gordan maps. Let $\iota_{ijk} : V_i \otimes V_j \otimes V_k \to \mathbb{C}$ be a $3j$ intertwining map and u, v and w be arbitrary vectors in V_i, V_k and V_k respectively. Clebsh-Gordan symbols and $3j$ symbols are related via the following evaluation

$$\iota_{ijk}(u \otimes v \otimes w) = \frac{\epsilon(i,j,k)}{\sqrt{\dim k}}\, (w, C^k_{ij}(u \otimes v)), \tag{1.5.36}$$

where $\epsilon(i,j,k)$ is a sign usually chosen to be $(-1)^{-i+j-k}$, where $-i+j-k \in \mathbb{Z}$. The evaluation of the above equation on the vectors $u = e^i_\alpha$, $v = e^j_\beta$ and $w = e^k_\gamma$ reads

$$\left(\begin{array}{ccc} i & j & k \\ \alpha & \beta & \gamma \end{array} \right) = \frac{(-1)^{-i+j-k}}{\sqrt{\dim k}} \epsilon^k_{\gamma\delta} \left(\begin{array}{cc|c} \delta & i & j \\ k & \alpha & \beta \end{array} \right) = \frac{(-1)^{-i+j+\gamma}}{\sqrt{\dim k}} \left(\begin{array}{c|cc} -\gamma & i & j \\ k & \alpha & \beta \end{array} \right), \tag{1.5.37}$$

where the left hand side is a $3j$ symbol. The above relation can be put into a more compact form by using the epsilon tensor to raise and lower indices, i.e. to change between the representation and its dual. We use the convention that indices are raised from the right and lowered from the left, that is, picturing only one column of the symbol,

$$\left(\begin{array}{c} i \\ \alpha \end{array} \right) = \epsilon^i_{\alpha\beta} \left(\begin{array}{c} \beta \\ i \end{array} \right), \quad \text{and} \quad \left(\begin{array}{c} \alpha \\ i \end{array} \right) = \left(\begin{array}{c} i \\ \beta \end{array} \right) \epsilon^{i\,\beta\alpha}.$$

Note that this implies the following property

$$\left(\begin{array}{c} i \\ \alpha \end{array} \right) \left(\begin{array}{c} \alpha \\ i \end{array} \right) = (-1)^{2i} \left(\begin{array}{c} \alpha \\ i \end{array} \right) \left(\begin{array}{c} i \\ \alpha \end{array} \right). \tag{1.5.38}$$

By raising and lowering the indices on a $3j$ symbol, it is possible to construct intertwiners between any three representation spaces and their duals. Using the symmetry under permutations of the $3j$ symbol

$$\begin{pmatrix} i & j & k \\ \alpha & \beta & \gamma \end{pmatrix} = (-1)^{i+j+k} \begin{pmatrix} i & k & j \\ \alpha & \gamma & \beta \end{pmatrix}, \tag{1.5.39}$$

which implies that the symbol is even under even permutations of the columns, the relation between $3j$ symbols and Clebsch-Gordan coefficients can be put in the form

$$\begin{pmatrix} k & i & j \\ \gamma & \alpha & \beta \end{pmatrix} = \frac{(-1)^{-i+j-k}}{\sqrt{\dim k}} \left(\begin{array}{c|cc} k & i & j \\ \gamma & \alpha & \beta \end{array}\right). \tag{1.5.40}$$

We can now use the $3j$ symbol as the building block for another diagrammatic calculus. A $3j$ symbol is represented as an ordered vertex with three lines. The clockwise ordering of the lines at a vertex is denoted with a $+$ symbol and the anticlockwise ordering with a $-$. Each line of the vertex is oriented with the convention that ingoing lines correspond to a map from the representation space and outgoing lines are a map from the dual. This implies that

$$\begin{pmatrix} i & j & k \\ \alpha & \beta & \gamma \end{pmatrix} =$$

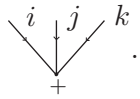

and

$$\begin{pmatrix} \alpha & \beta & \gamma \\ i & j & k \end{pmatrix} =$$

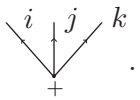

Note that unlike the Kauffmann-Lins vertices, these can be drawn in any orientation on the page as it is the arrows and $\pm$ that describes the ordering.

The $3j$ symbols are normalised

$$\begin{pmatrix} i & j & k \\ \alpha & \beta & \gamma \end{pmatrix} \begin{pmatrix} \alpha & \beta & \gamma \\ i & j & k \end{pmatrix} = Y(i,j,k), \tag{1.5.41}$$

where $Y(i,j,k) = 1$ if i, j and k are admissible and zero otherwise, summation is assumed on the indices α, β, γ. Diagrammatically, this means that the theta network is equal to (zero or) one

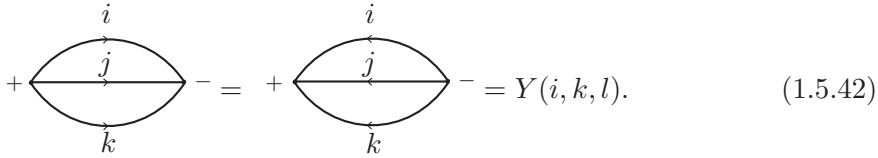

$$= Y(i,k,l). \tag{1.5.42}$$

With the rule that lines can only be joined if the arrows are pointing the same direction. Note that changing the orientation of an arrow on an internal line of a diagram produces a factor $(-1)^{2k}$ if k is the spin label on the line.

The corresponding intertwiner has norm (squared) given by $(-1)^{2k}Y(i,j,k)$, in accordance with the results found in the group integral section.

Changing the ordering at a vertex is equivalent to a permutation of the arguments of the $3j$ thus we have the diagrammatic identity

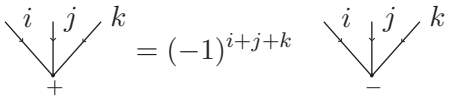

(1.5.43)

This emphasises the need to have an ordering label at the vertices.

The $6j$ symbol is defined by the following contraction of $3j$ symbols

$$\left\{ \begin{array}{ccc} j_1 & j_2 & j_3 \\ j_4 & j_5 & j_6 \end{array} \right\} = \left(\begin{array}{ccc} \alpha_1 & \alpha_2 & \alpha_3 \\ j_1 & j_2 & j_3 \end{array} \right) \left(\begin{array}{ccc} j_1 & \alpha_5 & j_6 \\ \alpha_1 & j_5 & \alpha_6 \end{array} \right) \left(\begin{array}{ccc} \alpha_6 & j_4 & j_2 \\ j_6 & \alpha_4 & \alpha_2 \end{array} \right) \left(\begin{array}{ccc} \alpha_4 & j_5 & j_3 \\ j_4 & \alpha_5 & \alpha_3 \end{array} \right).$$

Accordingly, the $6j$ symbol is equal to the following tetrahedral spin network evaluation

$$\left\{ \begin{array}{ccc} j_1 & j_2 & j_3 \\ j_4 & j_5 & j_6 \end{array} \right\} =$$

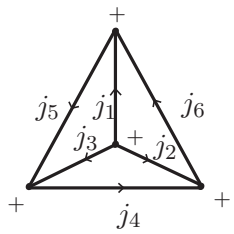

(1.5.44)

Comparing the analytical formula given in [10], one can see that this is the same as the Kauffmann-Lins 6j formula 1.5.24. Note that reversing an arrow on a spin j line of the diagram produces a factor $(-1)^{2j}$ because of (1.5.38). This emphasises the need to have the arrows in the diagram. Thanks to the symmetries of the $3j$ symbol, the $6j$ symbol network is invariant under any permutation of the vertices.

Diagrammatics and Recoupling identities

The analogues of the diagrammatic identities given in the previous section can now be described. These will look very similar but have some important differences (usually minus signs.) The first that we use is the second orthogonality of the $3j$ symbols

$$\left(\begin{array}{ccc} i & \gamma & \delta \\ \alpha & k & l \end{array} \right) \left(\begin{array}{ccc} k & l & \beta \\ \gamma & \delta & j \end{array} \right) = \frac{(-1)^{2j}}{\dim j} \, \delta^i_j \, \delta^\beta_\alpha \, Y(i,k,l). \tag{1.5.45}$$

This is the analogue of Schur's lemma The diagrammatic version is

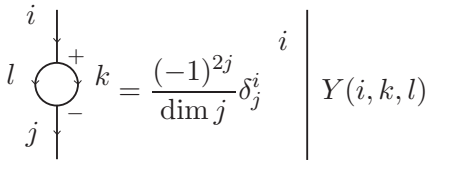

(1.5.46)

The recoupling identity in this formalism is given by

$$\begin{pmatrix} \beta & i & m \\ j & \alpha & \epsilon \end{pmatrix} \begin{pmatrix} \epsilon & \gamma & l \\ m & k & \delta \end{pmatrix} = \sum_n C_n \begin{pmatrix} i & l & \theta \\ \alpha & \delta & n \end{pmatrix} \begin{pmatrix} n & \beta & \gamma \\ \theta & j & k \end{pmatrix}, \tag{1.5.47}$$

where

$$C_n = \dim n \, (-1)^{i+k+m+n} \begin{Bmatrix} i & j & m \\ k & l & n \end{Bmatrix}.$$

In graphical language, the recoupling theorem yields

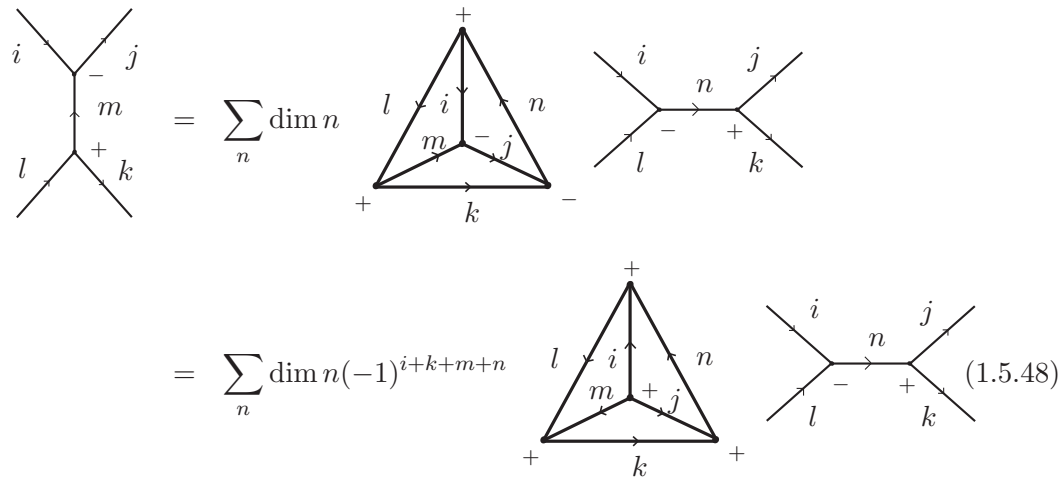

(1.5.48)

A consequence of the recoupling identity is the following property

$$\begin{pmatrix} i & \delta & n \\ \alpha & l & \epsilon \end{pmatrix} \begin{pmatrix} l & j & \theta \\ \delta & \beta & m \end{pmatrix} \begin{pmatrix} m & k & \epsilon \\ \theta & \gamma & n \end{pmatrix} = \begin{Bmatrix} i & k & j \\ m & l & n \end{Bmatrix} \begin{pmatrix} i & j & k \\ \alpha & \beta & \gamma \end{pmatrix}. \tag{1.5.49}$$

Diagrammatically, this yields the fusion move displayed below

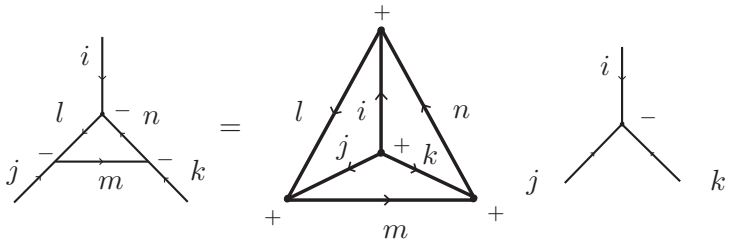

(1.5.50)

1.5.4 Group integrals

We now express integrals of tensor products of representations in terms of $3j$ symbols. We use the fact that

$$\int_{\mathrm{SU}(2)} dg \, \pi^k(g) = \delta_0^k.$$

Using this and the Clebsch-Gordan decomposition, we can compute the integrals of the other tensor products. The first is the bivalent integration.

$$\begin{aligned}\int_{\mathrm{SU}(2)} dg\, \pi^i(g)^\alpha{}_\beta\, \pi^j(g)^\gamma{}_\delta &= \sum_{k,\epsilon,\zeta} \left(\begin{array}{cc|c} \alpha & \gamma & k \\ i & j & \zeta \end{array}\right) \left(\begin{array}{c|cc} \epsilon & i & j \\ k & \beta & \delta \end{array}\right) \int_{\mathrm{SU}(2)} dg\, \pi^k(g)^\zeta{}_\epsilon \\ &= \left(\begin{array}{cc|c} \alpha & \gamma & 0 \\ i & j & 0 \end{array}\right) \left(\begin{array}{c|cc} 0 & i & j \\ 0 & \beta & \delta \end{array}\right) \\ &= \frac{\delta^{ij}}{\dim j}\, \epsilon^{j\,\alpha\gamma} \epsilon^j_{\beta\delta}, \end{aligned} \tag{1.5.51}$$

where we have used [10]

$$\left(\begin{array}{cc|c} \alpha & \beta & 0 \\ i & j & 0 \end{array}\right) = \frac{\delta^{ij}}{\sqrt{\dim j}} (-1)^{j-\alpha} \delta_{\beta,-\alpha} = (-1)^{2j} \frac{\delta^{ij}}{\sqrt{\dim j}} \epsilon^{j\,\alpha\beta},$$

in the last step. Note that 1.5.51 often appears in the literature with lowered indices and delta functions instead of ϵ^j. From this result one can prove the orthogonality of characters.

Using the above, one can compute the three-valent integral. The calculation is displayed below.

$$\begin{aligned}\int_{\mathrm{SU}(2)} dg\, \pi^i(g)^\alpha{}_\beta\, \pi^j(g)^\gamma{}_\delta \pi^k(g)^\epsilon{}_\zeta &= \sum_{l,\eta,\theta} \left(\begin{array}{cc|c} \alpha & \gamma & l \\ i & j & \theta \end{array}\right) \left(\begin{array}{c|cc} \eta & i & j \\ l & \beta & \delta \end{array}\right) \int_{\mathrm{SU}(2)} dg\, \pi^l(g)^\theta{}_\eta \pi^k(g)^\epsilon{}_\zeta \\ &= \frac{1}{\dim k} \sum_{\eta,\theta} \left(\begin{array}{cc|c} \alpha & \gamma & k \\ i & j & \theta \end{array}\right) \epsilon^{k\,\theta\epsilon} \epsilon^k_{\eta\zeta} \left(\begin{array}{c|cc} \eta & i & j \\ k & \beta & \delta \end{array}\right) \\ &= \left(\begin{array}{ccc} \alpha & \gamma & \epsilon \\ i & j & k \end{array}\right) \left(\begin{array}{ccc} i & j & k \\ \beta & \delta & \zeta \end{array}\right). \end{aligned} \tag{1.5.52}$$

As for the Kauffman-Lins diagrams, a group integral is represented by a box, only now the lines entering and leaving the box will have an arrow. The above formula is then

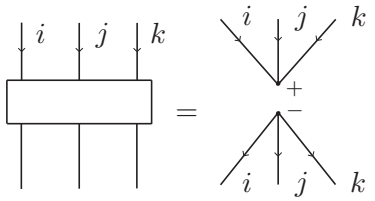

(1.5.53)

To calculate the same integral, but with one group element inverted, one uses the following formula which essentially comes from the fact that for $SU(2)$ the conjugate representation is equivalent to the standard one.

$$\pi^i(g^{-1})^\alpha{}_\beta = (-1)^{2j} \epsilon^{j\,\alpha\gamma} \pi^i(g)^\delta{}_\gamma \epsilon^j_{\delta\beta}. \tag{1.5.54}$$

From the above, we immediately obtain that

$$\int_{\mathrm{SU}(2)} dg\, \pi^i(g)^\alpha{}_\beta\, \pi^j(g)^\gamma{}_\delta \pi^k(g^{-1})^\epsilon{}_\zeta = (-1)^{2k} \begin{pmatrix} \alpha & \gamma & k \\ i & j & \zeta \end{pmatrix} \begin{pmatrix} i & j & \epsilon \\ \beta & \delta & k \end{pmatrix}.$$

The diagram is the same but with the appropriate arrow reversed. Using the invariance of the Haar measure under inversion $g \mapsto g^{-1}$ this gives the final case of two group elements inverted. These will be used later when tensor products of group elements and their inverses will appear in all combinations.

1.6 The Ponzano-Regge model

We can now apply the graphical calculus techniques to equation (1.4.11). Each dual edge has a group element associated to it and the formula contains a character with each of the group elements in the dual face. An orientation must be chosen for each dual edge and this orientation determines whether g or g^{-1} appears in the character. The partition function is invariant under a change of orientation since g and g^{-1} are in the same conjugacy class and the character is invariant under conjugation.

To represent the characters diagrammatically, we use that the characters are related to a loop diagram with a group element inserted 1.5.29. We can now draw the loops for each character, noting that each group element will appear in three different characters. We can draw the section of the partition function corresponding to a single dual vertex graphically using Kauffmann-Lins cable diagrams as

$$\prod_{E=1}^{6} (-1)^{2j_E}(2j_E+1)$$

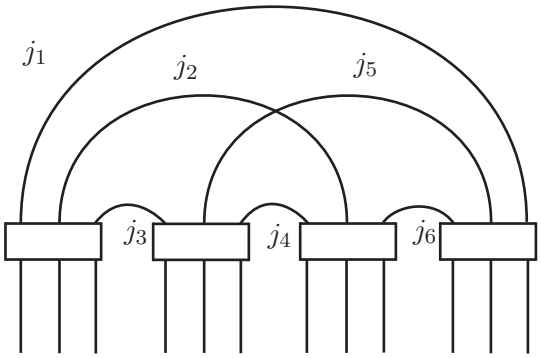

(1.6.1)

The $(-1)^{2j_E}$ arise from the repeated use of equation (1.5.29). Performing the group inte-

grals with equation (1.5.31) gives us

$$\frac{\prod_{E=1}^{6}(-1)^{2j_E}(2j_E+1)}{\theta(j_1,j_2,j_3)\theta(j_2,j_4,j_6)\theta(j_1,j_5,j_6)\theta(j_3,j_4,j_5)}$$

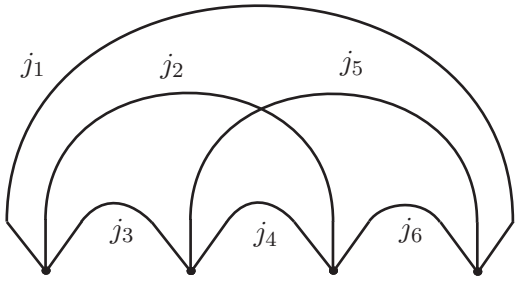

(1.6.2)

So the amplitude associated to each dual vertex is the tetrahedral network. The Ponzano-Regge amplitude for the triangulation Δ_M of some manifold M can thus be formally written as

$$\mathcal{Z}_{PR}(\Delta_M) = \sum_{j_E} \prod_{edges\ E} (-1)^{2j_E}(2j_E+1) \prod_{triangles\ \Delta} \frac{1}{\theta(j_1,j_2,j_3)} \prod_{tetrahedra\ \sigma}$$

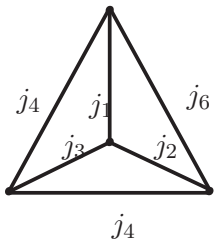

(1.6.3)

or in terms of the 6j symbol

$$\mathcal{Z}_{PR}(\Delta_M) = \sum_{j_E} \prod_{edges\ E} (-1)^{2j_E}(2j_E+1) \prod_{triangles\ \Delta} (-1)^{j_1+j_2+j_3} \prod_{tetrahedra\ \sigma} \left\{ \begin{array}{ccc} j_1 & j_2 & j_3 \\ j_4 & j_5 & j_6 \end{array} \right\} \tag{1.6.4}$$

This may be divergent and require regularisation, this will be discussed in the next section. $\mathcal{Z}_{PR}$ is formally equivalent to $\mathcal{Z}_{GR}$ defined previously, i.e. they agree if they are finite.

Note that there is a freedom in choosing the normalisation and the phase of the 3-valent intertwiners on the boundary and the above formula is for a particular choice of phase. We may write $\mathcal{Z}_{PR}(\Psi, \Delta_M)$ where Ψ contains the information about these phases and normalisations. If no mention is made of the boundary phase choice Ψ we will assume it to be standard one - i.e. normalised 3-valent Kauffmann-Lins intertwiners - to agree with 1.6.4.

1.6.1 Examples

Applying the Ponzano-Regge formula to some simple triangulations, gives the following simple examples for the partition function

The tetrahedron The amplitude for a single tetrahedron is given by

$$\mathcal{Z}_{PR} = \prod_{E=1}^{6} (-1)^{2k_E}(2k_E+1)(-1)^{2(k_1+k_2+k_3+k_4+k_5+k_6)} \left\{ \begin{array}{ccc} k_1 & k_2 & k_3 \\ k_4 & k_5 & k_6 \end{array} \right\} \tag{1.6.5}$$

The 3-ball Three tetrahedra can be glued together to make a triangulation of the 3-ball with one interior edge

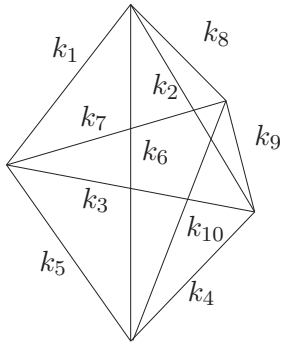

The amplitude is

$$\begin{aligned} \mathcal{Z}_{PR} &= \sum_{k_6} \prod_{E=1}^{10} (-1)^{2k_E}(2k_E+1)(-1)^{2(k_3+k_7+k_9)-k_1-k_2-k_4-k_5-k_6-k_8-k_{10}} \\ &\quad \times \left\{ \begin{array}{ccc} k_1 & k_2 & k_3 \\ k_4 & k_5 & k_6 \end{array} \right\} \left\{ \begin{array}{ccc} k_1 & k_6 & k_5 \\ k_{10} & k_7 & k_8 \end{array} \right\} \left\{ \begin{array}{ccc} k_2 & k_8 & k_9 \\ k_{10} & k_4 & k_6 \end{array} \right\}. \end{aligned} \tag{1.6.6}$$

The 3-sphere The triangulation of S^3 with two tetrahedra with each face identified is given by

$$\begin{aligned} \mathcal{Z}_{PR} &= \sum_{k_E=1}^{6} \prod_{E=1}^{6} (-1)^{2k_E}(2k_E+1)(-1)^{2(k_1+k_2+k_3+k_4+k_5+k_6)} \\ &\quad \times \left\{ \begin{array}{ccc} k_1 & k_2 & k_3 \\ k_4 & k_5 & k_6 \end{array} \right\} \left\{ \begin{array}{ccc} k_1 & k_2 & k_3 \\ k_4 & k_5 & k_6 \end{array} \right\}. \end{aligned} \tag{1.6.7}$$

The solid torus A triangulation of the solid torus with three tetrahedra is given by

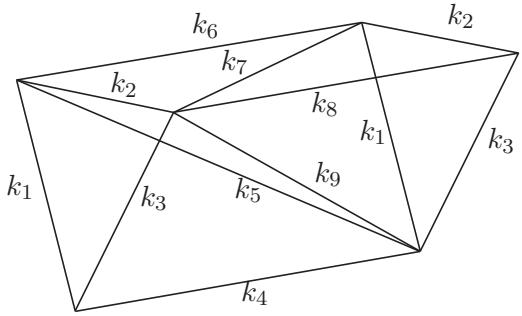

The two triangles with edges k_1, k_2, k_3 are identified. The Ponzano-Regge amplitude is given by

$$\begin{aligned}\mathcal{Z}_{PR}(\Psi,\mathbb{T}) &= \prod_{E=1}^{6}(-1)^{2k_E}(2k_E+1)(-1)^{2k_4+2k_6+2k_8-k_3-k_5-k_9} \\ &\times \left\{ \begin{array}{ccc} k_1 & k_2 & k_3 \\ k_8 & k_9 & k_7 \end{array} \right\} \left\{ \begin{array}{ccc} k_1 & k_2 & k_3 \\ k_9 & k_4 & k_5 \end{array} \right\} \left\{ \begin{array}{ccc} k_1 & k_5 & k_6 \\ k_2 & k_7 & k_9 \end{array} \right\}. \quad (1.6.8)\end{aligned}$$

1.7 Properties of the Ponzano-Regge model

1.7.1 Regularisation

The Ponzano-Regge amplitude given above may turn out to be divergent and require regularization. Ponzano and Regge originally proposed the following regularisation

$$\mathcal{Z}_{PR} = N_\lambda^{-V} \sum_{j_E=0}^{\lambda} \prod_E (-1)^{2j_E}(2j_E+1) \prod_\Delta (-1)^{j_1+j_2+j_3} \prod_\sigma \left\{ \begin{array}{ccc} j_1 & j_2 & j_3 \\ j_4 & j_5 & j_6 \end{array} \right\} \quad (1.7.1)$$

Where $N_\lambda = \sum_{i=0}^{\lambda}(2i+1)$ and λ is some positive number. Whilst this regularization works for some simple cases, an example where it fails was given in [17]. The divergence in the Ponzano-Regge model arises when the internal spin labels are not constrained by the spins on the boundary and this leads to an infinite sum. A triangulation in which the spin labels are restricted to a finite set of values is called *non-tardis* in [17] and by definition this gives a finite partition function.

We will briefly discuss two important methods of regularising the Ponzano-Regge formula. The first of which views the divergence as an SU(2) gauge invariance that must be fixed, the second uses representation theory of a quantum group instead of SU(2) to restrict the sum over spin labels.

Fixing the gauge symmetry

The divergence can be seen from the lattice BF theory point of view as the result of the rotation and translation symmetries, which are equivalent to diffeomorphism symmetry on-shell [2]. These are fixed as follows

SU(2) **Symmetry:** The rotation symmetry is fixed in the following way. One chooses a maximal tree T^* in the edges of the dual triangulation and sets each of the group elements associated to the edges of the tree to the identity by inserting the observable

$$\prod_{e\in T^*} \delta(g_e). \quad (1.7.2)$$

This can be derived from a Faddeev-Popov gauge fixing procedure with the associated determinant equal to one.

Translation Symmetry: The translation symmetry is fixed by choosing a tree T on the edges of the triangulation and setting the frame fields to zero, $e_E = 0, \forall E \subset T$. For the formulation of the Ponzano-Regge model in terms of characters, this is given by inserting

$$\prod_{E \in T} \frac{\delta_{j_E,0}}{\dim j_E} \tag{1.7.3}$$

In the graphical calculus an extra factor of $(-1)^{2j_E}$ needs to be inserted for each edge of the tree.

It was shown in [17] that this type of regularisation only gives a finite partition function under certain conditions on the topology of the manifold.

Regularisation with a cosmological constant

An interesting regularisation of the Ponzano-Regge model was found by Turaev and Viro [18] when they constructed an 3-manifold invariant from representation theory of the quantum deformation of the universal enveloping algebra of $\mathfrak{sl}(2)$. This is referred to in the literature as the Turaev-Viro model and while we will not use this explicitly, no discussion of regularisation would be complete without it.

The Turaev-Viro amplitude corresponds to using spin networks with Kauffman's parameter $A \neq \pm 1$. The parameter A is taken to be a $2r$-th root of unity, i.e. $A = \sqrt{q} = e^{\frac{i\pi}{2r}}$. Instead of the 6j symbol, the resulting spin network evaluation gives a "q-deformed" Kauffman-Lins 6j symbol, the dimension is replaced by the quantum dimension, and crucially the sums appearing in the partition function are restricted.

By studying the asymptotics of the q-6j symbol, or by relating the amplitude to Chern-Simons theory, the deformation parameter can be shown to be related to a positive cosmological constant [19]. The Chern-Simons path integral for manifold M is given by

$$Z_{CS}(M) = \int [dA] \exp\left(i\frac{k}{4\pi} \int_M \mathrm{tr}(A \wedge dA + \frac{2}{3} A \wedge A \wedge A) \right) \tag{1.7.4}$$

for some k, where A is an $SU(2)$ connection (a 1-form). The Turaev-Viro amplitude was shown to be equivalent to the square of Z_{CS} which, by a suitable field redefinition, can be written as a path integral over 3d gravity with cosmological constant

$$\Lambda = \left(\frac{4\pi}{k} \right)$$

with k related to the quantum group paramter by $k = r - 2$.

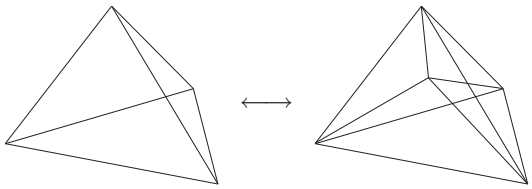

Figure 1.1: The 1-4 Pachner move.

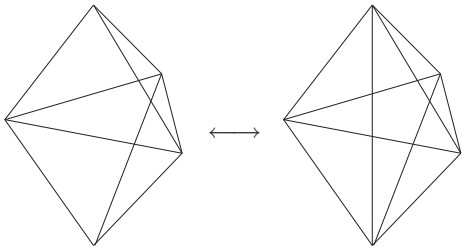

Figure 1.2: The 2-3 Pachner move.

1.7.2 Topological invariance

With an appropriate regularisation procedure, the Ponzano-Regge model is topologically invariant. By this, we mean that it depends only on the boundary triangulation and boundary data but not the triangulation of the interior of the 3-manifold. This feature is due to the fact that gravity in three dimensions has no local degrees of freedom and only admits flat solutions. The same is not true in four dimensions so that fact that the current 4d spin foam models depend on the underlying triangulation is not considered a problem. The dependence on the triangulation can be dealt with by summing over triangulations with a group field theory (see chapter 4), or may be removed by a suitable renormalisation procedure.

The proof that the Ponzano-Regge model is a topological invariant proceeds using the Pachner moves. Any two piecewise linear isomorphic spaces are related by a finite (although possibly very large) sequence of elementary moves. In three dimensions, the moves are the 1-4 move and the 2-3 move, see figures 1.1 and 1.2.

In general, Pachner moves in n dimensions can be found by considering the different possible ways to split up the boundary of an $n+1$ simplex. We can now show the topological invariance by showing that the Ponzano-Regge amplitude is unchanged by both the Pachner moves. This can be done in a number of ways, we illustrate one method below. The regularisation is important because the 1-4 move will lead to a divergence without it

Cable diagrams

Here we use Kauffmann-Lins cable diagrams to prove the invariance [14], the angular momentum diagram proof is essentially the same.

1-4 Move: For the 1-4 move, the relevant part of the partition function for four tetrahedra is

$$\sum_{j_7,j_8,j_9,j_{10}} \prod_{j_E=7}^{10} (-1)^{2j_E}(2j_E+1)$$

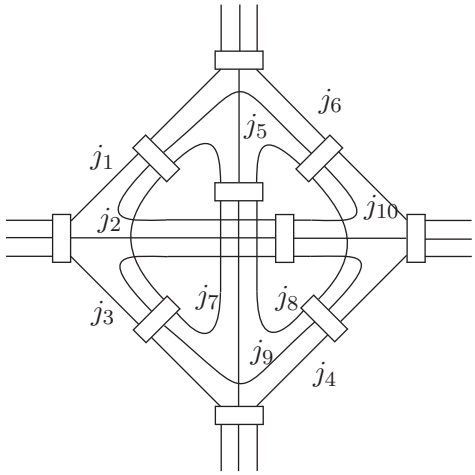

(1.7.5)

Using the gauge fixing tree to fix the Lorentz symmetry, we have

$$\sum_{j_7,j_8,j_9,j_{10}} \prod_{j_E=7}^{10} (-1)^{2j_E}(2j_E+1)$$

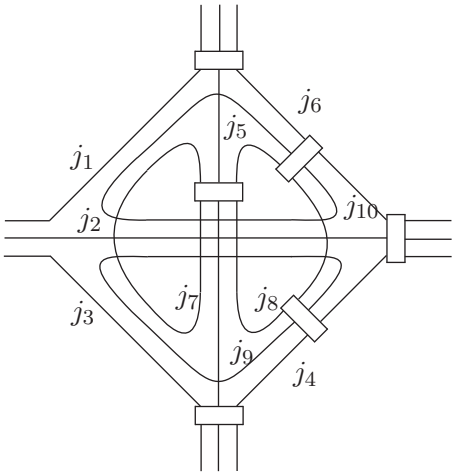

(1.7.6)

Using (1.5.32) on the loop with spin label j_7

$$\sum_{j_8,j_9,j_{10}} \prod_{j_E=8}^{10} (-1)^{2j_E}(2j_E+1) \quad \text{(1.7.7)}$$

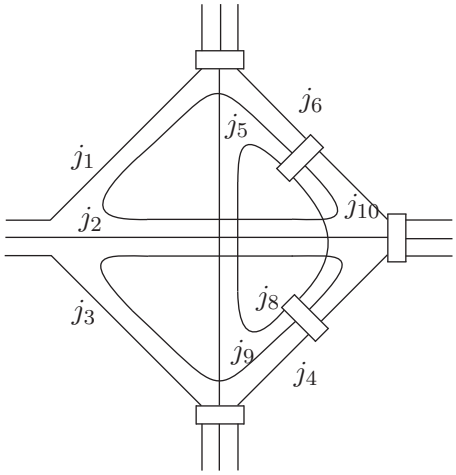

and again on the j_9 and j_{10} loops, leaves us with

$$\sum_{j_8}(-1)^{2j_8}(2j_8+1) \quad \text{(1.7.8)}$$

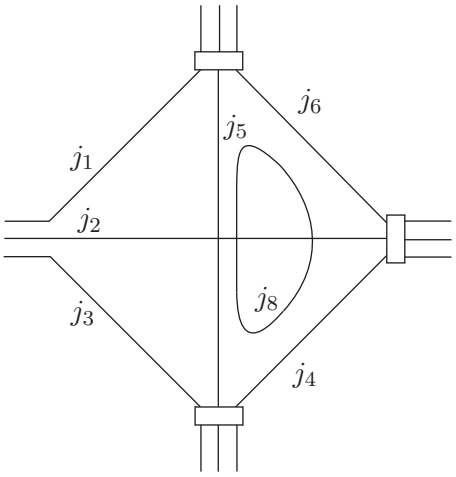

We now take into account the fixing of the translation symmetry with the tree T. This removes the final interior j_8 loop by setting the spin label to zero and the dimension factors cancel. Note that T will also remove some of the loops on the exterior part of the diagram, say j_4, j_5, j_6, however we are only looking at the part that changes under a Pachner move

so we will not add this alteration to the diagram. We are left with

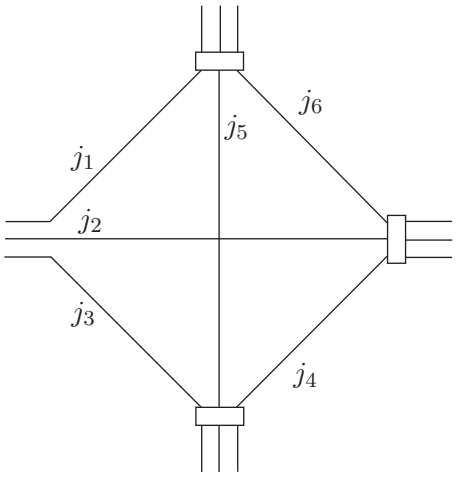

(1.7.9)

Which is the relevant part of the gauge fixed partition function for a single tetrahedron.

3-2 Move The partition function for three tetrahedra is given by

$$\sum_{j_{10}}(-1)^{2j_{10}}(2j_{10}+1)$$

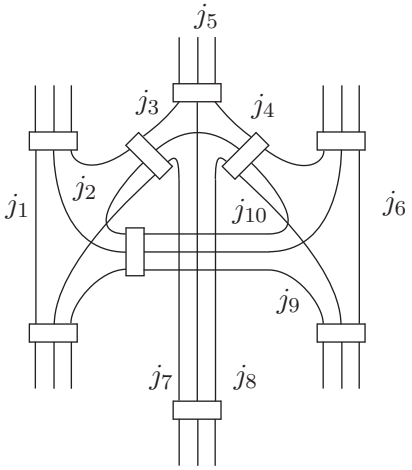

(1.7.10)

With the dual gauge fixing tree

$$\sum_{j_{10}}(-1)^{2j_{10}}(2j_{10}+1)$$

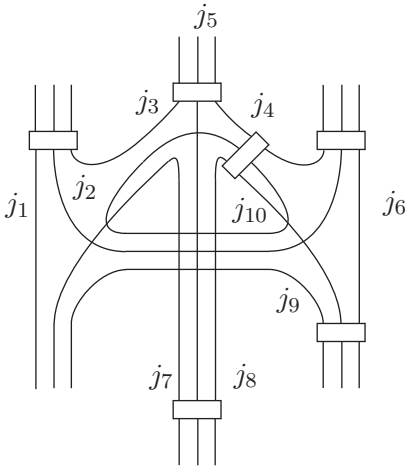

(1.7.11)

Using equation (1.5.32) on the j_{10} loop leaves

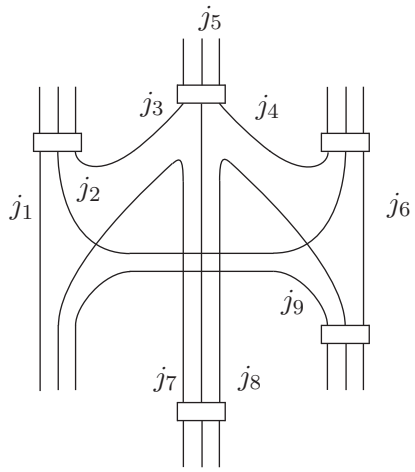

(1.7.12)

However, the partition function for two tetrahedra sharing a face is given by

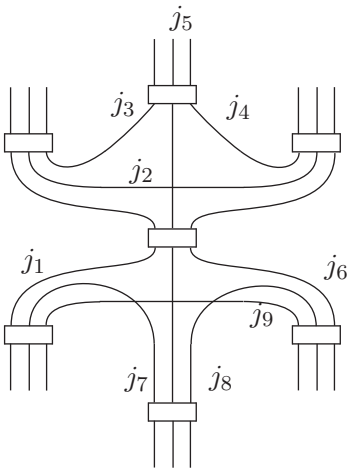

(1.7.13)

which is equivalent to the previous diagram with an appropriate choice of dual tree. The gauge fixing of the translation symmetry can be ignored here as the 3-2 move does not create a divergence as in the 1-4 case.

Hence we have shown that the regularised Ponzano-Regge model is invariant under the 3d Pachner moves and is a topological invariant.

1.7.3 Transition amplitudes

The Ponzano-Regge model gives a method of computing transition amplitudes between simplicial geometries. Suppose for simplicity that we have a triangulated manifold M with disjoint boundaries M_1, M_2 and that we fix a Regge metric g_{M_1} on M_1 and g_{M_2} on M_2.

This means that a half integer is assigned to each edge of the triangulation in M_1, M_2, i.e.

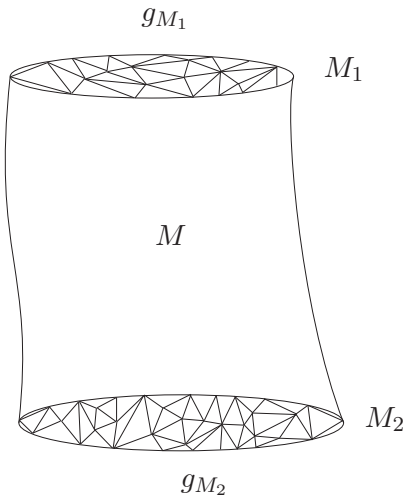

(1.7.14)

Constructing the Ponzano-Regge model for M with the spin labels fixed on M_1, M_2 then (assuming it is finite) gives a possible way to compute the transition amplitude between the initial state g_{M_1} and the final state g_{M_2}.

$$\langle g_{M_2}|g_{M_1}\rangle_{PR} = \sum_{j_E \in M-\partial M} \prod_{edges\ E} (-1)^{2j_E}(2j_E+1) \prod_{triangles\ \Delta} (-1)^{j_1+j_2+j_3} \prod_{tetrahedra\ \sigma} \times \begin{Bmatrix} j_1 & j_2 & j_3 \\ j_4 & j_5 & j_6 \end{Bmatrix} \tag{1.7.15}$$

This amplitude is of course a topological invariant since the PR model is. More generally, one can consider transition amplitudes between g_{M_1} and g_{M_2} but without a fixed topology on the interior. This can be achieved with a Group Field Theory which provides a sum over triangulations with a fixed boundary (see Chapter 4 or [4, 20]).

1.7.4 Ponzano-Regge on the boundary

We will now discuss a useful property of the Ponzano-Regge model that allows us to express the partition function $\mathcal{Z}_{PR}$ of a manifold with boundary as the evaluation of a spin network dual to the boundary triangulation. This is based on the result of Moussouris [21] which states that

Lemma 1. (Moussouris algorithm) *Using the recoupling identity and Schur's lemma, any planar spin network can be expressed in terms of sums of products of 6j symbols and dimension factors. This will be equal to the Ponzano-Regge model for the 3-ball with a boundary triangulation dual to the spin network and some triangulation of the interior.*

Note that this applies only to spin networks that can be drawn in the plane and thus correspond to triangulations of B^3. We will now describe the inverse of this procedure (reverse Moussouris algorithm) and generalise it to higher genus manifolds.

The reverse Moussouris algorithm for B^3 Start with a triangulation Δ_{B^3} of B^3, for simplicity we consider non-tardis triangulations. The claim is that $\mathcal{Z}_{PR}(\Delta_{B^3})$ can be expressed in terms of a planar spin network topologically dual to the triangulation of the boundary ∂B^3. We start by noting that for a triangulation with a single tetrahedron, the amplitude is expressed in terms of a tetrahedral network dual to the boundary of the tetrahedron so satisfies the claim. We now need to proceed inductively to build up arbitrary non-tardis triangulations by gluing on additional tetrahedra. We need only consider gluing tetrahedra on one or two common faces as an more than this will not give a non-tardis triangulation.

One face: If we glue two tetrahedra on a single common face then $\mathcal{Z}_{PR}$ is given by two tetrahedral networks with three common labels meeting at a vertex (see below). One can replace the two intertwiners by an integration over the tensor product of three SU(2) group variables

$$\int_{\mathrm{SU}(2)} dg D^i(g) \otimes D^j(g) \otimes D^k(g) = \frac{1}{\theta(i,j,k)}$$

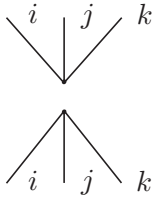

(1.7.16)

but, since the diagrams are invariant, these group elements can be reabsorbed leaving only the theta network from the normalisation which cancels with the face amplitudes in the Ponzano-Regge amplitude.

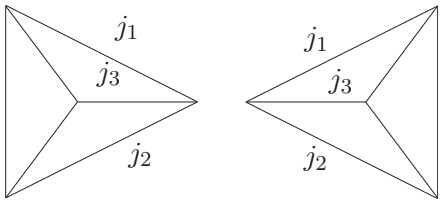

$$= \theta(j_1, j_2, j_3)$$

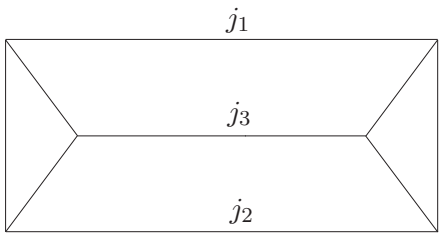

(1.7.17)

Now, one can see that this remaining spin network can be drawn dual to the surface of two tetrahedra glued on a common face.

Two faces: We start by writing the relevant part of the partition function for a tetrahe-

dron glued onto two faces of an existing triangulation

$$\sum_j (-1)^{2j}(2j+1)\frac{1}{\theta(j,a,b)\theta(j,e,d)\theta(b,k,e)\theta(k,d,a)}$$

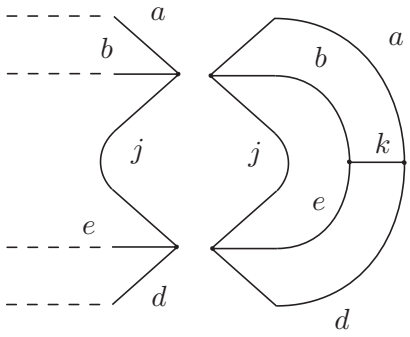

(1.7.18)

The edge corresponding to the spin j label is now internal so there is a summation. We can now apply the recoupling identity to the a, b, j, e, d edges which removes the tetrahedral network, two thetas, the dimension and the summation to give

$$\frac{1}{\theta(b,k,e)\theta(k,d,a)}$$

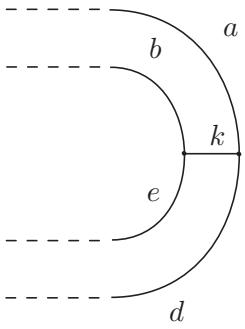

(1.7.19)

Which is a spin network dual to the new boundary of the triangulation with the canonical intertwiners. This can be seen explicitly in the (slightly degenerate) example of two tetrahedra being glued on two common faces.

The reverse Moussouris algorithm for the solid torus For the solid torus $\mathbb{T} = D^2 \times S^1$, the procedure differs slightly as the spin network dual to the boundary triangulation will no longer be planar. We will use the fact that the solid torus can be reduced to the 3-ball by cutting along a disc. Since we are considering non-tardis triangulations, it will be possible to reduce a triangulation $\Delta_{\mathbb{T}}$ of $\mathbb{T}$ to a triangulation $\Delta_{\mathbb{B}^3}$ of $\mathbb{B}^3$ by cutting along a disc, but such that the boundary of the disc contains at least three edges and no internal vertices (e.g. the triangulation described in section 1.6.1). Suppose there are n edges on the boundary of the disc, then there will be $n-2$ triangles, and the resulting triangulation will be that of the 3-ball with two identical discs. The Ponzano-Regge amplitude for $\Delta_{\mathbb{T}}$ with this cut will look like the amplitude for a 3-ball, but with the same spin labels associated to this cut and a summation over these labels since they were interior edges for $\Delta_{\mathbb{T}}$.

As above, we replace the $n-2$ valent intertwiners and the summations with a group

integral

$$\int_{\mathrm{SU}(2)} dg\ D^{j_1}(g) \otimes D^{j_2}(g) \otimes ... \otimes D^{j_{n-2}}(g) \tag{1.7.20}$$

However, we can no longer absorb these group elements into the remaining spin network. We are left with the following: $\mathcal{Z}_{PR}(\Delta_{\mathbb{T}})$ can be expressed as a spin network evaluation dual to the boundary triangulation, but with an integral over a group element inserted for each edge of the spin network that crosses the cut. Note that if we had chosen a different cut, then this can be compensated for in the amplitude by moving the group elements around using the invariance properties of the intertwiners.

As an example, consider the triangulation of the solid torus described in section 1.6.1 We choose the cutting disc $\mathbb{D}$ to be the triangle k_1, k_2, k_3 and perform the cut that reduces $\mathbb{T}$ to the 3-ball. A net for constructing the triangulation on the boundary is given by

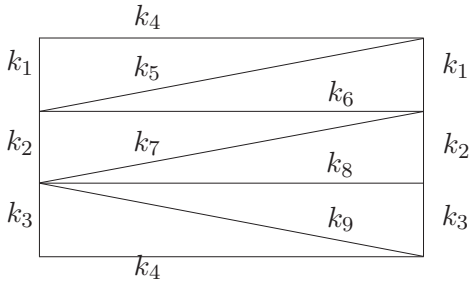

The Ponzano-Regge amplitude can be expressed as the following spin network evaluation on the boundary, with a group integral inserted on each of the dual edges that cross $\mathbb{D}$.

$$\mathcal{Z}_{PR}(\Psi, \mathbb{T}) = \int_{\mathrm{SU}(2)} dh$$

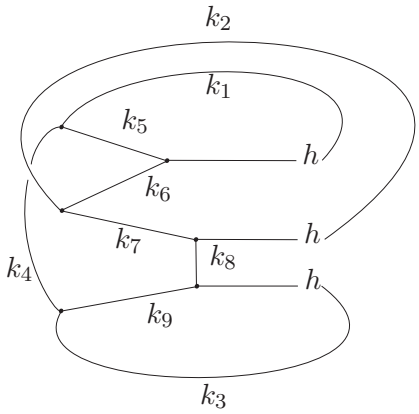

Expressing this spin network in terms of 6j symbols gives equation (1.6.8).

The reverse Moussouris algorithm for handlebodies of genus g This obviously generalises to higher genus handlebodies by repeated use of the above procedure. We first note that it is always possible to construct a non-tardis triangulation of a genus g handlebody Σ_3. Start with a triangulation of the 3-ball that has at least g distinct (i.e.

do not share any common edges or vertices) pairs congruent triangles on the boundary. Identify these triangles on the boundary pairwise and this provides a triangulation of Σ_3.

By definition, a genus g handlebody always admits a set of cuts $\mathbb{D}_i$ $i = 1, ..., g$ that reduce it to the 3-ball. For later use, we denote the set of cuts by C and for simplicity, we will also assume that we are working with the set of 'standard cuts' [22].

By repeated use of the methods described for the torus, we have the following:

Let Δ_{Σ^3} be a triangulation of a handlebody Σ^3 with a set of trivialising cuts C with the edge in $\partial\Delta_{\Sigma^3}$. The Ponzano-Regge amplitude can be expressed as the evaluation of a spin network dual to $\partial\Delta_{\Sigma^3}$ with a set of SU(2) elements h_i inserted on each of the edges that cross a cut i, with an integral over each of the group elements. Schematically, we write this as

$$\mathcal{Z}_{PR}(\Sigma^3) = \int_{\mathrm{SU}(2)} \prod_{i\in C} \mathrm{d}h_i \langle (\partial\Sigma^3)^*_{h_i} \rangle. \tag{1.7.21}$$

1.7.5 Asymptotics of the 6j symbol

The key piece of information that led Ponzano and Regge to suggest their model for 3d quantum gravity was their realisation that, in the limit of large spins, the behaviour of the 6j symbol could be described by the exponential of the Regge action for a tetrahedron. They did not provide a proof for their formula but gave numerical examples that illustrated how accurate the formula was, the proof was provided much later by Roberts in [23]. Since then, other (often simpler) methods of proving the formula have been found such as [24] and higher order corrections added [25].

We will look at the limit in which all of the spin labels in the 6j symbol are rescaled by some $\lambda \in \mathbb{N}$, i.e. $k \mapsto \lambda k$, and we take $\lambda \to \infty$. In this limit, the 6j symbol is related to the geometry of a tetrahedron with edge lengths $l = \lambda k + \frac{1}{2}$. For consistency with later chapters, we will label the faces of the tetrahedron by the numbers 1 to 4 and the edges by the two faces that share that edge. Eg k_{12} is the edge between the triangles labelled 1 and 2.

The formula is

$$\left\{ \begin{array}{ccc} \lambda k_{12} & \lambda k_{13} & \lambda k_{14} \\ \lambda k_{23} & \lambda k_{24} & \lambda k_{34} \end{array} \right\} \to \frac{1}{\sqrt{12\pi \mathrm{Vol}(\tau)}} \cos\left(\sum_{a<b} (\lambda k_{ab} + \frac{1}{2}) \Theta_{ab}(\tau) + \frac{\pi}{4} \right) \tag{1.7.22}$$

$\mathrm{Vol}(\tau)$ is the volume of the tetrahedron and $\Theta_{ab}(\tau)$ are the dihedral angles (the angles between the outward normals to the triangles a and b.)

Whilst this result was interesting and provided the motivation for the Ponzano-Regge model, it is important to check that the asymptotic formula for triangulations larger than

a single tetrahedron give the correct semiclassical limit. This will be the subject of the next chapter.

Chapter 2

Generalizing the Ponzano-Regge asymptotic formula

In this chapter, we will discuss the generalisation of the asymptotic formula for the 6j symbol to an asymptotic formula for the Ponzano-Regge model for larger triangulations. In particular, the results will cover triangulations of handlebodies. This chapter is based on [C].

2.1 Rewriting the Ponzano-Regge amplitude

The standard method of evaluating amplitudes of spin foam models in the semiclassical regime is to use the stationary phase approximation [26]. This requires the amplitude to be expressed as the exponential of some action. We will discuss this in more detail later but the next sections will focus on rewriting the Ponzano-Regge amplitude in this form. To achieve this, we will use coherent intertwiners. For the rest of the chapter we assume that we are considering a closed, compact 3-manifold with boundary M. In particular, M will be a handlebody of genus g.

2.1.1 Coherent intertwiners

A coherent intertwiner (or coherent triangle) refers to the use of SU(2) coherent states to express the standard SU(2) intertwiners in a different basis that is more suitable for studying the semiclassical behaviour of spin networks and spin foam amplitudes. Coherent states were first used in spin foam models by Livine and Speziale in [27] and have proved very useful in asymptotic calculations.

We begin with the definition and a summary of the important properties of SU(2) coherent

states. The subject is covered in detail by Perelomov in [28].

SU(2) **coherent states:** An SU(2) coherent state $\alpha_k(\mathbf{n},\theta)$ is a vector in the spin k representation space V_k that has maximum spin projection in the direction of some unit 3-vector $\mathbf{n}$.

$$L.\mathbf{n}\alpha_k(\mathbf{n},\theta) = ik\alpha_k(\mathbf{n},\theta) \tag{2.1.1}$$

$L = \frac{i}{2}\sigma^i$ are the SU(2) Lie algebra generators and the state $\alpha_k(\mathbf{n},\theta)$ depends on both the direction $\mathbf{n}$ and some angle θ as this equation only determines the coherent state up to a phase. So a choice of $\mathbf{n}$ does not specify a coherent state, and in order to properly define the state one must pick a representative of the U(1) equivalence class of states that correspond to the same $\mathbf{n}$. Perelemov chooses this phase by demanding that the states are defined by $|k,\mathbf{n}\rangle_{\text{Perelomov}} = g|k,k\rangle$, where g is the rotation taking the vector $\mathbf{z} = (0,0,1)$ to $\mathbf{n}$ around the vector $\mathbf{m} = \mathbf{z}\times\mathbf{n}$. Later, we will give a prescription for specifying the *relative* phase of coherent intertwiners such that the Ponzano-Regge amplitude does not depend on the choice of U(1) angle.

Coherent states have a number of useful properties that we will use later.

- These states transform with a phase under the group elements generated by $L.\mathbf{n}$ and the label $\mathbf{n}$ transforms covariantly under the SO(3) action of SU(2). That is for $g \in \text{SU}(2)$ with corresponding SO(3) element $\hat{g}$:

$$g\alpha_k(\mathbf{n},\theta) = e^{ik\phi}\alpha_k(\hat{g}\mathbf{n},\theta) \tag{2.1.2}$$

- The k representation can be constructed as the symmetric subspace of $2k$ copies of the fundamental representation. In this picture coherent states decompose into a tensor product of coherent states in the fundamental representation, i.e.

$$\alpha_k(\mathbf{n},\theta) = \left(\alpha_{\frac{1}{2}}(\mathbf{n},\theta)\right)^{2k} \tag{2.1.3}$$

  Consequently the group action factorizes:

$$g\alpha_k(\mathbf{n},\theta) = g\bigotimes_{i=1}^{2k}\alpha_{\frac{1}{2}}(\mathbf{n},\theta) = \bigotimes_{i=1}^{2k} e^{i\frac{\phi}{2}}\alpha_{\frac{1}{2}}(\hat{g}\mathbf{n},\theta). \tag{2.1.4}$$

- The modulus squared of the Hermitian inner product of coherent states is given by:

$$|\langle\alpha_k(\mathbf{n}_1,\theta_1),\alpha_k(\mathbf{n}_2,\theta_2)\rangle|^2 = \left(\frac{1}{2}(1+\mathbf{n}_1.\mathbf{n}_2)\right)^{2k}, \tag{2.1.5}$$

- Under the action of the standard antilinear structure on SU(2) (see [29]) the coherent state changes as:

$$L.\mathbf{n}J\alpha_k(\mathbf{n},\theta) = -ikJ\alpha_k(\mathbf{n},\theta) \tag{2.1.6}$$

  The antilinear map J is given by multiplication by the epsilon tensor in the spin k representation followed by complex conjugation. J commutes with SU(2) elements.

Intertwiners in the coherent state basis: An n-valent SU(2) coherent intertwiner can be written as

$$\iota(\mathbf{n}_i,\theta_i) = \int_{\mathrm{SU}(2)} \mathrm{d}X \bigotimes_{i=1}^{n}(X\alpha_{k_i}(\mathbf{n}_i,\theta_i)) \in \mathrm{Inv}_{\mathrm{SU}(2)}(V_{k_1}\otimes V_{k_2}\otimes ...\otimes V_{k_n}) \tag{2.1.7}$$

This state is clearly an SU(2) invariant state. As we noted that SU(2) acts covariantly as SO(3) on the labels $\mathbf{n}_i$ this choice is only dependent on an unspecified phase as we left open which eigenstates of $L.\mathbf{n}_i$ we are using. In particular it does not depend on the remaining parity $P = \mathrm{O}(3)/\mathrm{SO}(3)$ as this acts on the plane of the triangle as an SO(3) element.

Thus choosing normalized $\alpha_k(\mathbf{n},\theta)$ compatible with the boundary spin labels fixes the intertwiner states up to a parity choice and up to a phase. These two data will be fixed by considering the gluing of the boundary.

Asymptotic behaviour of coherent intertwiners It is interesting to consider the behaviour of the intertwiners in the large spin regime $k_i \to \lambda k_i, \lambda \to \infty$. The norm of the coherent intertwiners (given by the Hermitian inner product)

$$f_{\mathrm{Coh}}(\mathbf{n}_i,k_i) = \int_{\mathrm{SU}(2)} dX \prod_{i=1}^{n}(\alpha_k(\mathbf{n},\theta))^{\dagger}\mathbf{X}\alpha_{\mathbf{k}}(\mathbf{n},\theta) \tag{2.1.8}$$

was studied in the limit of large spins in [27] using the stationary phase approximation. Note that the phase dependence cancels in the inner product and the norm depends only on $\mathbf{n}$ and k It was found that f_{Coh} was exponentially suppressed for large λ unless the closure condition is satisfied

$$\sum_{i=1}^{n} k_i\mathbf{n}_i = 0 \tag{2.1.9}$$

In the three valent case, this is interpreted as the closure condition for a triangle with edges given by $\mathbf{v}_i = k_i\mathbf{n}_i$. So a coherent intertwiner only exists in the semiclassical regime if its variables admit a geometrical interpretation as a triangle.

In the 4-valent case, there is a geometrical interpretation with $\mathbf{A}_i = k_i\mathbf{n}_i$ as the normals to the faces of a tetrahedron.

Geometric quantisation of the shape space of polyhedra shows that sets of n vectors subject to the closure condition are in fact sufficient to span the space of n-valent intertwiners [30].

2.1.2 Regge states - a canonical phase choice for the boundary

We are almost ready to use the coherent intertwiners to express the Ponzano-Regge amplitude in a form suitable for stationary phase analysis, but first we will discuss a canonical phase choice for the intertwiners.

When the PR amplitude is expressed in terms of coherent intertwiners, the partition function is no longer a function of just the spin labels associated to the edges on the boundary, but it now also depends on the $\mathbf{n}_{ab}$. The set $\{k_{ab}, \mathbf{n}_{ab}\}$ of half integers and 3-vectors associated to each edge on the boundary of the triangulation will be referred to as *boundary data*.

Note that because of the closure condition, we can pick the boundary data to lie in a single plane. We choose the plane orthogonal to $\mathcal{N} = (0, 0, 1)$. The unit vectors $\mathbf{n}_{ab} \in S^2$ are labelled by the dual edge $ab \in \mathcal{E}$, or equivalently by the two triangles a and b to which it belongs. Then the triangles formed by the edges $k_i\mathbf{n}_i$ along with $\mathcal{N}$ have the same orientation with respect to $\mathbb{R}^3$.

Now there exists an element $\hat{g}_{ab} \in \mathrm{SO}(3)$ such that:

$$\begin{aligned} -\mathbf{n}_{ba} &= \hat{g}_{ab}\mathbf{n}_{ab} \\ \mathcal{N} &= \hat{g}_{ab}\mathcal{N} \end{aligned} \tag{2.1.10}$$

So $\hat{g}_{ab}$ lies in the SO(2) subgroup of SO(3) that preserves $\mathcal{N}$. There are two possible choices of SU(2) element corresponding to this $\hat{g}_{ab}$ and we make some choice of lift for each triangle.

The canonical choice of phase for the boundary state is as follows. Since $\alpha_k(-\mathbf{n}_{ab}, \theta_{ab})$ is proportional to $g_{ab}\alpha_k(\mathbf{n}_{ba}, \theta_{ba})$, then we fix the phase of the ba state relative to that of the ab state

$$J\alpha_k(\mathbf{n}_{ba}, \theta_{ba}) = g_{ab}\alpha_k(\mathbf{n}_{ab}, \theta_{ab}) \tag{2.1.11}$$

We call coherent states with the above relative state choice Regge states, and denote them $|\mathbf{n}, k\rangle$ Their image under the antilinear structure is $|-\mathbf{n}, k\rangle = J\,|\mathbf{n}, k\rangle$, and states in the fundamental representation are denoted $|\mathbf{n}\rangle$.

We can now write the boundary state for the whole manifold as the following

$$\Psi(k_i, \mathbf{n}_i) = \int \left(\prod_{a \in \mathcal{V}} \mathrm{d}X_a \right) \bigotimes_{cd \in \mathcal{E}} X_c \ |\mathbf{n}_{cd}, k_{cd}\rangle \tag{2.1.12}$$

Where $\mathcal{V}$ is the set of vertices and we can choose any representative of the U(1) equivalence class for the ab-th state. A different choice will result in some phase factor which will be cancelled by the ba-th state.

2.1.3 The Amplitude in terms of coherent states

We begin with B^3, the 3d ball. To evaluate the spin network defining our amplitude in terms of these coherent intertwiners we choose a particular diagrammatic representation of the planar graph. To obtain the spin network evaluation of this graph we then contract the intertwiners chosen using the epsilon inner product defined in terms of the Hermitian inner product by $(\alpha, \beta) = \langle J\alpha|\beta\rangle$. Number the triangles in the graph from left to right. We then assume that the coherent intertwiners have been specified with respect to this planar representation of the graph as well. Then we have no crossings in the diagram and we can explicitly write the contraction of coherent intertwiners as:

$$\begin{aligned}\mathcal{Z}_{PR}(\Psi, B^3) &= \int \prod_{a\in\mathcal{V}} \mathrm{d}X_a \prod_{bc\in\mathcal{E}} \left(X_b \left|\mathbf{n}_{bc}, k_{bc}\right\rangle, X_c \left|\mathbf{n}_{cb}, k_{bc}\right\rangle\right) \\ &= \int \prod_{a\in\mathcal{V}} \mathrm{d}X_a \prod_{bc\in\mathcal{E}} \left\langle -\mathbf{n}_{bc}, k_{bc}\right| X_b^\dagger X_c \left|\mathbf{n}_{cb}, k_{cb}\right\rangle \\ &= \int \prod_{a\in\mathcal{V}} \mathrm{d}X_a \prod_{bc\in\mathcal{E}} \left\langle -\mathbf{n}_{bc}\right| X_b^\dagger X_c \left|\mathbf{n}_{cb}\right\rangle^{2k_{bc}} \end{aligned} \tag{2.1.13}$$

Where we have written $|\mathbf{n}_{cb}\rangle$ for $|\mathbf{n}_{cb}, \frac{1}{2}\rangle$. This formula is just the Z_{PR} for B^3 defined in chapter 1 but expressed on the boundary. The boundary phase is now different as the coherent intertwiners are used rather than the standard 3-valent KL intertwiners.

For the higher genus manifolds, the amplitude contains additional group elements when expressed on the boundary. Call $\tilde{\mathcal{E}}$ the set of edges not crossing circles and $\mathcal{E}_j$ the set of edges crossing circle $j \in C$. The amplitude is then given by

$$\begin{aligned}\mathcal{Z}_{PR}(\Psi, \Sigma^3) &= (-1)^\chi \int \prod_{a\in\mathcal{V}} \mathrm{d}X_a \prod_{j\in C} \mathrm{d}h_j \prod_{bc\in\tilde{\mathcal{E}}} \left\langle -\mathbf{n}_{bc}\right| X_b^\dagger X_c \left|\mathbf{n}_{cb}\right\rangle^{2k_{bc}} \\ &\quad \times \prod_{l\in C} \prod_{de\in\mathcal{E}_l} \left\langle -\mathbf{n}_{de}\right| X_d^\dagger h_l X_e \left|\mathbf{n}_{ed}\right\rangle^{2k_{de}} \end{aligned} \tag{2.1.14}$$

Where $(-1)^\chi$ is a sign factor incurred in the spin network evaluation when connecting up the glued edges in the spin network evaluation. This can then be written as

$$\mathcal{Z}_{PR}(\Psi, \Sigma^3) = (-1)^\chi \int \prod_{i\in V} dX_i \prod_{j\in C} dh_j e^S \tag{2.1.15}$$

with the action given by

$$S = \sum_{ab\in\tilde{\mathcal{E}}} 2k_{ab} \ln \left\langle \mathbf{n}_{ab}\right| JX_a^\dagger X_b \left|\mathbf{n}_{ba}\right\rangle + \sum_{l\in C} \sum_{de\in\mathcal{E}_l} 2k_{de} \ln \left\langle \mathbf{n}_{de}\right| JX_d^\dagger h_l X_e \left|\mathbf{n}_{ed}\right\rangle. \tag{2.1.16}$$

Note that the ambiguity in the logarithm of a complex number does not affect the amplitude.

2.1.4 Symmetries of the action

The action (2.1.16) has the following symmetries (up to $2\pi i$)

- *Continuous.* A global rotation $Y \in \mathrm{SU}(2)$ acting on each X_a and h_i as $X_a \to Y X_a$ and $h_i \to Y h_i Y^{-1}$. This represents a rigid motion of the whole manifold.
- *Discrete.* At each triangle a the transformation $X_a \to \epsilon_a X_a$ with $\epsilon_a = \pm 1$ leaves a factor $\epsilon_a^{\sum_{b,ab\in\mathcal{E}} 2k_{ab}}$. As the admissibility conditions are satisfied on each triangle, this factor equals one. Similarly we have an arbitrary sign ϵ_i on h_i as the edges on which h_i act satisfy the admissibility condition for intertwiners.

This latter symmetry will be used to compensate for the ambiguity of the lifts of SO(3) to SU(2) in the higher genus handlebodies.

2.1.5 Relation to the standard intertwiner phase choice

The standard choice of phase for an intertwiner, defined by chromatic evaluation [9], gives real numbers for a spin network evaluation. We will now show that with the Regge phase choice the amplitude is real so can only differ from the chromatic evaluation by ± 1 and a normalisation factor. Note that since the Regge choice has all the $\mathbf{n}_{ab}$ orthogonal to $\mathbf{e}_z$, the rotation $e^{-i\pi \mathbf{e}_z\cdot\sigma}$ rotates $\mathbf{n}_{cb}$ to $-\mathbf{n}_{cb}$ and leaves $\mathbf{e}_z$ invariant. Under this rotation, the coherent state $|\mathbf{n}_{cb}\rangle$ will transform as

$$e^{-i\pi \mathbf{e}_z\cdot\sigma} |\mathbf{n}_{cb}\rangle = e^{i\phi} J |\mathbf{n}_{cb}\rangle \tag{2.1.17}$$

for some phase ϕ.

Consider a single term in the amplitude (2.1.14), and rewrite it inserting the identity:

$$\begin{aligned}
\langle -\mathbf{n}_{bc}| X_b^\dagger X_c |\mathbf{n}_{cb}\rangle &= \langle -\mathbf{n}_{bc}| e^{i\pi \mathbf{e}_z\cdot\sigma}(e^{-i\pi \mathbf{e}_z\cdot\sigma} X_b^\dagger)(X_c e^{i\pi \mathbf{e}_z\cdot\sigma}) e^{-i\pi \mathbf{e}_z\cdot\sigma} |\mathbf{n}_{cb}\rangle \\
&= \langle \mathbf{n}_{bc}| J^\dagger e^{i\pi \mathbf{e}_z\cdot\sigma} \tilde{X}_b^\dagger \tilde{X}_c e^{-i\pi \mathbf{e}_z\cdot\sigma} g_{cb} J |\mathbf{n}_{bc}\rangle \\
&= \langle \mathbf{n}_{bc}| J^\dagger e^{-i\phi} J^\dagger \tilde{X}_b^\dagger \tilde{X}_c g_{cb} J e^{i\phi} J |\mathbf{n}_{bc}\rangle \\
&= \langle \mathbf{n}_{bc}| J^\dagger J^\dagger \tilde{X}_b^\dagger \tilde{X}_c J |\mathbf{n}_{cb}\rangle \\
&= \overline{\langle -\mathbf{n}_{bc}| \tilde{X}_b^\dagger \tilde{X}_c |\mathbf{n}_{cb}\rangle}
\end{aligned} \tag{2.1.18}$$

where we have defined the transformation $\tilde{X}_c = X_c e^{i\pi \mathbf{e}_z\cdot\sigma}$, which can be absorbed on the group integration in (2.1.14) and the fact that $J |\mathbf{n}_{cb}\rangle = |-\mathbf{n}_{cb}\rangle$. We have used the Regge

phase choice (2.1.11) from going from the first to the second line and the fact that the SU(2) transformations are all in fact in the same U(1) subgroup (and hence commute). From going to the second to the third line we have noted that we are acting with opposite rotations on the same state. Hence we get that $\mathcal{Z}_{PR}(\Psi, \Sigma^3) = \overline{\mathcal{Z}_{PR}(\Psi, \Sigma^3)}$ which is thus real.

2.2 Asymptotic formula

We wish to study the semiclassical limit of the amplitude $Z_{PR}(\Psi, \Sigma^3)$ when the boundary spin labels are large. To do this, we homogeneously rescale the spin labels by an integer λ and consider the limit $\lambda \to \infty$. The corresponding boundary state Ψ_λ is denoted $\Psi_\lambda = \Psi(\lambda k_i, \mathbf{n_i})$. We will see that a certain type of immersion of the boundary data will play a dominant role in the asymptotic formula. These immersions are referred to as cut immersions.

A *cut immersion* $\mathfrak{i} \in \mathfrak{I}$ is an immersion of the manifold obtained from $\partial\Sigma^3$ by the trivializing cuts $\partial\mathbb{D}_i$, $i \in C$, i.e. it is an immersion $\imath(\partial\Sigma^3 - \{\cup_{i\in C}\partial\mathbb{D}_i\}) \hookrightarrow \mathbb{R}^3$. This condition is topological but here a cut immersion is also required to be an isometry, i.e. the mapping is such that the discrete metric given by the edge lengths agrees with the standard metric on $\mathbb{R}^3$. Furthermore, we require the existence of SO(3) elements that identify the two sides of the cut, i.e. $\hat{h}_i \in \mathrm{SO}(3)$ such that $\hat{h}_i(\imath(\partial\mathbb{D}_i^+)) = \imath(\partial\mathbb{D}_i^-)$, where $\partial\mathbb{D}_i^-$ and $\partial\mathbb{D}_i^+$ are the elements of the boundary $\partial(\partial\Sigma^3 - \partial\mathbb{D}_i)$ created by the removal of $\partial\mathbb{D}_i$ from $\partial\Sigma^3$ [1] . Note that for the 3-ball, there are no trivialising cuts and the notion of a cut immersion reduces to the usual immersion.

Given a set $\mathcal{B} = \{\mathbf{n}_{ab}, k_{ab}\}_{a\neq b}$ of boundary data we denote as $\mathfrak{I}$ the set of cut immersions of the polyhedral surface $\partial\Sigma^3$ with edge lengths k_{ab} in $\mathbb{R}^3$ up to rigid motion.

There are usually a number of different possible cut immersions for a particular set of boundary data and cuts. The cut immersions for a different choice of cuts can be obtained by a homotopy on the surface. We treat any cut immersions that are related in this way as equivalent. An example of a cut immersion of the boundary of the solid torus is given in Figure 2.1.

Such an immersion is called rigid if every continuous deformation of it requires changing the edge lengths, and flexible otherwise. We denote the subset of rigid immersions $\mathfrak{I}_r \subset \mathfrak{I}$. Through every immersion in $\mathfrak{I}$ passes a set of immersions that can be continuously deformed into each other, for simplicity it is assumed that these are manifolds with dimension

[1] Note that since $\mathbb{D}_i$ is transversal to generators of $H_1(\Sigma^3)$, its removal changes the connectivity of Σ^3 and creates two new boundaries, $\mathbb{D}_i^-$ and $\mathbb{D}_i^+$.

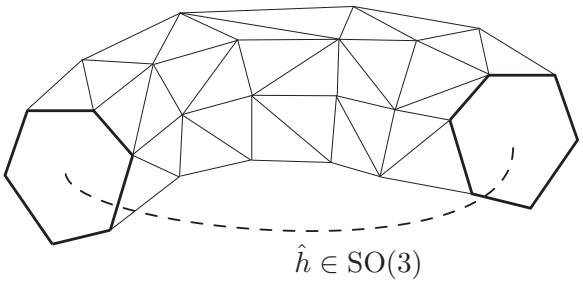

Figure 2.1: A cut immersion for a particular boundary triangulation of a torus. The cutting circles are shown in bold and there is an $\hat{h} \in \mathrm{SO}(3)$ that identifies them.

d. We call these *flexifolds* and denote them $\mathfrak{f}$, we denote the set of flexifolds $\mathfrak{F}$. We then define $\mathfrak{F}_{\max}$ to be the set of flexifolds in $\mathfrak{F}$ of maximal dimension $d_{\max}$. With this definition the rigid immersions are a special case of a flexifold with dimension $d = 0$. We assume from now on that the flexifolds $\mathfrak{f}$ do not intersect.

In the limit $\lambda \to \infty$ we have the following:

Asymptotic Formula

For a triangulated handlebody Σ^3, with boundary data $\{k_{ab}, \mathbf{n}_{ab}\}$

1. If $\mathfrak{I}$ is not empty we have that:

$$\begin{aligned} \mathcal{Z}_{PR}(\psi_\lambda, \Sigma^3) &= \left(\frac{2\pi}{\lambda}\right)^{\frac{3(|\mathcal{V}|+|C|-1)-d_{\max}}{2}} \sum_{\mathfrak{f}\in\mathfrak{F}_{\max}} N_{\mathfrak{f}} \cos\left(\lambda \sum_{ab\in\mathcal{E}} k_{ab}\Theta^{\mathfrak{f}}_{ab} + \phi^{\mathfrak{f}}_{ab}\right) \\ &\quad + O\left(\left(\frac{1}{\lambda}\right)^{\frac{3(|\mathcal{V}|+|C|)-d_{\max}}{2}}\right) \end{aligned} \tag{2.2.1}$$

   The coefficient $N_{\mathfrak{f}}$, the dihedral angle $\Theta^{\mathfrak{f}}_{ab}$ and the phase $\phi^{\mathfrak{f}}_{ab}$ are independent of λ and will be described later. The $\phi^{\mathfrak{f}}_{ab}$ and the dihedral angle $\Theta^{\mathfrak{f}}_{ab}$ are evaluated on an arbitrary immersion $\mathfrak{i}$ in $\mathfrak{f}$. It can be shown that these are independent of the cuts. Thus for any particular edge we can evaluate the dihedral angle by moving the cut away from it. $|\mathcal{V}|$ is the number of triangles (or equivalently vertices in the set $\mathcal{V}$) and $|C|$ is the number of cutting circles. $d_{\max}$ is the dimension of the flexifolds $\mathfrak{f} \in \mathfrak{F}_{\max}$, and $N_{\mathfrak{f}}$ now also contains an integral over the union of flexifolds in $\mathfrak{f}$.

2. If no immersions in $\mathbb{R}^3$ exist the amplitude is exponentially suppressed:

$$\mathcal{Z}_{PR}(\psi_\lambda, \Sigma^3) = o(\lambda^{-n}) \quad \forall n \in \mathbb{N} \tag{2.2.2}$$

Note that in the simple case where the boundary data only admits rigid immersions, ie if $d_{\max} = 0$, then the sum becomes a sum over the rigid immersions $\mathfrak{i} \in \mathfrak{I}_r$ and we have that:

$$\begin{aligned} \mathcal{Z}_{PR}(\psi_\lambda, \Sigma^3) &= \left(\frac{2\pi}{\lambda}\right)^{\frac{3(|\mathcal{V}|+|C|-1)}{2}} \sum_{\mathfrak{i}\in\mathfrak{I}_r} N_\mathfrak{i} \cos\left(\lambda \sum_{ab\in\mathcal{E}} k_{ab}\Theta^\mathfrak{i}_{ab} + \phi^\mathfrak{i}_{ab}\right) \\ &\quad + O\left(\left(\frac{1}{\lambda}\right)^{\frac{3(|\mathcal{V}|+|C|-1)}{2}+1}\right) \end{aligned} \tag{2.2.3}$$

since $d_{\max} = 0$. Since the immersions are now rigid, the coefficient $N_\mathfrak{i}$, the dihedral angles $\Theta^\mathfrak{i}_{ab}$ and the phase $\phi^\mathfrak{i}_{ab}$ are evaluated on the cut immersion $\mathfrak{i}$.

2.3 Proof of the asymptotic formula

We now prove the above statement using the stationary phase approximation described in the appendix. We will find the stationary and critical points of the action and give them a geometrical interpretation. This can then be used to evaluate the action at the critical points in terms of the geometrical quantities.

2.3.1 Critical points

The critical points of the action (2.1.16) are those such that $\mathrm{Re}S = 0$. These are the only ones that contribute in the limit $\lambda \to \infty$ as can be seen by considering the exponential of a complex number

$$e^{\lambda(a+ib)} \tag{2.3.1}$$

where $a \leq 0$. This will obviously be suppressed in the large λ limit unless $a = 0$.

First, we introduce some more notation. The action of the elements X_b on the coherent states will produce a new coherent state

$$|\mathbf{n}'_{ab}\rangle = X_a |\mathbf{n}_{ab}\rangle \tag{2.3.2}$$

We will denote the corresponding rotated three vectors by

$$\mathbf{n}'_{ab} = \hat{X}_a \mathbf{n}_{ab} \tag{2.3.3}$$

where $\hat{X}_a$ is the SO(3) element corresponding to X_a.

We will first consider critical points for edges that are not on one of the cutting circles. Using (2.1.5), we can see that the real part of the action is given by

$$\mathrm{Re}S = \sum_{ab\in\tilde{E}} k_{ab} \ln \frac{1}{2}(1 - \mathbf{n}'_{ab} \cdot \mathbf{n}'_{ba}). \tag{2.3.4}$$

This does not depend on the coherent state phases as it is real. Using this formula, we can see that $\mathrm{Re}S = 0$ when $\mathbf{n}'_{ab} = -\mathbf{n}'_{ba}$ for all ab, or explicitly in terms of SO(3) rotations

$$\hat{X}_a \mathbf{n}_{ab} = -\hat{X}_b \mathbf{n}_{ba}. \tag{2.3.5}$$

The critical points for an edge that crosses a cutting circle i differ by the inclusion of the h_i

$$\hat{X}_a \mathbf{n}_{ab} = -\hat{h}_i \hat{X}_b \mathbf{n}_{ba}. \tag{2.3.6}$$

2.3.2 Stationary points

The stationary points are found by varying the action with respect to each of the group variables X_a. The variation of an SU(2) group variable and its inverse is

$$\delta X = TX \qquad \delta X^{-1} = -X^{-1}T \tag{2.3.7}$$

for an arbitrary $\mathfrak{su}(2)$ Lie algebra element $T = \frac{1}{2} i T^j \sigma_j$. The stationary points are given by $\delta S = 0$ and lead to the following equation

$$\sum_{b:\ b\neq a} k_{ab}\ \mathbf{V}_{ab} = 0 \tag{2.3.8}$$

where

$$\mathbf{V}_{ab} = \frac{\langle -\mathbf{n}_{ab} | X_a^{-1}\, \boldsymbol{\sigma}\, X_b | \mathbf{n}_{ba} \rangle}{\langle -\mathbf{n}_{ab} | X_a^{-1} X_b | \mathbf{n}_{ba} \rangle}, \tag{2.3.9}$$

These equations can then be evaluated at the critical points using $\langle \mathbf{n} | \sigma^i | \mathbf{n} \rangle = n^i$ to give

$$\sum_{b:\ b\neq a} k_{ab}\ \mathbf{n}_{ab} = 0 \tag{2.3.10}$$

which is the closure constraint for an immersed triangle.

The stationary phase condition for the h_i variables is the same but in this case we obtain

$$\sum_{ab\in C_i} k_{ab}\ \mathbf{n}'_{ab} = 0 \tag{2.3.11}$$

Which is the closure condition for edges on the circle i immersed in $\mathbb{R}^3$. Note that unlike the closure condition for the triangle, this relation involves the $\mathbf{n}'_{ab}$ as each edge belongs to a different triangle.

If the critical points are not isolated but form a manifold of critical points, then we denote this manifold by

$$\mathcal{C}_X = \{(X_1, ..., X_{|V|}, h_1, ..., h_{|C|}) \in \mathrm{SU}(2)^{|\mathcal{V}|+|C|} : \delta S = 0, \mathrm{Re}(S) = 0\} \tag{2.3.12}$$

2.3.3 Geometric Analysis

In this section we will discuss the relation of the stationary and critical points to geometry. We begin by relating them to the cut immersions described above, we then discuss the Regge action for this type of immersion - in particular what happens at the trivializing cuts. We can then relate the group variables and the Regge gluing maps to the dihedral rotation which will require resolving some sign ambiguities from the lift of the geometric SO(3) quantities to SU(2). We can then evaluate the action at the critical points and show that it reduces to the Regge action for a cut immersion.

Geometry of the critical points

The critical points correspond to immersions of the surface geometry defined by the boundary data cut along the trivializing cuts. This is easy to see as the critical and stationary equations simply enforce the existence of a consistent set of edge vectors to be associated to each edge. Precisely formulated we have that:

Lemma 2. (Geometry) *Given a set of boundary data $\mathcal{B}$ satisfying the closure constraint on each triangle, the solutions X_a, h_i to the critical and stationary point equations* (2.3.5), (2.3.6) *and* (2.3.11) *correspond to immersions of a geometric triangulated 2-manifold with boundary in $\mathbb{R}^3$. This manifold is the one obtained by cutting the boundary manifold $\partial\Sigma^3$ along the trivialising cuts C and has a boundary $\bigcup_{i\in C}\partial\mathbb{D}_i^+ \cup \partial\mathbb{D}_i^-$. This immersion is subject to the constraint that a set of $\hat{h}_i \in \mathrm{SO}(3)$ exists that map the immersion of $\partial\mathbb{D}_i^+$ to the parity flipped $P(\partial\mathbb{D}_i^-)$, that is, the immersion of $\partial\mathbb{D}_i^+$ is congruent and oppositely oriented to the immersion of $\partial\mathbb{D}_i^-$ (i.e. Figure 2.1).*

The edge vectors of the immersion are given by

$$\mathbf{v}_{ab}(\mathfrak{i}) = k_{ab}\hat{X}_a\mathbf{n}_{ab}.$$

Its orientation is the one induced by the vectors on each face.

Proof: The closure condition means that all of the edges associated to a triangle close in $\mathbb{R}^3$ and the edges do give a triangle. Start with all of the triangles immersed in the plane orthogonal to the z axis $\mathcal{N}^\perp$. The group elements then rotate these triangles out of the plane such that the edges of the triangles satisfy (2.3.5), i.e. they are antiparallel in adjacent triangles. For a 3-ball this is enough to give an immersion, but for higher genus handlebodies the critical points on the cut must be used. The critical point equations on the cuts ensure that there is a rotation that identifies the cut circles.

□

If there is a manifold of dimension $d > 0$ of critical points then Lemma 2 holds for each critical point in $\mathcal{C}_X$. Since these critical points lie on a manifold, there is a continuous deformation of the immersed surface that does not change the edge lengths. Hence these critical points reconstruct flexible immersions and we arrive at the flexifolds $\mathfrak{f}$ described in section 2.2. We will now label the critical manifolds by $\mathcal{C}_\mathfrak{f}$, where $\mathfrak{f}$ is the flexifold that it describes.

The Regge Action for Handlebodies

The boundary Regge action for a convex polyhedral body embedded in $\mathbb{R}^3$ is given by $S_R = \sum l_{ab}\Theta_{ab}$ where l_{ab} are the edge lengths and Θ_{ab} are the dihedral angles. The dihedral angle is the angle between the two normals to adjacent triangles $\cos\Theta_{ab} = \mathcal{N}_a \cdot \mathcal{N}_b$ and we take $0 \leq \Theta_a < \pi$. In the previous section we found that our critical points corresponded to a particular type of immersions in $\mathbb{R}^3$, these may not be convex, embeddings, or even have a well defined notion of outward, e.g. a sphere with a dent such that the dent passes through the sphere at another point. We give a slight generalization of the Regge action to accommodate this.

Firstly, our choice of normals to triangles such that they agree with the standard orientation of $\mathbb{R}^3$ gives a suitable notion of "outward", even though in the cut immersion some of these normals may end up pointing inward. These normals are given by

$$\mathcal{N}_a = \hat{X}_a \mathcal{N}.$$

The dihedral rotation is the unique rotation $\hat{D}_{ab} \in \mathrm{SO}(3)$ that rotates the normal $\mathcal{N}_a$ to $\mathcal{N}_b$ and leaves the edge $\mathbf{v}_{ab}(\mathfrak{i})$ of the immersion unchanged. That is

$$\mathcal{N}_b = \hat{D}_{ab}\mathcal{N}_a$$

and

$$\mathbf{v}_{ab}(\mathfrak{i}) = \hat{D}_{ab}\mathbf{v}_{ab}(\mathfrak{i}).$$

The dihedral angle is the rotation parameter associated with $\hat{D}_{ab}$. A lift of this rotation to an SU(2) element can thus be written as

$$\begin{aligned} D_{ab} &= \exp\left(\Theta^{\mathfrak{i}}_{ab}\,\frac{\mathbf{v}_{ab}(\mathfrak{i})}{|\mathbf{v}_{ab}(\mathfrak{i})|}.L\right) \\ &= \exp\left(\Theta^{\mathfrak{i}}_{ab}\,\mathbf{n}'_{ab}.L\right) \in \mathrm{SU}(2) \end{aligned} \tag{2.3.13}$$

where L are SU(2) generators and we require $-\pi < \Theta^{\mathfrak{i}}_{ab} \leq \pi$. We then call $\Theta^{\mathfrak{i}}_{ab}$ the dihedral angle. As $\mathbf{v}_{ab}(\mathfrak{i}) = -\mathbf{v}_{ba}(\mathfrak{i})$ this definition clearly implies $\Theta^{\mathfrak{i}}_{ab} = \Theta^{\mathfrak{i}}_{ba}$. If we have a surface defining a convex subspace of $\mathbb{R}^3$ this definition reduces to the usual definition up to a global sign.

For handlebodies with $g > 0$, the immersed surface will have a boundary given by a collection of circles. We define the dihedral rotation at these edges to be such

$$\hat{h}_i \mathcal{N}_b = \hat{D}_{ab} \mathcal{N}_a$$

and

$$-\hat{h}_i \mathbf{v}_{ba}(\mathfrak{i}) = \mathbf{v}_{ab}(\mathfrak{i}) = \hat{D}_{ab} \mathbf{v}_{ab}(\mathfrak{i}).$$

i.e., we use the group element $\hat{h}_i$ to move the normal $\mathcal{N}_b$ such that $\mathcal{N}_a$ can be rotated into it. The Regge action of a cut immersion is then given by

$$S_R = \sum k_{ab} \Theta_{ab}$$

with the above definitions of Θ_{ab}

This definition does not depend on the choice of trivialising cut, which we see as follows. Moving the cut will have the effect of rotating the variables on the boundary of the surface by h_i. So $\mathcal{N}_a$ changes to $h_i^{-1}\mathcal{N}_a$ and v_{ab} to $h_i^{-1} v_{ab}$. Thus we have $\mathcal{N}_b = \tilde{D}_{ab} h_i^{-1} \mathcal{N}_a$ and $v_{ab} = \tilde{D}_{ab} h_i^{-1} v_{ab}$. By comparing the equations before and after the move, we have $\tilde{D}_{ab} = h_i^{-1} D_{ab} h_i$. So the dihedral rotation changes only by conjugation and its eigenvalues are unchanged.

By repeating this procedure the cut can be changed to any other standard cut. Thus the Regge action defined here is indeed invariant under moving the cuts. Thus we have $\mathcal{N}_b = \tilde{D}_{ab} h_i^{-1} \mathcal{N}_a$ and $v_{ab} = \tilde{D}_{ab} h_i^{-1} v_{ab}$. Therefore by direct comparison we have $\tilde{D}_{ab} = h_i^{-1} D_{ab} h_i$ and the dihedral rotation changes only by conjugation, its eigenvalues are unchanged.

The Group variables at the Critical Points

We now consider the relation between the SO(3) dihedral rotations and the SU(2) elements that appear in the action. As for the g_{ab}, we must lift the dihedral rotation to an SU(2) element D_{ab}. We will then see that the X_a are a gauge transformation that relates the Regge gluing maps and the dihedral rotation. There is a sign ambiguity arising from the choice of spin lift for the D_{ab} but we will see that the discrete symmetry of the action can be used to compensate for this. We will proceed by first noting that the dihedral rotations can be considered as SO(3) connections before discussing in some detail the lift to SU(2).

Connections: Consider the following diagram which applies to two adjacent triangles that are not on a cutting circle:

$$\begin{array}{ccc} t_a & \xrightarrow{X_a} & \tau_a \\ {\scriptstyle g_{ab}}\downarrow & & \downarrow{\scriptstyle (-1)^{\nu_{ab}} D_{ab}} \\ t_b & \xrightarrow[X_b]{} & \tau_b \end{array} \tag{2.3.14}$$

Here t_a is the boundary triangle at $\mathcal{N}^\perp$ with edge vectors given by $k_{ab}\mathbf{n}_{ab}$ and τ_a is the triangle rotated according to its location in the surface, which according to the geometry lemma 2 has edge vectors given by $\mathbf{v}_{ab}(\mathfrak{i}) = k_{ab}\hat{X}_a\mathbf{n}_{ab}$. The SO(3) action of this diagram immediately commutes, as can be seen by acting on $\mathbf{n}_{ab}$ and $\mathcal{N}$. This implies that the X_a act as gauge transformations relating the SO(3) connections $\hat{D}_{ab}$ and $\hat{g}_{ab}$ away from the circles. To analyse the lift to SU(2) connections we define a sign $(-1)^{\nu_{ab}}$ that makes it commute as SU(2). The discrete sign symmetry $X_a \to \epsilon_a X_a$ of the action can be seen as acting on this sign by $(-1)^{\nu_{ab}} \to \epsilon_a\epsilon_b(-1)^{\nu_{ab}}$.

Now, for two triangles whose common edge is on a cutting circle i, in the same way we have a commuting diagram as

$$\begin{array}{ccc} t_a & \xrightarrow{X_a} & \tau_a \\ {\scriptstyle g_{ab}}\downarrow & & \downarrow{\scriptstyle (-1)^{\nu_{ab}} D_{ab}} \\ t_b & \xrightarrow[h_i X_b]{} & \tau_b \end{array} \tag{2.3.15}$$

and additionally have $(-1)^{\nu_{ab}} \to \epsilon_a\epsilon_b\epsilon_i(-1)^{\nu_{ab}}$. Together these diagrams can be interpreted as saying that $\hat{D}_{ab}$ is indeed a gauge transformation obtained from the connection given by $\hat{g}_{ab}$ away from the cuts and $\hat{g}_{ab}\hat{h}_i$ on the cut.

Spin Lift: Now we will fix the signs emerging from the spin lifts of the dihedral angle by exploring the discrete sign symmetry in h_i and X_a. Recall that the discrete sign freedom of the action $X_a \to \epsilon_a X_a$ emerged from a different choice of spin frame for each triangle. Now, we show that the discrete sign symmetry related to the cuts $h_i \to \epsilon_i h_i$ corresponds to different choices of spin structures for the manifold Σ^3. Then, using the fact that $(-1)^{\nu ab}D_{ab}$ is a gauge transform of the connection g_{ab} we can fix the symmetries by adjusting the spin frames and the spin structure such that $(-1)^{\nu_{ab}} = 1$. Thus we will show that:

Lemma 3. *The signs $(-1)^{\nu_{ab}}$ arising from the spin lift on each face not on the cut obey $(-1)^{\nu_{ab}} = \kappa_{ab} = \kappa_a\kappa_b$ for some $\kappa_a = \pm 1$. The signs for a face on the cut, i.e. $ab \in i \in C$ obey $(-1)^{\nu_{ab}} = \kappa_{ab} = \kappa_a\kappa_b\kappa_i$ where κ_i parametrizes the spin structures of Σ^3.*

Proof. First of all, by (2.3.3) a lift of the dihedral rotations, $\kappa_{ab}D_{ab}$, are just a gauge transformation of the g_{ab}. Now recall that $\hat{g}_{ab} \in \mathrm{SO}(3)$ are parallel translations on the boundary triangles according to the Levi-Civita connection of the associated metric, with g_{ab} being the parallel translation of the respective spin connection (a lift of $\hat{g}_{ab}$ to SU(2)).

But when the geometry around a vertex is continuously deformed to the flat geometry, the g_{ab} holonomy of a trivial cycle around said vertex has to go to the identity rotation,

as opposed to a 2π rotation. This implies that for the holonomy around a vertex through triangles a, b and c (which of course consists of a trivial cycle), we have

$$\kappa_{ca}\kappa_{bc}\kappa_{ab}D_{ca}D_{bc}D_{ab} = \kappa_{ca}\kappa_{bc}\kappa_{ab} = 1$$

which implies that locally we must have $\kappa_{ab} = \kappa_a\kappa_b$. The problem now is that if there are non-trivial cycles, i.e. $g \neq 0$, we may not be able to extend this globally, i.e. κ_{ab} may not be globally pure gauge.

In other words, for trivial cycles the lift of the holonomy given by the $\kappa_{ab}D_{ab}$ is fixed to be the same as that given by D_{ab}. But not so for the holonomy of a non-trivial cycle; there exist inequivalent spin structures on a manifold. These have a one-to-one correspondence with the elements of $H_1(\Sigma^3, \mathbb{Z}_2)$, and so are 2^g in number. Hence for a non-trivial cycle, dual to the sequence of triangles $\Delta_{a_0}\cdots\Delta_{a_n}\Delta_{a_0}$ crossing the circle $i \in C$, we have

$$\kappa_{a_n a_0}\kappa_{a_{n-1}a_n}\cdots\kappa_{a_0 a_1}D_{a_n a_0}D_{a_{n-1}a_n}\cdots D_{a_0 a_1} = \kappa_i D_{a_n a_0}D_{a_{n-1}a_n}\cdots D_{a_0 a_1} \tag{2.3.16}$$

where a κ_i is introduced whenever there is an implicit choice of spin structure; i.e. it parametrizes the different spin structures associated with the cut.

We reconcile this case with the $g = 0$ one by keeping the form $\kappa_{ab} = \kappa_a\kappa_b$ for all the edges ab that do not lie on a circle, i.e. $ab \notin i$ for any $i \in C$. Then by (2.3.16) immediately we must have for $ab \in i$, $\kappa_{ab} = \kappa_i\kappa_a\kappa_b$. Since our chosen basis for $H_1(\Sigma^3, \mathbb{Z}_2)$ generates all cycles, we can see that this form of κ_{ab} has all the right properties demanded by our equations and accounts for the different spin structures.

Therefore, taking advantage of the discrete sign symmetry, we can choose the spin structure to be compatible with the one chosen for the lift of g_{ab} and thus we will have $(-1)^{\nu_{ab}} \to \epsilon_i\epsilon_a\epsilon_b(-1)^{\nu_{ab}}$ makes $(-1)^{\nu_{ab}} = 1$. $\square$.

The Action at the Critical Points

We can now easily evaluate the action at the critical points. We evaluate at the symmetry related critical point at which $(-1)^{\nu_{ab}} = 1$. By equation (2.3.13) we have that

$$(X_a(\mathfrak{i}))^{-1}D_{ab}X_a(\mathfrak{i}) = \exp\left(\Theta^{\mathfrak{i}}_{ab}\,\mathbf{n}_{ab}.L\right) \tag{2.3.17}$$

Acting with X_a^{-1} by the left of the commuting diagram equations, using the notation $X_{ab}(\mathfrak{i}) = (X_a(\mathfrak{i}))^{-1}X_b(\mathfrak{i})$ if not on a circle and $X_{ab}(\mathfrak{i}) = (X_a(\mathfrak{i}))^{-1}h_iX_b(\mathfrak{i})$ if on, we get

$$X_{ab}(\mathfrak{i})g_{ab} = (X_a(\mathfrak{i}))^{-1}D_{ab}X_a(\mathfrak{i}) = \exp\left(\Theta_{ab}\,(\mathbf{n}_{ab}.L\right) \tag{2.3.18}$$

where we have used (2.3.17).

It is now straightforward to evaluate the matrix elements in the amplitude. Now consider the matrix elements $\langle -\mathbf{n}_{ab}| X_{ab} |\mathbf{n}_{ba}\rangle$ appearing in the action. Using the gluing condition this becomes $\langle -\mathbf{n}_{ab}| X_{ab} g_{ab} |-\mathbf{n}_{ab}\rangle$. Finally, by (2.3.18) this is just $e^{\frac{i}{2}\Theta^{\mathfrak{i}}_{ab}}$. Thus we have overall that:

$$\langle -\mathbf{n}_{ab}| X_{ab} |\mathbf{n}_{ba}\rangle = e^{\frac{i}{2}\Theta^{\mathfrak{i}}_{ab}} \tag{2.3.19}$$

Finally, we obtain that the action evaluated at the critical points is (i times) the Regge action for the immersed surface $\mathfrak{i}$.

$$S = i \sum_{ab\in\mathcal{E}} k_{ab}\Theta^{\mathfrak{i}}_{ab} \tag{2.3.20}$$

For the flexible immersions, the action is the same for all points on the critical manifold so we evaluate it on an arbitrary immersion in the flexifold.

Parity Note that for every cut immersion $\mathfrak{i}$, the parity related immersion $P\mathfrak{i}$ will also appear in the asymptotic formula. Parity is an element of O(3) such that $P : \mathbf{n} \to -\mathbf{n}$. Acting with an element of SO(3) on all of the edges does not change anything, in fact this is the continuous symmetry that we fixed earlier, but parity will change the sign of the dihedral angle. The two equations defining D_{ab} are invariant under parity, and the dihedral rotation is unchanged. Thus by the definition of the dihedral angle we have

$$D_{ab} = \exp\left(\Theta^{\mathfrak{i}}_{ab}\,(-\frac{\mathbf{v}_{ab}}{|\mathbf{v}_{ab}|}(P\sigma)).L\right)$$

and so $\Theta^{P\mathfrak{i}}_{ab} = -\Theta^{\mathfrak{i}}_{ab}$.

Thus after fixing the continuous symmetry we will obtain two solutions who's actions are the complex conjugate of each other.

2.3.4 Hessian

The stationary phase formula requires us to calculate the Hessian of the action S to determine the weights with which the stationary points contribute to the action. This will be a $3(|\mathcal{V}| + |C|) \times 3(|\mathcal{V}| + |C|)$ matrix defined by

$$H = \begin{pmatrix} H_{XX} & H_{Xh} \\ H_{hX} & H_{hh} \end{pmatrix}. \tag{2.3.21}$$

Where

$$\begin{aligned} (H_{XX})^{ij}_{cd} &= \left(\frac{\partial^2 S}{\partial X^i_c \partial X^j_d}\right), \qquad (H_{hX})^{ij}_{pd} = \left(\frac{\partial^2 S}{\partial h^i_p \partial X^j_d}\right), \\ (H_{Xh})^{ij}_{cq} &= \left(\frac{\partial^2 S}{\partial X^i_c \partial h^j_q}\right), \qquad (H_{hh})^{ij}_{pq} = \left(\frac{\partial^2 S}{\partial h^i_p \partial h^j_q}\right). \end{aligned} \tag{2.3.22}$$

The global SU(2) symmetry of the action implies that there is a redundant integration in I. This will cause the determinant of the Hessian to be zero unless it is gauge fixed. To solve this, we make the change of variables $X_a \to X_b X_a$ for some $b \in \{1, ..., |\mathcal{V}|\}$. This has the effect of removing the X_b variables and the integral gives a volume of SU(2) which can be normalised to one as it is compact. The remaining Hessian is now a $3(|\mathcal{V}| + |C| - 1) \times 3(|\mathcal{V}| + |C| - 1)$ matrix. The submatrix H_{XX} at the critical points, is given by

$$\left(\frac{\partial^2 S}{\partial X_c^i \partial X_c^j}\right)\Bigg|_{\delta S=0, \mathrm{Re} S=0} = \frac{1}{2} \sum_{b\neq c, bc\in E} k_{cb} \left(\delta^{ij} - n'^i_{cb} n'^j_{cb}\right) \tag{2.3.23}$$

for the diagonal terms. The off diagonal part is

$$\begin{aligned}\left(\frac{\partial^2 S}{\partial X_c^i \partial X_d^j}\right)\Bigg|_{\substack{\delta S=0\\ \mathrm{Re} S=0}} &= -\frac{1}{2}\sum_E (\delta_{c\ s(E)}\delta_{d\ t(E)} + \delta_{d\ s(E)}\delta_{c\ t(E)}) \\ &\quad \times \left(\delta^{ij} - i\epsilon^{ijk} n^k_{s(E)t(E)} - n'^i_{s(E)t(E)} n'^j_{s(E)t(E)}\right). \end{aligned} \tag{2.3.24}$$

So one can see that only the off-diagonal elements that represent two neighbouring triangles are non zero. The (H_{hh}) submatrix will be diagonal since each term in the action only contains one h_p term (ie, each dual edge only crosses one cut.)

$$\left(\frac{\partial^2 S}{\partial h_p^i \partial h_p^j}\right)\Bigg|_{\delta S=0, \mathrm{Re} S=0} = \frac{1}{2} \sum_{b\neq c, bc\in C_p} k_{cb} \left(\delta^{ij} - n'^i_{cb} n'^j_{cb}\right) \tag{2.3.25}$$

The mixed terms H_{Xh}, H_{Xh} will be non zero only for triangles with an edge on the cut

$$\left(\frac{\partial^2 S}{\partial X_c^i \partial h_q^j}\right)\Bigg|_{\substack{\delta S=0\\ \mathrm{Re} S=0}} = -\frac{1}{2} \sum_{\substack{ab\in \mathcal{E}_q\\ c=a,b}} k_{ab} \left(\delta^{ij} - i\epsilon^{ijk} n^k_{ab} - n'^i_{ab} n'^j_{ab}\right) \tag{2.3.26}$$

Note that

$$(X_a(\mathfrak{i}))^{-1} D_{ab} X_a(\mathfrak{i}) = \exp\left(-\Theta^{\mathfrak{i}}_{ab}\left(\mathbf{n}_{ab}(\mathfrak{i})\right).L\right)^{-1} = \left((X_a(P\mathfrak{i}))^{-1} D_{ab} X_a(P\mathfrak{i})\right)^{-1} \tag{2.3.27}$$

where we used that $D_{ab} = \exp\left(\Theta^{\mathfrak{i}}_{ab}\left(-\frac{\mathbf{v}_{ab}(P\mathfrak{i})}{|\mathbf{v}_{ab}(P\mathfrak{i})|}\right).L\right)$ on the second equality. By (2.3.18) we then have $(X_{ab}(\mathfrak{i}) g_{ab}) = (X_{ab}(P\mathfrak{i}) g_{ab})^{-1}$, so if we replace the $X_{ab}(\mathfrak{i})$ in $\langle -\mathbf{n}_{ab}| X_{ab}(\mathfrak{i}) |\mathbf{n}_{ba}\rangle$ with the parity related one we now obtain the complex conjugate:

$$\begin{aligned}\langle -\mathbf{n}_{ab}| X_{ab}(\mathfrak{i}) g_{ab} |-\mathbf{n}_{ab}\rangle &= \langle -\mathbf{n}_{ab}| \left(X_{ab}(P\mathfrak{i}) g_{ab}\right)^{-1} |-\mathbf{n}_{ab}\rangle \\ &= \overline{\langle -\mathbf{n}_{ab}| X_{ab}(P\mathfrak{i}) g_{ab} |-\mathbf{n}_{ab}\rangle} \\ &= \overline{\langle -\mathbf{n}_{ab}| X_{ab}(P\mathfrak{i}) |\mathbf{n}_{ba}\rangle} \end{aligned} \tag{2.3.28}$$

Thus we can see that the action of parity on the Hessian matrix will also result in complex conjugation when evaluated at the critical points.

2.3.5 Proof of the formula

We can now evaluate the stationary phase approximation to the amplitude $\mathcal{Z}_{PR}(\Psi_\lambda, \Sigma^3)$ defined in (2.1.14). First we fix the symmetries of the action. This is done by dropping the group integration at an arbitrary vertex. We have seen that the critical point equations describe cut immersions of the boundary data in $\mathbb{R}^3$ and if the cut immersion is rigid, i.e. in $\mathfrak{I}_r$, then the critical points are isolated.

For the isolated critical points we can explicitly evaluate the stationary phase approximation. Having fixed one group integration we are left with a $3(|\mathcal{V}| + |C| - 1)$ dimensional integration. The overall scaling of these points is thus $\left(\frac{2\pi}{\lambda}\right)^{3(|\mathcal{V}|+|C|-1)/2}$. Further we obtain a set of $2^{3(|\mathcal{V}|+|C|-1)}$ critical points for each immersion from the spin lift of each SU(2). Finally the derivatives in the Hessian as defined above are taken with respect to a parametrization of SU(2) with volume $(4\pi)^2$, so we need to rescale by this factor. Using equation (2.3.19) and lemma 3 we have seen that the amplitude itself evaluates to the Regge action of the cut immersion:

$$\ln \langle -\mathbf{n}_{ab}| X_{ab} |\mathbf{n}_{ba}\rangle^{2k_{ab}} = ik_{ab}\Theta^{\mathfrak{i}}_{ab}.$$

Taking all these factors together we can approximate the contributions of the isolated critical points to the partition function as:

$$\begin{aligned}
\mathcal{Z}_{PR}(\Psi_\lambda, \Sigma^3) &= (-1)^\chi \left(\frac{2\pi}{\lambda}\right)^{\frac{3(|\mathcal{V}|+|C|-1)}{2}} \left(\frac{2}{(4\pi)^2}\right)^{\frac{3(|\mathcal{V}|+|C|-1)}{2}} \\
&\times \left[\sum_{\mathfrak{i}\in\mathfrak{I}_r} \frac{1}{\sqrt{\det H_{\mathfrak{i}}}} \exp\left(i\lambda \sum_{ab\in\mathcal{E}} k_{ab}\Theta^{\mathfrak{i}}_{ab}\right) + \frac{1}{\sqrt{\det H_{\mathfrak{i}}}} \exp\left(-i\lambda \sum_{ab\in E} k_{ab}\Theta^{\mathfrak{i}}_{ab}\right)\right] \\
&+ O\left(\left(\frac{1}{\lambda}\right)^{\frac{3(|\mathcal{V}|+|C|-1)}{2}+1}\right)
\end{aligned} \tag{2.3.29}$$

Since parity complex conjugates the action and since the Hessian matrix changes to its complex conjugate with parity, we can absorb the phase of the determinant into the exponentials and combine the terms from the immersion $\mathfrak{i}$ and the parity related immersion $P\mathfrak{i}$ into a cosine.

$$\begin{aligned}
\mathcal{Z}_{PR}(\Psi_\lambda, \Sigma^3) &= 2(-1)^\chi \left(\frac{1}{4\pi\lambda}\right)^{\frac{3(|\mathcal{V}|+|C|-1)}{2}} \\
&\times \sum_{\mathfrak{i}\in\mathfrak{I}_r} \frac{1}{\sqrt{|\det H_{\mathfrak{i}}|}} \cos\left(i\lambda \sum_{ab\in\mathcal{E}} k_{ab}\Theta^{\mathfrak{i}}_{ab} - \frac{1}{2}\mathrm{Arg}(\det H_{\mathfrak{i}})\right) \\
&+ O\left(\left(\frac{1}{\lambda}\right)^{\frac{3(|\mathcal{V}|+|C|-1)}{2}+1}\right),
\end{aligned} \tag{2.3.30}$$

where $\Theta^{\mathfrak{i}}_{ab}$ is the dihedral angle of the edge ab in the cut immersion $\mathfrak{i} \in \mathfrak{I}_r$.

If there are any flexible immersions of the boundary data then there will be a manifold of critical points. By definition the action must have the same value on every point of the critical manifold. The Hessian therefore has zero modes along the directions of the flexifold and we must treat the integral as having further symmetries in the neighbourhood of the flexifold. The generalised stationary phase formula in the appendix takes care of this and changes the scaling of the contribution of these critical points by $\lambda^{d_{\max}/2}$, where $d_{\max}$ is the dimension of the flexifold. Therefore these immersions dominate the rigid immersions if they exist, their contribution is given by:

$$\begin{aligned}\mathcal{Z}_{PR}(\Psi_\lambda, \Sigma^3) &= (-1)^\chi \left(\frac{2\pi}{\lambda}\right)^{\frac{3(|\mathcal{V}|+|C|-1)-d_{\max}}{2}} \left(\frac{2}{(4\pi)^2}\right)^{\frac{3(|\mathcal{V}|+|C|-1)-d_{\max}}{2}} \\ &\quad \times \left[\sum_{\mathfrak{f}\in\mathfrak{F}_{\max}} L^{\mathfrak{f}} \exp\left(i\lambda \sum_{ab\in\mathcal{E}} k_{ab}\Theta^{\mathfrak{f}}_{ab}\right) + \overline{L^{\mathfrak{f}}} \exp\left(-i\lambda \sum_{ab\in\mathcal{E}} k_{ab}\Theta^{\mathfrak{f}}_{ab}\right)\right] \\ &\quad + O\left(\left(\frac{1}{\lambda}\right)^{\frac{3(|\mathcal{V}|+|C|-1)-d_{\max}}{2}+1}\right) \end{aligned} \tag{2.3.31}$$

$\Theta^{\mathfrak{f}}_{ab}$ is the dihedral angle of the edge ab of a particular cut immersion $\mathfrak{i}$ in the flexifold $\mathfrak{f}$. As the action is constant along the flexifold it does not matter where we evaluate it. $L^{\mathfrak{f}}$ is given by

$$L^{\mathfrak{f}} = \int_{\mathcal{C}_{\mathfrak{f}}} d\sigma_{\mathcal{C}_{\mathfrak{f}}}(y) \frac{a(y)}{\sqrt{\det H^{\top}_{\mathfrak{f}}(y)}} \tag{2.3.32}$$

where $H^{\top}_{\mathfrak{f}}$ is the Hessian matrix for the transverse directions which we can not give a general formula for. Combining the exponentials into cosines as above we obtain part one of the main theorem.

Finally, if no immersions of the boundary data exist then there are no solutions to the critical point equations and the stationary phase formula gives that the amplitude is suppressed. □

2.4 Example: The Tetrahedron

Here we apply the above results to the well known case of the asymptotics of the amplitude for a single tetrahedron which, with an appropriate choice of normalisation for the boundary intertwiners, will correspond to the 6j symbol. This is a special case of theorem 2.2 so the proof is the same as above. In particular, the critical and stationary point equations are the same and the action evaluated at these points reduces to the Regge action for a tetrahedron. Since the asymptotic formula for the tetrahedron is already known, we must

verify that our formula agrees with this result. This also provides further evidence that the asymptotic formula for the 4d case derived using the same methods in [29] is correct. We begin by noting that, up to parity, the boundary data of a tetrahedron has only one immersion so the sum in the asymptotic formula disappears.

2.4.1 Normalisation and scaling behaviour

We can now compare our theorem with the Ponzano-Regge asymptotic formula for the 6j symbol. The Ponzano-Regge formula is

$$\left\{ \begin{array}{ccc} \lambda k_{12} & \lambda k_{13} & \lambda k_{14} \\ \lambda k_{23} & \lambda k_{24} & \lambda k_{34} \end{array} \right\} \rightarrow \frac{1}{\sqrt{12\pi \mathrm{Vol}}} \cos\left(\sum_{a<b} (\lambda k_{ab} + \frac{1}{2})\Theta_{ab} + \frac{\pi}{4} \right) \tag{2.4.1}$$

where Vol is the volume of a geometric tetrahedron with edge lengths $\lambda k_{ab} + \frac{1}{2}$ and Θ_{ab} are the dihedral angles. Note that the formula scales as $\lambda^{-3/2}$ due to the volume term. Currently, our formula for the tetrahedron contains the Regge action but the amplitude, phase term and scaling do not obviously agree with (2.4.1). We will first consider the intertwiner normalisation, which will be necessary to obtain the correct scaling behaviour and some numerical factors, and then evaluate the Hessian numerically to check the agreement of the remaining terms. The main drawback of the coherent state approach occurs here as it is very difficult to obtain an analytic formula for the determinant of the Hessian matrix.

Intertwiner normalisation

For the 6j symbol, the three valent intertwiners are normalised by dividing by the square root of the theta spin network. The coherent intertwiners that we replaced these with, however, are not normalised.

The normalisation of the coherent intertwiner is given in terms of the three edge vectors of the triangle $\mathbf{n}_1, \mathbf{n}_2, \mathbf{n}_3$ by the Hermitian inner product

$$\begin{aligned} f_\Delta(\mathbf{n}_i, k_i) &= \int_{\mathrm{SU}(2)} dX \prod_{i=1}^{3} \langle \mathbf{n}_i, k_i | X | \mathbf{n}_i, k_i \rangle \\ &= \int_{\mathrm{SU}(2)} dX \exp S_\Delta \end{aligned} \tag{2.4.2}$$

where

$$S_\Delta = \sum_{i=1}^{3} 2k_i \ln \langle \mathbf{n}_i | X | \mathbf{n}_i \rangle. \tag{2.4.3}$$

This integral can be calculated exactly using [9, 28], the result being

$$f_\Delta = \frac{(1 - \mathbf{n}_1.\mathbf{n}_2)^p (1 - \mathbf{n}_1.\mathbf{n}_2)^q (1 - \mathbf{n}_1.\mathbf{n}_2)^r (p+q)!(q+r)!(p+r)!}{2^{p+q+r}(p+q+r+1)!p!q!r!}. \tag{2.4.4}$$

Where $p = k_1 + k_2 - k_3$, $q = k_2 + k_3 - k_1$ and $r = k_1 + k_3 - k_2$.

The asymptotics of this intertwiner normalisation can also be found using stationary phase [27]. The stationarity of the action S_Δ gives the closure condition and the action evaluated on the critical points $\pm I$ gives zero.

$$\begin{aligned} f_\Delta(\mathbf{n}_i, \lambda k_i) &\sim \left(\frac{2\pi}{\lambda}\right)^{3/2} \frac{2}{(4\pi)^2} \frac{1}{\sqrt{\det H_\Delta}} \\ &= \frac{1}{\sqrt{2^3 \pi \lambda^3 \det H_\Delta}} \end{aligned} \tag{2.4.5}$$

The additional factor 2 comes from the fact that both I and $-I$ are critical points that give the same contribution to the action. H_Δ is the Hessian matrix of the action which is given by

$$\begin{aligned} H_\Delta^{ij} &= \frac{\partial^2 S_\Delta}{\partial X^i \partial X^j} \\ &= \frac{1}{2} \sum_l k_l (\delta^{ij} - n_l^i n_l^j) \end{aligned} \tag{2.4.6}$$

We can now normalise our formula such that it agrees with the standard normalisation by dividing by a factor $(f_{\Delta_a})^{1/2}$ for each triangle a.

Numerical calculations

With the intertwiner normalisations included in the asymptotic formula, we obtain

$$\begin{aligned} \left\{ \begin{array}{ccc} \lambda k_{12} & \lambda k_{13} & \lambda k_{14} \\ \lambda k_{23} & \lambda k_{24} & \lambda k_{34} \end{array} \right\} &= \frac{\mathcal{Z}_{PR}(\Psi_\lambda, \sigma)}{\prod_{p=1}^4 \sqrt{f_{\Delta_p}}} \\ &= \left(\frac{2\pi}{\lambda}\right)^{9/2} \frac{2^4}{((4\pi)^2)^3 \sqrt{|\det H|}} \frac{1}{\prod_{p=1}^4 \sqrt{f_{\Delta_p}}} \\ &\quad \times \cos\left(\sum_{a<b} \lambda k_{ab} \Theta_{ab} - \frac{1}{2} \mathrm{Arg}(\det H) \right) \end{aligned} \tag{2.4.7}$$

Note that we have the correct scaling behaviour once the additional scaling factors from the intertwiners are included. The normalisation terms are real so do not contribute any additional phase.

The formula for the equilateral tetrahedron with both the exact and approximate intertwiner normalisation was compared to the 6j symbol and the Ponzano-Regge asymptotic formula using Mathematica in Figure 2.2. We see that our formula differs from the Ponzano Regge formula for low spins. The only point where our formula differs from Ponzano Regge is in the fact that the Ponzano Regge asymptotics are given in terms of the dihedral angles and volume of the tetrahedron with edge lengths $\lambda k_{ab} + \frac{1}{2}$. Therefore the dihedral

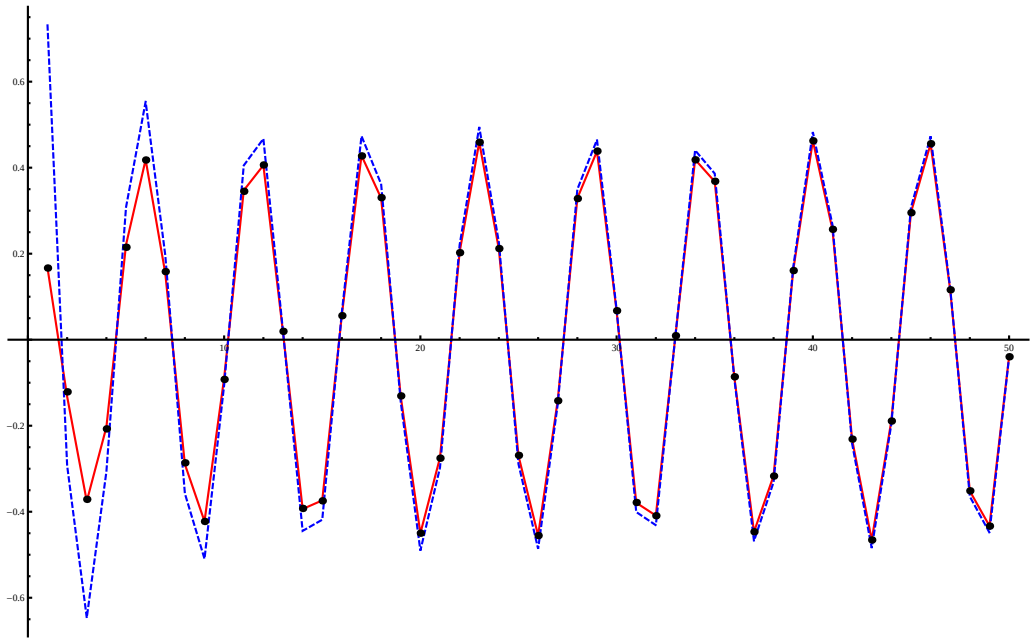

Figure 2.2: Comparison of the 6j symbol (dots), the PR formula (red line) and equation (2.4.7) (blue dashed line) against the scaling λ. The scaling factor $\lambda^{-3/2}$ has been removed to make the comparison easier at low spins.

angles and volume change nontrivially with λ. A stationary phase approximation extracts only the scaling behaviour with respect to lambda in the asymptotic regime and cannot register this type of low spin behaviour. This agrees as well as the PR formula for larger spins, however the agreement for very low values is not as good - Figure 2.2.

2.5 Example: Steffen's flexible polyhedron

Here we discuss an example for which the second part of theorem 2.2 is relevant, that is we describe a set of boundary data that admits a flexible immersion. This particular example is taken from a flexible polyhedron with half integer edge lengths consisting of fourteen boundary triangles which was found by K. Steffen [31]. A net for constructing this polyhedron is given in Figure 2.3 and the corresponding spin network in Figure 2.4. Since Steffen's polyhedron admits a flex in one direction, we know that the flexifold is at least one dimensional. As a polyhedron, it is not allowed to self intersect but there may be other immersions with flexibility in more than one dimension. Applying the asymptotic formula with the same intertwiner normalisation as the tetrahedron in section 2.4, we would expect the scaling to be $\lambda^{-17/2}$.

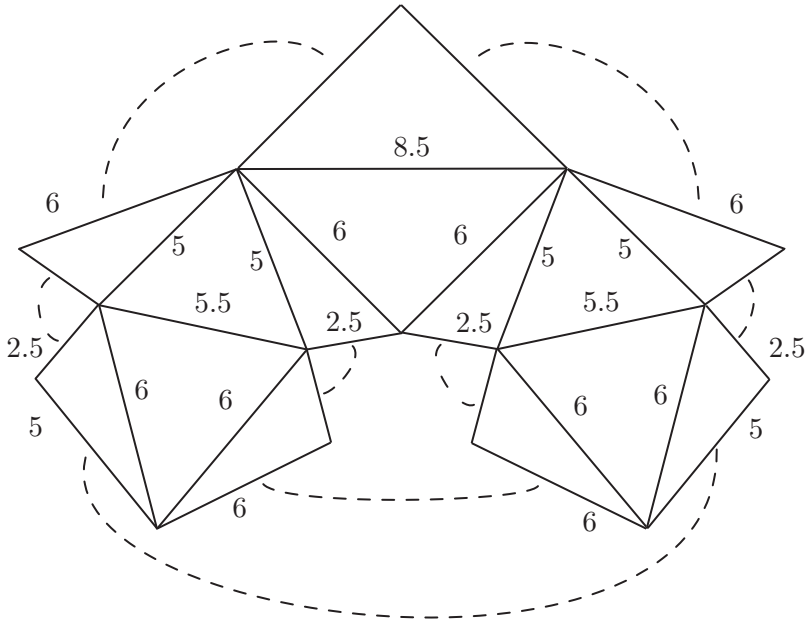

Figure 2.3: A net showing a set of boundary data that reconstructs Steffen's flexible polyhedron.

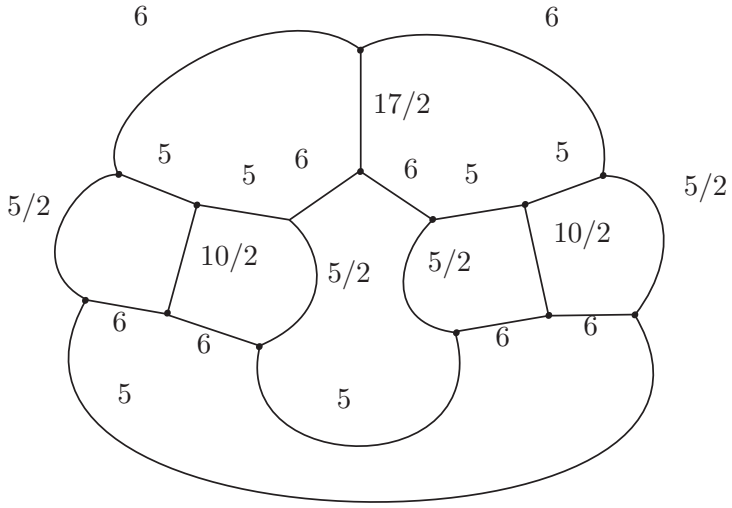

Figure 2.4: The spin network corresponding to Steffen's flexible polyhedron.

2.6 Discussion and Conclusions

2.6.1 Rigidity of cut immersions

We have seen that if the boundary data allows for a flexible immersion then this immersion will dominate in the large λ limit. Ideally, we would like to know if flexible immersions exist just by looking at the boundary data. Unfortunately, knowing whether or not a polyhedron is rigid or flexible is a difficult and still unsolved problem. It is known that convex polyhedra are rigid but this does not cover the immersions that are obtained here. In particular, Steffen's polyhedron is non-convex.

If the boundary data is topologically $\mathcal{S}^2$ then a theorem by Steinitz [32] applies that states that any simplicial complex with underlying space homeomorphic to a 2-sphere admits a simplexwise linear embedding into $\mathbb{R}^3$ whose image is strictly convex. This embedding will indeed be rigid and we can conclude that for the ball $\mathfrak{I}_r$ will always be non-empty.

There are other results on the rigidity of bar frameworks, a graph embedded in Euclidean space with fixed linear edges, but these results do not help here.

2.6.2 Surface immersions vs interior immersions

With the asymptotic analysis performed above, we explicitly obtain a sum over immersions of the boundary data weighted by the cosine of the Regge action for the immersed surface. Previously, asymptotics of the Ponzano-Regge model for larger triangulations could only be considered by taking the product of the asymptotic formula for each 6j symbol. We now illustrate schematically that, in a simple example, that this is in fact equivalent to the asymptotic formula above.

We will consider the case of two tetrahedra σ_1, σ_2 glued along a common triangle Δ and use the boundary normalisation that agrees with the 6j symbol. The partition function then reads

$$\mathcal{Z}_{PR}(\Psi_\lambda, \sigma_1 \cup_\Delta \sigma_2) = \begin{Bmatrix} \lambda k_1 & \lambda k_2 & \lambda k_3 \\ \lambda k_4 & \lambda k_5 & \lambda k_6 \end{Bmatrix} \begin{Bmatrix} \lambda k_1 & \lambda k_2 & \lambda k_3 \\ \lambda k_7 & \lambda k_8 & \lambda k_9 \end{Bmatrix} \tag{2.6.1}$$

We write the asymptotic formula for the 6j in terms of the Regge action S_σ for a tetrahedron σ

$$\begin{Bmatrix} \lambda k_1 & \lambda k_2 & \lambda k_3 \\ \lambda k_4 & \lambda k_5 & \lambda k_6 \end{Bmatrix} = N \left(\exp(i\lambda S_\sigma) + \exp(-i\lambda S_\sigma) \right) \tag{2.6.2}$$

Where several of the factors have been absorbed into the amplitude N. Asymptotically,

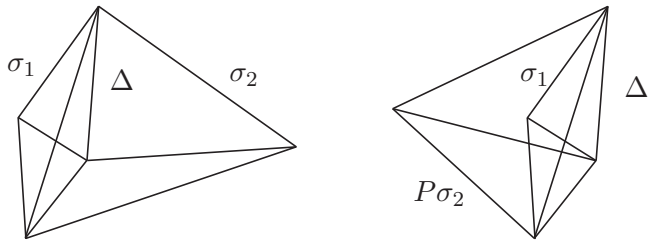

Figure 2.5: Two different possible immersions of the boundary data for two tetrahedra σ_1, σ_2 glued on a common triangle Δ.

this gives

$$\begin{aligned} \mathcal{Z}_{PR}(\Psi_\lambda, \sigma_1 \cup_\Delta \sigma_2) &= N_1 N_2 \left(\exp(i\lambda(S_{\sigma_1} + S_{\sigma_2})) + \exp(-i\lambda(S_{\sigma_1} + S_{\sigma_2})\right) \\ &\quad + N_1 N_2 \left(\exp(i\lambda(S_{\sigma_1} - S_{\sigma_2})) + \exp(-i\lambda(S_{\sigma_1} - S_{\sigma_2})\right) \\ &= N_1 N_2 \exp(\sum_{e\subset\Delta} k_e \pi) \left(\cos\left(\lambda(S_{\sigma_1 \cup_t \sigma_2}\right) + \cos\left(\lambda(S_{\sigma_1 \cup_\Delta P\sigma_2}\right)\right) \end{aligned} \tag{2.6.3}$$

Where $P\sigma$ is the parity related tetrahedron and we have used the fact that the Regge action for two tetrahedra becomes

$$S_{\sigma_1} + S_{\sigma_1} = S_{\sigma_1 \cup_\Delta \sigma_2} + \sum_{e\subset\Delta} k_e \pi. \tag{2.6.4}$$

Thus the formula gives a sum over the two different ways of immersing the boundary triangles in $\mathbb{R}^3$, see Figure 2.5 .

2.6.3 Boundary states

We also note that it is possible to select a particular immersion in the sum by choosing a boundary state peaked around a particular set of dihedral angles, see for example [33–35]. This boundary state also selects one overall orientation of the immersion which removes the parity related term in the asymptotic formula. For non-rigid immersions, the boundary state would also have the ability to select a particular configuration of the immersed surface which would stop these immersions dominating the integral.

2.6.4 Conclusions

In this chapter we addressed the problem of asymptotics of larger triangulations for the Ponzano-Regge model. We introduced coherent intertwiners and used the expression of the partition function as a spin network dual to the boundary triangulation. We applied the stationary phase approximation and found that the dominant contribution to the

asymptotics came from immersions of the boundary data in $\mathbb{R}^3$. This gives a concrete realisation of the suggestion of Ponzano and Regge that more than one geometry should contribute to the asymptotics of 3n-j symbols for larger values of n.

Interestingly, and unexpectedly, we found that spin networks contain some information about the rigidity properties of surfaces. The scaling properties of a spin network depend on how many directions the associated immersions can flex in. This aspect warrants further investigation.

The analysis presented here covered a large class of three manifolds but not all possible examples. In fact all closed orientable three manifolds may be decomposed into handle-bodies using a Heegard splitting. It would be interesting to investigate whether this fact can be used to determine the asymptotic contribution to the Ponzano-Regge model for this larger class of manifolds.

Finally, it would also be interesting to extend this analysis to the Turaev-Viro model where one would expect immersions in the space of constant positive curvature to be dominant.

Chapter 3

Fermions in 3d spin foam models

Previous chapters have focussed on spin foam models for pure gravity. However, if we are to make any useful predictions from a quantum theory of gravity, we will likely have to consider gravity coupled to matter. The work in this chapter involves the continued study and computation of observables in a model for 3d gravity coupled to fermions [36]. This approach extends the lattice BF theory derivation to include fermion fields at the dual vertices as in standard lattice gauge theory. The usual spin foam techniques can then be applied. The research in this chapter is contained in [D].

Other proposals for coupling matter in 3d spin foam models are the following. In [37], spinning particles are inserted on to the edges of the spin foam. This creates a non-zero deficit angle in the holonomy around the edge and in an appropriate limit this can be related to Feynman diagrams on non-commutative spacetime. Yang-Mills theory was coupled to 3d quantum gravity in [38], but due to the nature of the coupling the model contained an inverse volume operator which was difficult to implement in the spin foam formalism. One might expect the scalar field to be the natural starting point for the coupling of matter, however the relevant action contains an inverse frame field and, since the non-degeneracy condition is not imposed, it is not clear if it is well defined. An attempt based on a conformally equivalent action is given in [39].

In four dimensions there has been less success. The coupling of fermions is difficult to extend to this case as current 4d spin foam models are constructed using 2-forms and fermions couple to an odd power of the frame field (see discussion.) The natural extension of the particle coupling is to use extended matter, or strings [40].

In this chapter, we will discuss the classical and discrete coupling of fermions to gravity, we will then write a path integral and perform each of the integrals in order to obtain a spin foam model for various observables, such as the two point function. We then compute some examples.

3.1 Classical theory

We begin with a brief summary of the relevant continuum theory. The first order formalism described in chapter 1 must be used in order to couple fermions to 3d gravity. Our spacetime will be a connected, oriented, compact, three dimensional differential manifold M endowed with a Euclidean metric. In 3+0 dimensions, fermions are described by two component spinors ψ and the Hermitian conjugate spinor $\overline{\psi}$. The action is given by [36, 41]

$$\begin{aligned} S_F[e,w,\psi,\overline{\psi}] &= S[e,w] + \int_M \epsilon_{IJK} e^I \wedge e^J \wedge \overline{\psi}\sigma^K \nabla\psi - \epsilon_{IJK} e^I \wedge e^J \wedge \nabla\overline{\psi}\sigma^K\psi \\ &+ m\epsilon_{IJK} e^I \wedge e^J \wedge e^K \overline{\psi}\psi \end{aligned} \tag{3.1.1}$$

With the covariant derivative given by $\nabla\psi = (\partial_\mu\psi + w_\mu\psi)dx^\mu$ and m the bare mass parameter. Note that, unlike the Dirac action in flat space, we must include the Hermitian conjugate term in the action. In flat space, the Hermitian conjugate term can be removed by integrating by parts and dropping a boundary term. The first equation of motion is

$$d_w e = -\frac{\kappa}{4}\epsilon^I{}_{JK} e^J \wedge e^K \bar{\psi}\psi\sigma_I \tag{3.1.2}$$

which means that the frame field is no longer compatible with the connection and the fermion field has introduced torsion into the spacetime. The second is

$$F(w) = \frac{\kappa}{4}\{\, e^I \wedge (\bar{\psi}\sigma^J\nabla\psi - \nabla\bar{\psi}\sigma^J\psi) - m e^I \wedge e^J \bar{\psi}\psi \,\}\,\sigma_I\sigma_J \tag{3.1.3}$$

which states that the curvature is no longer zero. The classical theory can no longer be considered topological since there are additional degrees of freedom coming from the fermion field. This action still admits the rotational symmetry of pure 3d gravity but the translation symmetry

$$\begin{aligned} e &\rightarrow e + d_w\phi \\ w &\rightarrow w \end{aligned} \tag{3.1.4}$$

is no longer present.

We now will set $m = 0$ and consider massless fermions. As in the pure gravity case, we will proceed to write a discretised version of this action from which we can construct a spin foam model.

3.1.1 Simplicial theory

In order to write a simplicial theory for fermions coupled to gravity, we will need to use a more refined discretisation. We begin with some fixed triangulation Δ but we will subdivide it into the so-called wedges. To construct the wedges, take a dual face f around an edge E and connect the centre of each dual edge e to a point on E

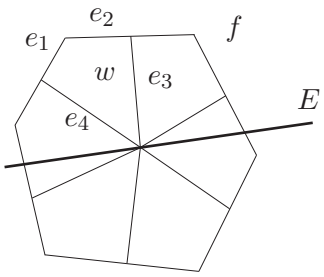

This splits the dual edge into wedges. The purpose of this is that there are six wedges within each tetrahedron, and each wedge is associated to an edge in the frame of a tetrahedron. So there are in fact several wedges associated to the same edge which makes it possible to measure a variable associated to this edge in different frames.

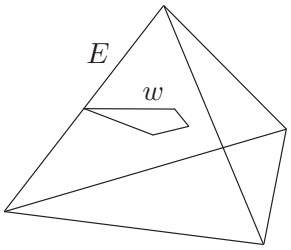

Simplicial fields. The frame field is discretised slightly differently on the derived complex Δ^+. A Lie algebra element is assigned to each wedge w, $\mathbf{e}_w = e^a_w \gamma_a \in \mathfrak{su}(2)$. So the different $\mathbf{e}_w$ around an edge measure the length of the edge in different tetrahedra. $\mathbf{e}_w$ is sometimes called the discretised frame field.

The holonomy variables are also constructed slightly differently on the wedges. We assign an SU(2) element $g_{\overline{e}}$ to each edge $\overline{e}$ of Δ^+. So we will have the holonomies along the half-edges of the original triangulation Δ but we will also have additional holonomies on the new edges in Δ^+

As before, reversing the orientation of an edge maps the associated group element into its inverse : $g_{e^{-1}} = g_e^\dagger$. The holonomy around a wedge w is written $G_w = \prod_{\bar{e}\in\partial w} g_{\bar{e}}$. An obvious starting point for each wedge holonomy is the dual vertex at the centre of the relevant tetrahedron.

We discretise the fermionic fields in a way that is natural from the point of view of lattice gauge theory [42]. Since the holonomies are associated to the dual edges, we must place the fermion fields at the dual vertices. So on each vertex v, there is a spinor ψ_v and its dual $\overline{\psi}_v$

Simplicial action. We can now define the discretised action in terms of these wedge variables. To define the Dirac part of the action, we write a matrix D_e associated to the

dual edges of the triangulation

$$D_e = \Sigma_e U_e - U_e \Sigma_{e^{-1}}, \tag{3.1.5}$$

$U_e := U(g_e)$ is the holonomy along the edge e in the fundamental representation, this will actually be a product of two of the group elements $g_{\overline{e}}$. Σ_e is the discretised version of the $\mathbf{e} \wedge \mathbf{e}$ term that appears in the continuum action. It is given by

$$\Sigma_e = \frac{1}{3} \sum_{w_e, w'_e} \mathbf{e}_{w_e} \mathbf{e}_{w'_e} \operatorname{sgn}(w_e, w'_e), \tag{3.1.6}$$

where the sum runs over all possible pairs of wedges that are in the tetrahedron dual to the vertex $s(e)$ and that meet at the edge e. The factor $\operatorname{sgn}(w_e, w'_e)$ equals ± 1 depending on the sign of the associated (coordinate) area bivector. D_e will be referred to as the Dirac operator. It is not a Dirac operator in the usual sense as it does not contain a lattice derivative, this appears in the action below with a sum over orientations of the dual edges.

We can now write the Dirac action

$$S_{\mathrm{D}}[\mathbf{e}_w, g_e, \overline{\psi}_v, \psi_v] = \frac{1}{8} \sum_{or(e)} \sum_{e} S_e, \tag{3.1.7}$$

where the sum is taken over all orientations $or(e)$ of all edges e of Δ^*, and

$$S_e = (\psi_{s(e)}, D_e \, \psi_{t(e)}), \tag{3.1.8}$$

with $s(e)$ and $t(e)$ respectively denoting label the source and target vertices of the edge e in the corresponding orientation, and the inner product $(,)$ being the standard Hermitian inner product on $\mathbb{C}^2$., i.e., introducing a basis of $\mathbb{C}^2$, $(\xi, \chi) = \overline{\xi}_A \chi^B \delta^A_B$.

The gravitational action is almost the same as that in chapter 1 but defined on the wedges

$$S_{\mathrm{GR}}[\mathbf{e}_w, g_{\bar{e}}] = \frac{1}{16\pi G} \sum_{w} \operatorname{tr}\left(\mathbf{e}_w G_w\right), \tag{3.1.9}$$

where the trace is in the spinor representation.

It was shown in [36] that $S_{\text{GR-D}} = S_{\mathrm{GR}} + S_{\mathrm{D}}$ converges to the continuum action for 3d general relativity coupled to fermions.

Symmetries. The symmetries of the coupled action will be different to the pure gravity case. In particular, since the theory is no longer topological, we only have the SU(2) symmetry at each vertex of Δ

$$\begin{aligned} \mathbf{e}_w &\mapsto k_v^{-1} \, \mathbf{e}_w \, k_v \\ G_w &\mapsto k_v^{-1} \, G_w \, k_v, \end{aligned} \tag{3.1.10}$$

for S_{GR}, and

$$\begin{aligned} g_e &\mapsto k_{s(e)}^{-1}\, g_e\, k_{t(e)} \\ \Sigma_e &\mapsto k_{s(e)}^{-1}\, \Sigma_e\, k_{s(e)} \\ \psi_v &\mapsto k_v^{-1}\psi_v \\ \overline{\psi}_v &\mapsto \overline{\psi}_v\, k_v, \end{aligned} \tag{3.1.11}$$

for S_{D}. In the first two lines, (3.1.10), the transformation acts on the variables assigned to all wedges w containing the vertex v, while the transformation (3.1.11) takes place on all edges e of Δ^*.

We also note a useful property of the Dirac matrix that will be used extensively later [36]

$$D_e^{AB} = -D_{e^{-1}}^{BA}, \tag{3.1.12}$$

where the indices have been raised and lowered with the standard symplectic metric ϵ_{AB} on $\mathbb{C}^2$. Our conventions are the following. The two-dimensional totally antisymmetric tensor is normalised such that $\epsilon_{01} = \epsilon^{01} = +1$, which implies that $\epsilon_{AB}\epsilon^{BC} = -\delta_A^C$. The raising and lowering of indices occurs according to

$$\chi^A = \epsilon^{AB}\chi_B, \text{ and } \xi_A = \xi^B\epsilon_{BA} = -\epsilon_{AB}\xi^B. \tag{3.1.13}$$

Simplicial observables. The observables $\mathcal{O}_{f,\mathcal{D}} := \mathcal{O}_f$ that we will calculate are polynomials of the fermion fields.

- ${\mathcal{O}_f}^A_B(x,y) = \psi_x^A\ \bar{\psi}_{yB}$: the gauge-variant two-point function of the fermionic field.
- $\mathcal{O}_f(e) = (\psi_{s(e)},\, V_e\, \psi_{t(e)})$, with $e = xy$ some path linking x to y and V_e the corresponding holonomy; the gauge-invariant Polyakov line.
- $\mathcal{O}_f(e,e') = (\psi_{s(e)},\, V_e\, \psi_{t(e)})(\psi_{s(e')},\, V_{e'}\, \psi_{t(e')})$, with the two-point function of the Polyakov line.

We can now define the expectation value of a fermionic observable $\mathcal{O}_f$

$$\langle \mathcal{O}_f \rangle_{\text{GR-D}} = \frac{1}{\mathcal{Z}_{\text{GR-D}}} \left(\prod_w \int_{\mathfrak{su}(2)} d\mathbf{e}_w \right) \left(\prod_{\bar{e}} \int_{\text{SU}(2)} dg_{\bar{e}} \right) \left(\int_{\mathcal{G}_\mathcal{D}} d\mu(\overline{\psi}_v,\, \psi_v) \right)\ \mathcal{O}_f\ e^{iS_{\text{GR-D}}}. \tag{3.1.14}$$

Here $d\mathbf{e}_w$ is the Lebesgue measure on $\mathfrak{su}(2)$, dg_e is the normalised Haar measure on SU(2), and the measure for the Grassmann variables $d\mu(\overline{\psi}_v,\, \psi_v)$ is given by

$$d\mu(\overline{\psi}_v,\, \psi_v) = \prod_{v=n}^{1} d\overline{\psi}_v \prod_{v=n}^{1} d\psi_v,$$

where n is the number of vertices of Δ^* and

$$d\overline{\psi}_v = \prod_{A=2}^{1} \frac{\partial}{\partial \overline{\psi}_{vA}}, \quad d\psi_v = \prod_{A=2}^{1} \frac{\partial}{\partial \psi_v^A}.$$

Finally, the normalisation factor

$$\mathcal{Z}_{\text{GR-D}} = \left(\prod_w \int_{\mathfrak{su}(2)} d\mathbf{e}_w\right) \left(\prod_{\bar{e}} \int_{\text{SU}(2)} dg_{\bar{e}}\right) \left(\int_{\mathcal{G}_\mathcal{D}} d\mu(\overline{\psi}_v,\, \psi_v)\right) \, e^{iS_{\text{GR-D}}} \tag{3.1.15}$$

is just the partition function without any field insertions.

Gauge fixing. According to a theorem in lattice gauge theory by Elitzur [43], the expectation value of a locally gauge dependent observable, such as the fermion two-point function, is zero without gauge fixing. This result is reproduced in the spinfoam formalism as the expectation value of a non-gauge fixed, locally gauge-dependent observable will result in spin network vertex amplitudes with a single open end which vanishes by Schur's Lemma. It is therefore crucial to appropriately fix the above gauge freedom in the naive expression (3.1.14). This is done in the same way as for the Ponzano-Regge model as described in chapter 1 [2]. In particular, we denote by Δ_T the triangulation with a choice of tree T and set $g_e = 1$ for all $e \in T$.

If the observables are gauge-invariant, one simply follows the standard Faddeev-Popov procedure associated to the above gauge-fixing prescription. If the observables are not gauge-invariant, there is no canonical path. One procedure to compute a gauge-variant observables in lattice gauge theory involves averaging over the gauge group to define a gauge invariant function which can then be computed [44]. Alternatively, following Faddeev and Popov, one can take the definition of a gauge dependent operator to include the necessary gauge fixing [45]

Using this gauge fixing, we take the following as the proper definition of the expectation value of an observable

$$\langle \mathcal{O}_f \rangle_{\text{GR-D}} = \frac{1}{\mathcal{Z}^{\Delta_T}_{\text{GR-D}}} \left(\prod_w \int_{\mathfrak{su}(2)} d\mathbf{e}_w\right) \left(\prod_{\bar{e}} \int_{\text{SU}(2)} dg_{\bar{e}}\right) \left(\int_{\mathcal{G}_\mathcal{D}} d\mu(\overline{\psi}_v,\, \psi_v)\right) \prod_{e\in T} \delta(g_e)\; \mathcal{O}_f \; e^{iS_{\text{GR-D}}}, \tag{3.1.16}$$

where the normalisation factor is the path integral (3.1.15) gauge fixed by the insertion of the simplicial gauge fixing function $\prod_{e\in T} \delta(g_e)$. For a gauge invariant observable, this reduces to equation (3.1.14) and for a gauge variant observable this will depend on T.

We will now proceed to evaluate equation (3.1.16) by computing each of the integrals.

3.2 Quantum theory

In the evaluation of (3.1.16), we will perform the fermionic integration first. The advantage of doing it in this order is that we will be left with the expectation value of some bosonic observable $\mathcal{O}_b$ inserted in the Ponzano-Regge model, i.e.

$$\langle \mathcal{O}_f \rangle_{\text{GR-D}} = \frac{1}{\mathcal{Z}_{\text{GR-D}}} \left(\prod_w \int_{\mathfrak{su}(2)} d\mathbf{e}_w \right) \left(\prod_{\bar{e}} \int_{\text{SU}(2)} dg_{\bar{e}} \right) \prod_{e \in T} \delta(g_e)\ \mathcal{O}_b\ e^{iS_{\text{GR}}}. \tag{3.2.1}$$

Where

$$\mathcal{O}_b = \left(\int_{\mathcal{G}_\mathcal{D}} d\mu(\overline{\psi}_v,\ \psi_v) \right)\ \mathcal{O}_f\ e^{iS_{\text{D}}}, \tag{3.2.2}$$

Also note that performing the fermionic integration without any field insertions gives just the determinant of the Dirac operator

$$\left(\int_{\mathcal{G}_\mathcal{D}} d\mu(\overline{\psi}_v,\ \psi_v) \right)\ e^{iS_{\text{D}}} = \det D.$$

So we can write

$$\langle \mathcal{O}_f \rangle_{\text{GR-D}} = \frac{\langle \mathcal{O}_b \rangle_{\text{GR}}}{\langle \det\ D \rangle_{\text{GR}}}, \tag{3.2.3}$$

The next step is to expand the bosonic observables $\mathcal{O}_b$ in fermionic paths. In standard lattice gauge theory this is much simpler due to the fact that one normally considers a (hyper)cubic lattice. The result is a sum over all possible paths on the lattice between vertices with a field insertion. For a triangulation, a much wider class of paths between two vertices is possible but the fermionic integration restricts these to be of a certain type which complicates the Feynman rules.

3.2.1 Feynman diagram expansion

Here we deal with the Berezin integrals and arrive at a set of Feynman rules for each of the different observables. We begin by Taylor expanding the exponential of the Dirac action. The Taylor expansion for Grassmann variables terminates at the second order term so we get

$$\mathcal{O}_b = \left(\int_{\mathcal{G}_\mathcal{D}} d\mu(\overline{\psi}_v,\ \psi_v) \right)\ \mathcal{O}_f\ \prod_e \left(1 + i\alpha\, S_e - \frac{\alpha^2}{2}(S_e)^2 \right) \left(1 + i\alpha\, S_{e^{-1}} - \frac{\alpha^2}{2}(S_{e^{-1}})^2 \right), \tag{3.2.4}$$

where $\alpha = 8(2\pi G)^2$ (we have rescaled the triad such that $e \to e/16\pi G$).

We can now use the definition of the Berezin integral.

$$\begin{aligned} \int d\psi 1 &= 0 \\ \int d\psi\psi &= 1 \end{aligned}$$

So the only terms that survive are those for which there is a spinor and its conjugate at every vertex v of Δ^*, i.e.

$$\int d\mu(\overline{\psi},\ \psi)\ \overline{\psi}_A\,\psi^B\,\overline{\psi}_C\,\psi^D = -\epsilon^{BD}\epsilon_{AC}. \tag{3.2.5}$$

The results of the integration at each vertex falls into two cases. The first if there is no field insertion at the vertex and the second if there is. We will consider each case separately.

A vertex with no field insertion: The amplitude for the oriented edge $S_e = (\psi_{s(e)}, D_e\,\psi_{t(e)})$ has a conjugate spinor $\overline{\psi}_{s(e)}$ at the source $s(e)$ of the edge and a spinor $\psi_{t(e)}$ at the target $t(e)$ of the edge e. Thus for the vertex to be completely saturated with two spinors and conjugate spinors, it must be the target of two edge amplitudes and the source of two others. Applying equation (3.2.5) to this situation, we see that the ϵ tensors will give a contraction for the Dirac matrices D_e of the two ingoing S_e terms. In order to properly contract the indices on the Dirac matrices we must use the antisymmetry property, for example consider just two ingoing edge amplitudes S_{e_1}, S_{e_2} at a vertex

$$... \times \overline{\psi}_{s(e_1)A} {D_{e_1}}^A{}_B \psi^B_{t(e_1)}\ \overline{\psi}_{s(e_2)E} {D_{e_2}}^E{}_F \psi^F_{t(e_2)} \times ... \tag{3.2.6}$$

Then assume we have performed the integration and this will result in an ϵ^{BF}, then we use the antisymmetry to flip the Dirac matrix for edge e_2

$$\begin{aligned} ... \times \overline{\psi}_{s(e_1)A} {D_{e_1}}^A{}_B\ \overline{\psi}_{s(e_2)E} \epsilon^{BF} {D_{e_2}}^E{}_F \times ... &= ... \times \overline{\psi}_{s(e_1)A} \overline{\psi}_{s(e_2)E} {D_{e_1}}^A{}_B\ \epsilon^{BF} (-{D_{e_2^{-1}}}^E{}_F) \times ... \\ &= ... \times \overline{\psi}_{s(e_1)A} \overline{\psi}_{s(e_2)E} {D_{e_1}}^A{}_B\ (-D^{BE}_{e_2^{-1}}) \times ... \end{aligned} \tag{3.2.7}$$

The same will occur for the two outgoing terms.

This process can be repeated for each of the vertices that do not have a field insertion and we will obtain products of Dirac matrices around closed loops that depend on the configurations of the S_e terms at each vertex. We can also note that each loop must have an even number of edges in as it is not possible to make a loop of odd length and still saturate all of the vertices in the loop.

A vertex with a field insertion: The situation is slightly different if the vertex has a field insertion, and differs again depending on whether the insertion is a ψ or $\overline{\psi}$. Assume the vertex has a spinor, then we will require three S_e terms from the Taylor expansion to saturate the vertex. One must be ingoing, to give the other spinor, and two must be outgoing to give the two conjugate spinors. Applying formula (3.2.5) will connect the two ingoing lines as before, but the Dirac matrix for the ingoing S_e term is left with a free index that will be contracted with one of the epsilon tensors in (3.2.5). If the vertex has a

co-spinor, then there must be one outgoing line and two ingoing. The two outgoing lines will be contracted by the integration and the Dirac matrix from the ingoing edge will be left un-contracted.

Note, that the result of the integration will only be non-vanishing if for every ψ, there is also a $\overline{\psi}$ field insertion. This is the case in all of the observables we consider. In this case, the fermionic integration gives a product of Dirac matrices along an open path between the vertex of the ψ insertion and the $\overline{\psi}$ insertion. This path will have an odd number of edges.

Admissible "Feynman graphs" The result of the Berezin integral with p spinor and p co-spinor insertions on the vertices $x_1, ..., x_{2p}$ of Δ^* can be stated as follows.

The only terms that remain after the integration correspond to a graph $\Gamma := \Gamma(x_1, ..., x_{2p})$ with oriented edges which contains a number of oriented loops $\mathcal{L}$ and p paths $\mathcal{P}$ connecting each of the spinors to each of the co-spinors. The graph must have the following properties

1. The length E_Γ of the graph is $2n - p$, where the length is the number of edges in the graph and n is the number of vertices in Δ^*.

2. The length $E_\mathcal{L}$ of each connected loop component $\mathcal{L}$ is even, while the length $E_\mathcal{P}$ of each path components $\mathcal{P}$ is odd

3. Each vertex $v \in \Delta^*$ has four edges of Γ meeting at it if there is no field insertion - i.e. two ingoing and two outgoing lines. If there is a field insertion then there is only one ingoing and one outgoing edge.

4. Each path $\mathcal{P}$ has the correct orientation. Every source $s(\mathcal{P})$ is at a vertex with a spinor and every target $t(\mathcal{P})$ is at a vertex with a co-spinor

5. Consecutive edges of the graph Γ cannot go back and forth along the same dual edge $e \in \Delta^*$ unless that particular connected component of Γ is of length two.

A graph satisfying all these properties will be called admissible.

A graphical method for admissible graphs: The admissible graphs for an observable can be obtained by a simple graphical method. Draw all possible sets of $2n$ arrows on Δ^* such that:1. each vertex without a field insertion has two ingoing and two outgoing arrows; 2. each vertex with a spinor has two outgoing and one ingoing arrow; 3. each vertex with a co-spinor has two ingoing and one outgoing arrow. Then at each vertex, connect the two ingoing arrows and/or the two outgoing arrows. When the lines are connected, flip the orientation of one of the arrows so that there is a consistent orientation along each

It does not matter which edges on the path are flipped as the orientation antisymmetry (3.1.12) means that the contribution from the graph is the same in either case.

For example, on a simple four point lattice with a field insertion $\psi_1\overline{\psi}_2$, the connecting of the arrows occurs as follows

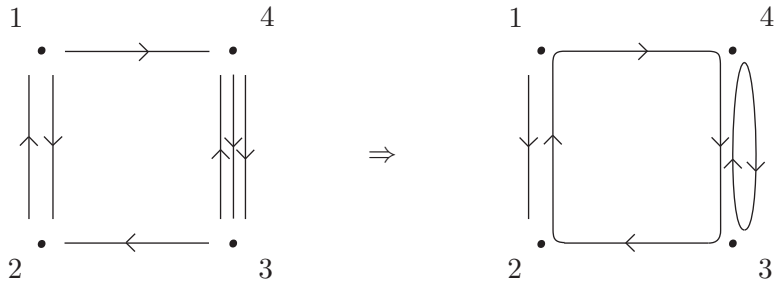

We are now ready to establish a set of 'Feynman rules' to obtain bosonic observables $\mathcal{O}_b$ in terms of the fermionic ones $\mathcal{O}_f$. These rules are as follows.

Feynman rules The Feynman rules for an observable $\mathcal{O}_f$ are the following

- Work out all of the possible admissible graphs for $\mathcal{O}_f$
- To each admissible graph $\Gamma(x_1, ..., x_{2p})$ assign an amplitude $I_{\Gamma(x_1,...,x_{2p})}$. This amplitude is constructed by assigning the ordered product of Dirac matrices

$$D_{\mathcal{P}} = (i\alpha)^{E_{\mathcal{P}}} \prod_{e\in\mathcal{P}} D_e$$

  to each open path $\mathcal{P}$, and

$$D_{\mathcal{L}} = (i\alpha)^{E_{\mathcal{L}}} \ \mathrm{tr} \prod_{e\in\mathcal{L}} D_e$$

  to each loop $\mathcal{L}$ in Γ. The orientation of the Dirac matrices should be consistent with the orientation of Γ.
- Assign a global sign $\epsilon_{\Gamma(x_1,...,x_{2p})} = \pm 1$ to each graph $\Gamma(x_1, ..., x_{2p})$ which controls the overall sign appearing as a result of raising and lowering some of the indices with the symplectic metric (see equation (3.1.13)), using the orientation antisymmetry (3.1.12), the 'see saw' property, and rearranging the fermionic fields to compute the full Berezin integral. In particular there will be a minus sign associated to each closed loop $\mathcal{L}$
- Sum over all such contributions:

$$\mathcal{O}_b = \sum_{\Gamma(x_1,...,x_{2p})} \epsilon_{\Gamma(x_1,...,x_{2p})} I_{\Gamma(x_1,...,x_{2p})}, \tag{3.2.8}$$

Conveniently, the factors of $1/2$ that appear in front of the $(S_e)^2$ terms in the Taylor expansion are cancelled by the fact that the $(S_{e^{-1}})^2$ term gives the same contribution. We absorb this factor and do not distinguish between these two supposedly different contributions.

Admissible graphs corresponding to observables We can now describe the admissible graphs for each different observable $\mathcal{O}_f$.

The partition function: The partition function $\mathcal{Z}_{\text{GR-D}}$ corresponds to the observable $\mathcal{O}_f = 1$, i.e. the number of field insertions p is zero. Here, there are no paths and Γ consists entirely of even length closed loops that touch each vertex twice. Two examples that are possible on any triangulation are a graph with a single loop that goes through each vertex twice and a graph with many components of length $E_{\mathcal{L}} = 2$ that has loops going back and forth between pairs of vertices.

The amplitude I_Γ for this Γ is thus given by

$$I_\Gamma = \prod_{\mathcal{L}} D_{\mathcal{L}}, \tag{3.2.9}$$

where the product is over all the loops $\mathcal{L} \subset \Gamma$. Hence, the corresponding bosonic observable $\mathcal{O}_b = \det D$ is given by

$$\det D = \sum_{\Gamma} \epsilon_\Gamma \prod_{\mathcal{L}} D_{\mathcal{L}}. \tag{3.2.10}$$

Fermion two point function: The admissible graphs $\Gamma(x_1, x_2)$ corresponding to the gauge-variant two-point function of the fermionic field

$$\mathcal{O}_f{}^A_B(x_1, x_2) = \psi^A_{x_1}\, \overline{\psi}_{x_2 B}.$$

have a single path $\mathcal{P}(x_1, x_2)$ going from x_1 to x_2 along with an admissible configuration of loops $\mathcal{L}$. The amplitude associated to $\Gamma(x_1, x_2)$ is

$$I_{\Gamma(x_1,x_2)}{}^A_B = D_{\mathcal{P}(x_1,x_2)}{}^A_B \left(\prod_{\mathcal{L}} D_{\mathcal{L}} \right). \tag{3.2.11}$$

Gauge invariant 2-point function: The bosonic observable corresponding to the gauge-invariant Polyakov line

$$\mathcal{O}_f(e) = (\psi_{s(e)},\, V_e\, \psi_{t(e)}),$$

has the same type of admissible graphs as the two-point function. The amplitudes have an additional V_e holonomy that closes up the path to make a trace

$$I_{\Gamma(x_1,x_2)} = \text{tr}\ \ V_e D_{\mathcal{P}(x_2,x_1)} \left(\prod_{\mathcal{L}} D_{\mathcal{L}} \right) \tag{3.2.12}$$

where $\mathcal{P}(x_2, x_1)$ is a path connecting the endpoints $x_2 = t(e)$ to $x_1 = s(e)$ of the Polyakov line.

Gauge invariant 4-point function: The graphs for the 4-point function

$$\mathcal{O}_f(e, e') = (\psi_{s(e)},\, V_e\, \psi_{t(e)})\, (\psi_{s(e')},\, V_{e'}\, \psi_{t(e')}),$$

are more complicated; there are two different types of admissible graph $\Gamma(x_1, ..., x_4)$. If x_1, x_2 and x_3, x_4 respectively label the source and target vertices of e and e' , then one of the admissible graphs has two paths that link x_2 to x_1 and x_4 to x_3. The amplitude for this type of graph is

$$I_{\Gamma(x_1,...,x_4)} = \text{tr}\ V_e D_{\mathcal{P}(x_2,x_1)}\ \text{tr}\ V_{e'} D_{\mathcal{P}(x_4,x_3)}\ \left(\prod_{\mathcal{L}} D_{\mathcal{L}}\right). \tag{3.2.13}$$

The second type of admissible graph also has two open paths but this time from x_2 to x_3 and x_4 to x_1. This type of graph has the amplitude

$$I_{\Gamma(x_1,...,x_4)} = \text{tr}\ V_e D_{\mathcal{P}(x_2,x_3)} V_{e'} D_{\mathcal{P}(x_4,x_1)}\ \left(\prod_{\mathcal{L}} D_{\mathcal{L}}\right). \tag{3.2.14}$$

At this stage, we have left all of the amplitudes in terms of the Dirac matrix D_e. This method of coupling fermions has the unfortunate feature that, since the Dirac matrix contains two terms

$$D_e = \Sigma_e\, U_e - U_e\, \Sigma_{e^{-1}}, \tag{3.2.15}$$

each admissible graph actually contributes a sum of 2^{E_Γ} terms to the expectation value. This can obviously result in a very large number of terms.

We distinguish between these terms by labelling each one with a number $c_\Gamma = 0, ..., 2^{E_\Gamma} - 1$ that refers to the configuration associated to the graph. An example of a such term, which we denote $c_\Gamma = 0$, can be obtained for each observable given above by replacing the Dirac matrix D_e with the quantity $\Sigma_e U_e$. In the term corresponding to, for example, $c_\Gamma = 1$, one of the edges has the factor $U_e \Sigma_{e^{-1}}$ instead of $\Sigma_e U_e$, etc. Hence, for each graph Γ the amplitude I_Γ is split into a sum of contributions

$$I_\Gamma = \sum_{c_\Gamma} I_{c_\Gamma}$$

and the bosonic observables are given by

$$\mathcal{O}_b = \sum_{\Gamma, c_\Gamma} \epsilon_\Gamma I_{c_\Gamma}. \tag{3.2.16}$$

This completes the fermionic integration, we will now address the gravitational sector of the model.

3.2.2 Gravitational integrals

The integration over the discretised frame field and connection will proceed as in sections 1.4 and 1.5 but with several additional complications. Namely, the partition function now contains an observable $\mathcal{O}_b$ that is a function of both $\mathbf{e}_w$ and U_e, and we have used the wedge variables in Δ^+ rather than just Δ.

We will first consider the gauge invariant observables and generalise the graphical methods to include the more complicated case covered here, then, with a few minor modifications, apply these to the gauge variant observables.

First, some more notation. We will write the expectation value of $\mathcal{O}_f$ as a sum over spin foams, each one associated to a different admissible graph

$$\langle \mathcal{O}_f \rangle_{\text{GR-D}} = \frac{1}{\langle \det D \rangle_{\text{GR}}} \sum_{\Gamma, c_\Gamma} \epsilon_\Gamma A_{c_\Gamma}. \tag{3.2.17}$$

The amplitude A_{c_Γ} associated to the graph Γ and to the configuration c_Γ is given by

$$A_{c_\Gamma} = \left(\prod_w \int_{\mathfrak{su}(2)} d\mathbf{e}_w \right) \left(\prod_{\bar{e}} \int_{\mathrm{SU}(2)} dg_{\bar{e}} \right) \prod_{e \in T} \delta(g_e)\ I_{c_\Gamma}(\mathbf{e}_w, U_e)\ \ \exp \sum_w \mathrm{tr}\left(\mathbf{e}_w G_w\right). \tag{3.2.18}$$

So to calculate the observable we must evaluate each A_{c_Γ} in the sum. In fact all this process really does is transfer the calculations into the language of representation theory. In order to actually compute the whole sum it may be better to perform the gravitational integrals using numerical methods as in lattice gauge theory. This is one of the difficulties of non-perturbative approaches.

Gauge invariant observables

For the gauge invariant observables, we will ignore the gauge fixing tree to simplify matters. In fact the expression is unchanged with the insertion of the gauge fixing since the Fadeev-Popov determinant is one and the Haar measures are normalised. We also consider just the $c_\Gamma = 0$ terms in I_{c_Γ}, these are the terms consisting only of the $\Sigma_e U_e$ terms in the Dirac operator. The other terms are obtained in the same way but we would have to keep track of much more information. The configuration is given by

$$I_0(\mathbf{e}_w, U_e) = (i\alpha)^{E_\Gamma} \left(\prod_\gamma \mathrm{tr} \prod_{\mathcal{P} \in \gamma} \prod_{e \in \mathcal{P}} \Sigma_e U_e V_{e(\mathcal{P})} \right) \left(\prod_{\mathcal{L}} \mathrm{tr} \prod_{e \in \mathcal{L}} \Sigma_e U_e \right). \tag{3.2.19}$$

Integration over simplicial triads. Here we discuss the integration over the $\mathbf{e}_w$. Since the Dirac matrices in the observable $\mathcal{O}_f$ contain polynomials of the discretised frame

fields, we will use the generating functional techniques to evaluate these terms [46]. Here the generating functional is given by inserting the exponentials of Lie algebra sources $J_w = J_w^a \gamma_a$ associated to the wedges into the amplitude A_{c_Γ}. The frame field then becomes a derivative with respect to these sources

$$\mathbf{e}_w \mapsto \frac{i}{2}\frac{\delta}{\delta J_w}.$$

The particular functions that we are interested in are the area operators $\Sigma_e = \Sigma_e^a \gamma_a$. Replacing the frame fields with derivatives these become

$$\hat{\Sigma}_e^a = -\frac{1}{12}\sum_{w_e, w_e'} \epsilon^{abc} \frac{\delta}{\delta J_{w_e}^b}\frac{\delta}{\delta J_{w_e'}^c}\,\mathrm{sgn}(w_e, w_e'), \tag{3.2.20}$$

The amplitude is now

$$A_0 = (i\alpha)^{E_\Gamma}\left[\left(\prod_\gamma \prod_{\mathcal{P}\in\gamma}\prod_{e\in\mathcal{P}} \hat{\Sigma}_e^{a_e}\right)\left(\prod_{\mathcal{L}}\prod_{e\in\mathcal{L}}\hat{\Sigma}_e^{b_e}\right)\left(A_0^{(a,b)}(J)\right)\right]_{J=0}, \tag{3.2.21}$$

with the generating functional, after integration over the simplicial triad as in chapter 1, given by

$$A_0^{(a,b)}(J) = \left(\prod_{\bar{e}}\int_{\mathrm{SU}(2)} dg_{\bar{e}}\right)\left(\prod_\gamma \mathrm{tr}\prod_{\mathcal{P}\in\gamma}\prod_{e\in\mathcal{P}}\gamma_{a_e}U_e V_{e(\mathcal{P})}\right)\left(\prod_{\mathcal{L}}\mathrm{tr}\prod_{e\in\mathcal{L}}\gamma_{b_e}U_e\right)\prod_w \delta\left(e^{J_w}G_w\right) \tag{3.2.22}$$

(a, b) represent the indices on the Lie algebra generators, a runs over all of the indices associated to the path $\mathcal{P}$ and b over the indices associated to the loop $\mathcal{L}$.

We now expand the delta function in terms of characters and we can compute the group integrals.

Group integrals. The group integrals are performed graphically in the same way as the Ponzano-Regge model but with a few important differences. First, consider the group variables that are on the interior of the dual faces f, i.e. in $\Delta^+ - \Delta^*$. Each one of these group variables appears in the amplitude twice. We use the orthogonality of characters to remove these group variables

$$\int_{\mathrm{SU}(2)} dg\ \chi_j(g_1 g)\chi_k(g^{-1}g_2) = \frac{\delta_{jk}}{\dim j}\chi_j(g_1 g_2), \tag{3.2.23}$$

diagrammatically this is

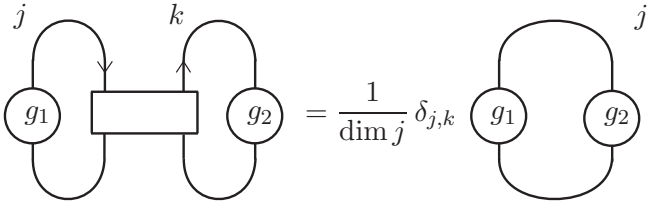

(3.2.24)

If we use this on each of the interior group elements then we see that it forces all of the spins j_w on the wedges belonging to the same face f to be equal $j_w = j_f$ for all w in f. The generating functional now reads

$$A_0^{(a,b)}(J) = \sum_{j_f} \prod_f \dim j_f A_0^{(a,b)}(j_f, J), \tag{3.2.25}$$

with

$$\begin{aligned} A_0^{(a,b)}(j_f, J) \;=\; & \left(\prod_e \int_{\mathrm{SU}(2)} dg_e\right) \left(\prod_\gamma \mathrm{tr} \prod_{\mathcal{P}\in\gamma} \prod_{e\in\mathcal{P}} \gamma_{a_e} U_e V_{e(\mathcal{P})}\right) \left(\prod_{\mathcal{L}} \mathrm{tr} \prod_{e\in\mathcal{L}} \gamma_{b_e} U_e\right) \\ & \times \prod_f \chi_{j_f}\left(e^{J_f^1} g_{e_f}^1 \ldots e^{J_f^m} g_{e_f}^m\right). \end{aligned}$$

The remaining edges $\bar{e}$ of Δ^+ have been recombined into edges e of Δ^* but the Lie algebra sources are still associated to the $m := m_f$ wedges in the face f. So we have that $g_{e_f} = g_{e_{w1}} g_{e_{w2}}^{-1}$ if $w1, w2$ are the two wedges that meet edge e in face f.

Next, we must generalise the integration over the tensor product of three representations to cases that include additional $j = 1/2$ holonomy matrices $U(g_e)$, i.e. if the dual edge contains an edge of Γ. The first case is if there is a single edge of Γ

$$\int_{\mathrm{SU}(2)} dg\, U(g) \otimes \pi^i(g) \otimes \pi^j(g) \otimes \pi^k(g) = \sum_s \iota_s\, \iota_s^*, \tag{3.2.26}$$

ι_s and ι_s^* are 4-valent intertwiners, the label s corresponds to the internal spin label that comes from decomposing them into the unique 3-valent intertwiners. Graphically this is

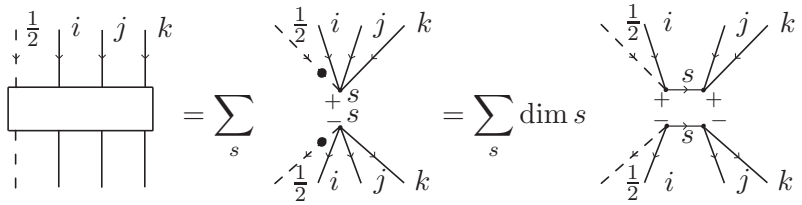

(3.2.27)

Note that we are now representing the spin half lines by dashed lines to make the path of the fermion clearer. The second case is if there are two spin half lines on a dual edge, this gives

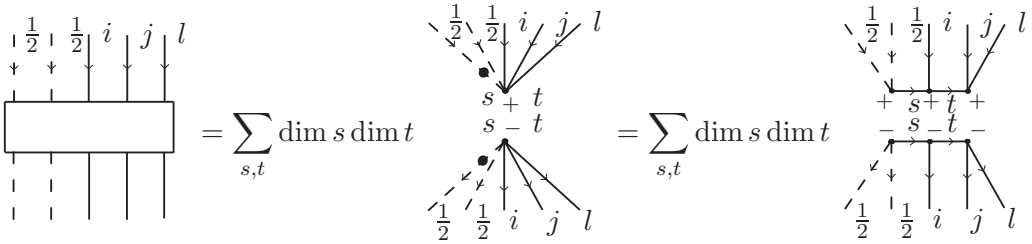

(3.2.28)

Depending on the path of the V_e holonomy in the definition of the observable, there may be more than two spin half holonomies on each dual edge. The formula generalises to these cases but this is the maximum that can occur just from Γ.

If we assume that we have performed all of these group integrals then the generating functional can be written as a state sum model as it will factorise into vertex amplitudes

$$A_0^{(a,b)}(j_f, J) = \prod_v A_v^{(a,b)}(j_f, J). \tag{3.2.29}$$

Each of the vertex amplitudes is a 6j symbol modified by the extra lines coming from Γ and with Lie algebra sources on each of the six edges. The modified generating functional amplitudes also have free indices given by the (a, b), we will now show how these are contracted with the source derivatives.

Grasping operators. The action of the source derivatives on the generating functional will produce what are called grasping operators in the literature. The derivative of the exponentiated current in the spin-j representation, at $J = 0$, gives the $\mathfrak{su}(2)$ Lie algebra generator in that representation

$$\frac{\delta}{\delta J^a}\pi^j(e^J)\Big|_{J=0} = \pi_*^j(\gamma_a). \tag{3.2.30}$$

We can represent these generators as three valent intertwiners between two spin-j representations and the vector representation

$$\pi_*^j \quad \in \quad \mathrm{Hom}(V_1, V_j \otimes V_j^*). \tag{3.2.31}$$

This is proportional to the standard 3-valent vertex

$$\pi_*^j(\gamma_a)^\alpha{}_\beta = \Theta(j)$$

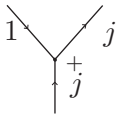

(3.2.32)

with the normalisation factor given by $\Theta(j)^2 := \Theta(1, j, j)^2 = j(j+1)(2j+1)$. So whenever there is a source derivative, we must insert a three valent vertex at the appropriate point in the spin network diagram. This is the "grasping" operation and results in a free index in the vector representation.

Now, recall the form of the $\hat{\Sigma}_e^a$

$$\hat{\Sigma}_e^a = -\frac{1}{12}\sum_{w_e, w_e'} \epsilon^{abc}\frac{\delta}{\delta J_{w_e}^b}\frac{\delta}{\delta J_{w_e'}^c}\,\mathrm{sgn}(w_e, w_e'), \tag{3.2.33}$$

this will act with a source derivative at pairs of wedges associated to a given triangle. In the spin network language, it will act by grasping two of the three lines (that are not part of Γ) meeting at a three-valent vertex. The two free indices created by the graspings are then contracted with the ϵ^{abc} appearing in $\hat{\Sigma}_e^a$. Since we have seen that ϵ^{abc} is an intertwiner this gives another vertex

$$\epsilon^{abc} = \sqrt{6}$$

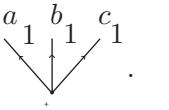

(3.2.34)

The final remaining index on the ϵ^{abc} is then contracted with the generator appearing in the relevant edge of Γ.

Performing this step for each $\hat{\Sigma}^a_e$, we arrive at a spin foam model for the observable

$$A_0 = (i\alpha)^{E_\Gamma} \prod_f \sum_{j_f} d_{j_f} \prod_v \sum_{s_v} A_v(j_f, s_v). \tag{3.2.35}$$

The sum over s_v refers to the spin labels in the decomposition of the higher valence vertices. All of the possible vertex amplitudes, including those for $c_\Gamma \neq 0$, are given in Figure 3.1. The graphical method for deriving these amplitudes will be summarised after we have dealt with the gauge variant amplitudes. For a particular triangulation and a particular graph/configuration, the obtained vertex amplitudes are recoupled in the following section.

Gauge dependent observables

For the gauge variant observables, the two point function, we must include the gauge fixing tree T in order to obtain a non-vanishing expectation value. As suggested by the name, these observables will depend on the choice of tree.

The amplitude associated to the admissible graphs for the two point function is

$$I_0(\mathbf{e}_w, U_e) = (i\alpha)^{E_\Gamma} \prod_{\mathcal{P}} \prod_{e\in\mathcal{P}} \Sigma_e U_e \left(\prod_{\mathcal{L}} \mathrm{tr} \prod_{e\in\mathcal{L}} \Sigma_e U_e \right). \tag{3.2.36}$$

The derivation is the same as for the gauge invariant case, however the inclusion of the gauge fixing tree means that the expectation value will be given by a spin network diagram for the whole triangulation. The amplitude can not be factorised into vertex amplitudes to give a state sum.

We write the generating functional schematically as

$$A_0^{(a,b)}(j_f, J) = \langle \bigotimes_l \pi^{j_l}(e^{J_l}), \bigotimes_n \iota_n \rangle, \tag{3.2.37}$$

where the inner product denotes the contraction of the indices according to the pattern of lines l and nodes n of the diagram. Acting with the grasping operators then gives

$$A_0 = (i\alpha)^{E_\Gamma} \prod_f \sum_{j_f} d_{j_f} \prod_v \sum_{s_v} A(j_f, s_v), \tag{3.2.38}$$

$A(j_f, s_v)$ is a spin network diagram that depends on Δ, T and Γ. It is actually a sum over diagrams because of the sum over graspings in each $\hat{\Sigma}^a_e$.

A summary of the graphical method is given by the following steps [14, 47]

- Draw the characters for each wedge as closed loops, labelled by the spin j_w, and the integrals over the group variables as cables in the appropriate places.

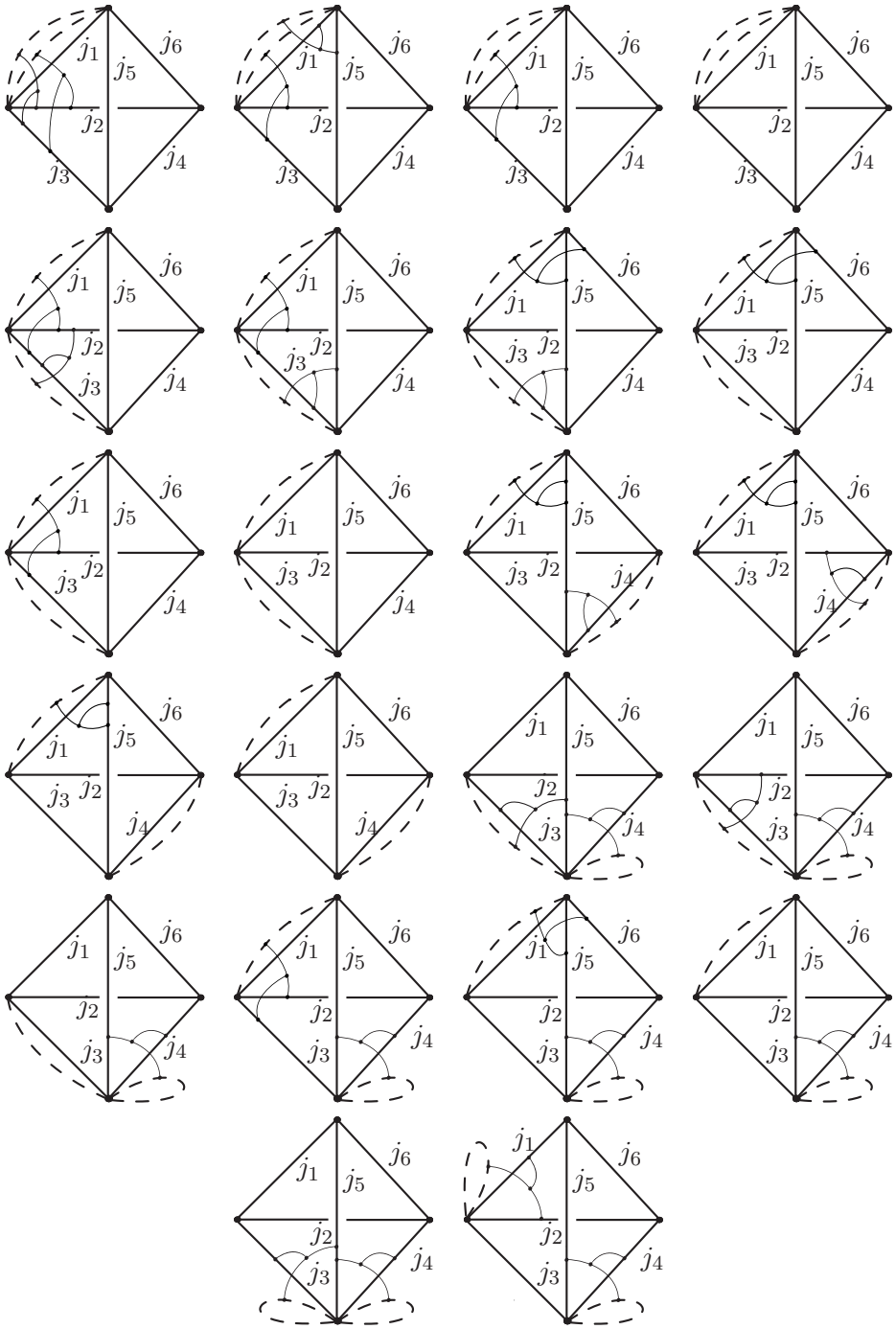

Figure 3.1: Spin network diagrams for the different possible vertex amplitudes A_v (up to symmetry) of the gauge invariant observables. The dashed lines are in the spin half representation and the curved lines denote the grasping operators in the spin one representation. To each diagram with a grasping, one must add the additional diagrams obtained by summing over the possible grapsings. Note that due to the V_e terms there can be additional spin half lines that have not been included in these diagrams.

- Draw a spin half line (a dashed line in our conventions) for every edge e of Γ.
- On each edge of Γ, add an open spin-1 line. This will be before the cables for the $c_\Gamma = 0$ but for $c_\Gamma \neq 0$, this can be after the cable. This is the generator appearing in D_e.
- For each edge e of Γ, pick two of the three j_w lines that meet at $s(e)$ and add an open spin-1 line. Sum over these pairs. This is the action of the grasping operators.
- On each edge of Γ, connect the spin-1 line from the generator to the two spin-1 lines from the graspings using a three valent vertex with three spin-1 lines, i.e. $\epsilon^{a_e b_e c_e}$.
- For the gauge variant observable remove the cables on the edge $e \in T$.
- Perform the integrals by replacing the boxes by the corresponding intertwiners.
- Put in all the numerical and normalisation factors and sum over the spins with a dimension factor $\dim j_f$ on each dual face.

Applying this at a single vertex, with just one fermion line for simplicity, will give diagrams of the following form

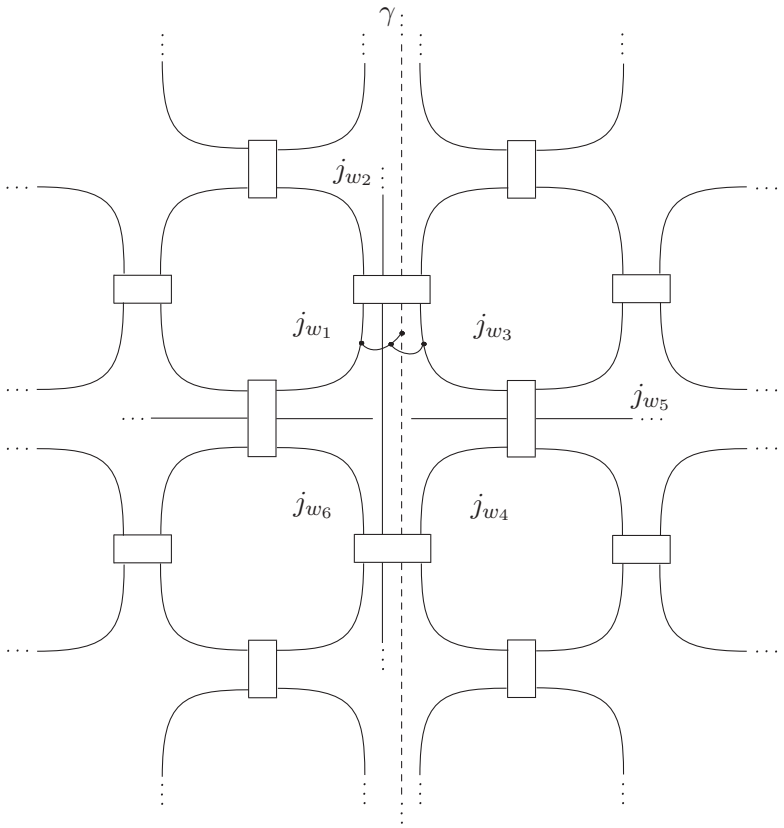

from which the vertex amplitudes or the relevant spin network diagram can be obtained.

We will now apply the methods described above to a simple example.

3.3 Explicit calculations: observables on $\mathcal{S}^3$

In this section, we give examples of the calculations described above for a space-time manifold homeomorphic to the three-sphere, i.e., $M \cong \mathcal{S}^3$. We consider the triangulation, denoted Δ, of $\mathcal{S}^3$ with the boundary of a 4-simplex[1] and label each vertex v of Δ^* (the pentachoron graph) by the labels $I, J = 1, ..., 5$ which implies that the edges e of Δ^* are labelled by couples IJ, with $I \neq J$, and the faces f of $\mathcal{D}^*$ are labelled by triples IJK, with $I \neq J \neq K$ corresponding to the three vertices belonging to the face. The Dirac part of the action (3.1.7) for Δ, with rescaled triad, is

$$S_{\text{D}} = \alpha \sum_{I \neq J} S_{IJ}. \tag{3.3.1}$$

The examples we will consider are the gauge invariant 2-point function $\mathcal{O}_f(e) = (\psi_{s(e)},\, V_e\, \psi_{t(e)})$, and the propagator $\mathcal{O}_f{}^A_B(x_1, x_2) = \psi^A_{x_1}\ \bar{\psi}_{x_2 B}$. We will now calculate the Berezin integrals explicitly to illustrate the Feynman rules for both observables.

3.3.1 Gauge invariant observable: 2-point function

For this observable we consider $\mathcal{O}_f(23) = (\psi_2,\, V_{253}\, \psi_3)$, with $V_{253} = V_{25}V_{53}$. The bosonic observable $\mathcal{O}_b$ formed by integrating the Grassmann variables is

$$\mathcal{O}_b = \left(\int_{\mathcal{G}_\mathcal{D}} d\mu(\overline{\psi}_I,\, \psi_I) \right)\ (\psi_2,\, V_{253}\, \psi_3)\ e^{iS_{\text{D}}}, \tag{3.3.2}$$

We will consider one relevant non-vanishing term in the Feynman expansion (3.2.4) in order to compute the amplitude I_Γ of a single admissible graph in equation (3.2.8).

$$\begin{aligned} \mathcal{O}_b \;=\; & ... + (i\alpha)^9 \left(\int_{\mathcal{G}_\mathcal{D}} d\mu(\overline{\psi}_I,\, \psi_I) \right)\ \overline{\psi}_{2A} V_{253}{}^A_{\ B} \psi^B_3 \\ & \times \overline{\psi}_{1C} D_{12}{}^C_D \psi^D_2\ \overline{\psi}_{2E} D_{23}{}^E_F \psi^F_3\ \overline{\psi}_{3G} D_{32}{}^G_H \psi^H_2\ \overline{\psi}_{3I} D_{34}{}^I_J \psi^J_4\ \overline{\psi}_{4K} D_{41}{}^K_L \psi^L_1 \\ & \times \overline{\psi}_{4M} D_{45}{}^M_N \psi^N_3\ \overline{\psi}_{5P} D_{54}{}^P_Q \psi^Q_4\ \overline{\psi}_{5R} D_{51}{}^R_S \psi^S_1\ \overline{\psi}_{1T} D_{15}{}^T_U \psi^U_5\ + ..., \end{aligned} \tag{3.3.3}$$

including the factor of 2 coming from the identical contribution of the S^2_{IJ} and S^2_{JI} terms. This corresponds to a particular Feynman graph which we denote $\Gamma(2, 3)$. Taking into account the order of the Grassmann variables, performing the integrals and contracting the indices leaves us with a global sign of $\epsilon_{\Gamma(2,3)} = -1$. This agrees with the usual QFT Feynman rules where one associates a minus sign to each closed loop.

[1] The (pseudo-)triangulation constructed from only two tetrahedra can not be used as it is not possible to properly define the action. This is because there is more than one edge connecting two vertices. While this is not problematic when working with theories of flat connections, it becomes highly ambiguous when dealing with non-trivial curvature.

Hence

$$\epsilon_{\Gamma(2,3)} I_{\Gamma(2,3)} = -(i\alpha)^9 \,\mathrm{tr}\,(D_{32}V_{253})\;\; \mathrm{tr}\,(D_{21}D_{15}D_{54}D_{41}D_{15}D_{54}D_{43}D_{32})\,. \tag{3.3.4}$$

Applying the graphical method described above gives us a number of admissible graphs, the graph $\Gamma(2,3)$ corresponding to the term in the Feynman expansion above is given by the following

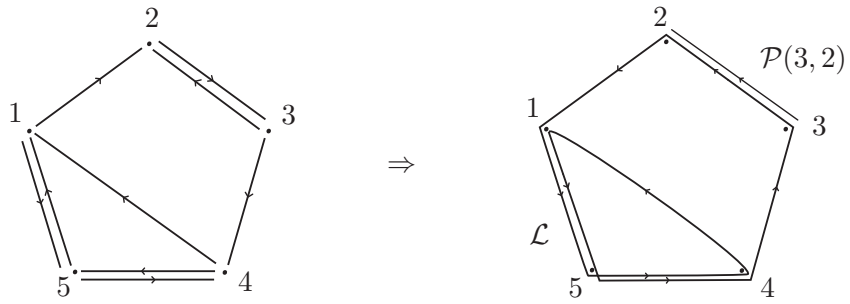

The path $\mathcal{P}(3,2)$ runs from vertex 3 to vertex 2 and has length $E_{\mathcal{P}} = 1$, and the loop term $\mathcal{L}$ has $E_{\mathcal{L}} = 8$ and passes through the following chain of vertices: 154154321. The overall length is therefore $E_{\Gamma(2,3)} = 2n - p = 9$. The Feynman rules in section 3.2 now associate a product of Dirac matrices D_e to the edges of $\Gamma(2,3)$ which gives equation (3.3.4).

This completes the fermionic integration, we can now consider the gravitational integration. As above, we will consider the $c = 0$ configuration $I^0_{\Gamma(2,3)}$, which is given by

$$\begin{aligned} I^0_{\Gamma(2,3)} \;&=\; (i\alpha)^9 \,\mathrm{tr}\,(\Sigma_{32}U_{32}V_{253}) \\ &\quad\times \mathrm{tr}\,(\Sigma_{21}U_{21}\Sigma_{15}U_{15}\Sigma_{54}U_{54}\Sigma_{41}U_{41}\Sigma_{15}U_{15}\Sigma_{54}U_{54}\Sigma_{43}U_{43})\,. \end{aligned} \tag{3.3.5}$$

Using this, one can apply the graphical methods of section 3.2 to obtain the generating functional and then the amplitude $A^0_{\Gamma(2,3)}$ of the graph $\Gamma(2,3)$.

$$\begin{aligned} A^0_{\Gamma(2,3)} \;&=\; \left(\frac{\alpha}{4}\right)^9 \prod_{I<J<K} \sum_{j_{IJK}} \dim j_{IJK}\,(-1)^{2(j_{145}+j_{123}+j_{245}+j_{234}+j_{135})} \\ &\quad\times \sum_{s_{15},t_{15}} \sum_{s_{23},t_{23}} \sum_{s_{45},t_{45}} \sum_{s_{14}} \sum_{s_{12}} \sum_{s_{25}} \sum_{s_{34}} \sum_{s_{35}} \\ &\quad\times \dim s_{15} \dim t_{15} \dim s_{14} \dim s_{12} \dim s_{23} \dim t_{23} \dim s_{25} \dim s_{34} \dim s_{35} \dim s_{45} \dim t_{45} \\ &\quad\times \Theta^2(j_{123})\Theta^2(j_{124})\Theta(j_{125})\Theta^2(j_{134})\Theta^2(j_{135})\Theta^4(j_{145})\Theta(j_{234})\Theta^2(j_{235})\Theta(j_{245})\Theta(j_{345}) \\ &\quad\times A_1(j_{1..}, s_{1.})A_2(j_{2..}, s_{2.})A_3(j_{3..}, s_{3.})A_4(j_{4..}, s_{4.})A_5(j_{5..}, s_{5.}) \end{aligned} \tag{3.3.6}$$

Here, the global factor is due to the multiplication of the $i\alpha$ factors coming from the Feynman rules with the factor $-i/4$ coming from the global contribution attached to each grasping ($i\sqrt{6}/2$ arising from the γ^a, $\sqrt{6}$ from the ϵ^{abc} tensor and $-1/12$ from the $\hat{\Sigma}^a_e$).

The signs are due to the Haar integrals, and the $\Theta(j_{IJK})$ terms come from the normalisation of the source derivatives. The vertex amplitudes A_I, $I = 1, ..., 5$, are given by evaluating the following spin networks.

$A_1 =$

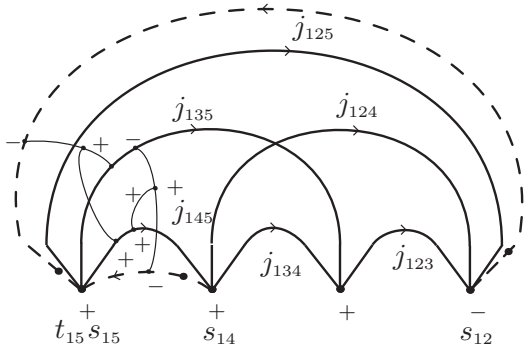

(3.3.7)

$A_2 =$

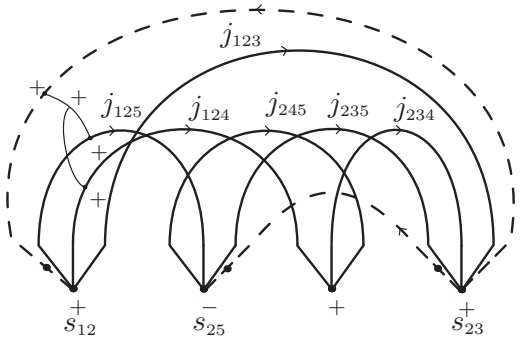

(3.3.8)

$A_3 =$

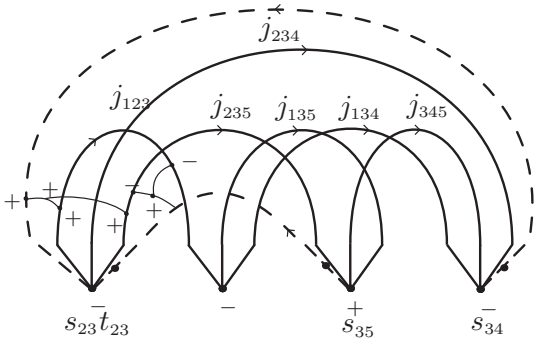

(3.3.9)

$A_4 =$

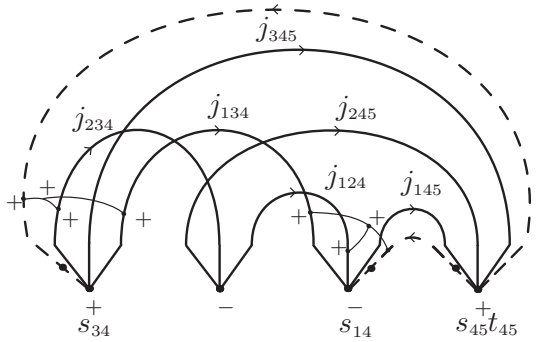

(3.3.10)

$A_5 =$ 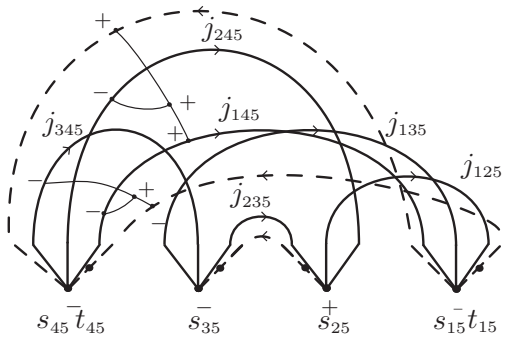

(3.3.11)

In order to write $A^0_{\Gamma(2,3)}$ explicitly, we will now recouple the vertex amplitudes appearing in the state sum in order to express them in terms of sums and products $6j$ symbols. We start by decomposing the vertices of valence four and five into three-valent vertices. Then, we repeatedly use the recoupling identities (1.5.46), (1.5.48), (1.5.50) displayed in the Appendix. As a result, we obtain the following decomposition of the vertex amplitudes $A_I(j_{IJK}, s_{IJ})$ appearing in equation (3.3.6).

$A_1 =$ 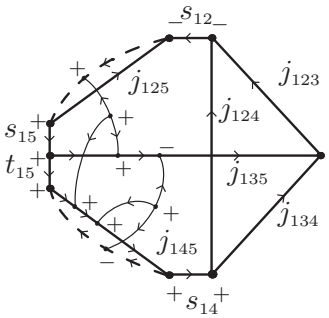

$$
\begin{aligned}
&\sum_{p,n,q} \dim n \ \dim p \ \dim q \\
&\times (-1)^{3n+q+j_{135}+s_{14}+2j_{123}+j_{134}+j_{124}+s_{12}+t_{15}+t_{15}} \\
&\times \begin{Bmatrix} j_{124} & j_{134} & s_{14} \\ j_{135} & s_{12} & j_{123} \end{Bmatrix} \begin{Bmatrix} s_{14} & j_{135} & s_{12} \\ j_{135} & n & 1 \end{Bmatrix} \begin{Bmatrix} 1 & s_{14} & n \\ j_{145} & \frac{1}{2} & \frac{1}{2} \end{Bmatrix} \\
&\times \begin{Bmatrix} 1 & s_{14} & q \\ j_{145} & \frac{1}{2} & \frac{1}{2} \end{Bmatrix} \begin{Bmatrix} s_{12} & j_{135} & n \\ j_{135} & p & 1 \end{Bmatrix} \begin{Bmatrix} \frac{1}{2} & n & j_{145} \\ 1 & j_{145} & q \end{Bmatrix} \\
&\times \begin{Bmatrix} j_{135} & p & n \\ 1 & t_{15} & s_{15} \end{Bmatrix} \begin{Bmatrix} 1 & 1 & 1 \\ s_{15} & s_{12} & p \end{Bmatrix} \begin{Bmatrix} \frac{1}{2} & t_{15} & j_{145} \\ 1 & j_{145} & n \end{Bmatrix} \\
&\times \begin{Bmatrix} 1 & \frac{1}{2} & \frac{1}{2} \\ j_{125} & s_{12} & s_{15} \end{Bmatrix}
\end{aligned}
$$

$A_2 =$ 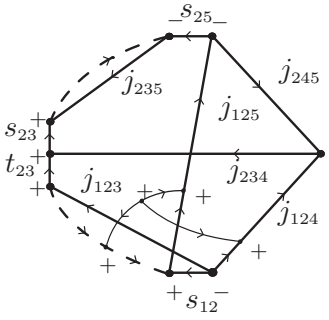

$$
\begin{aligned}
&\sum_{m,r} (\dim s_{23})^{-1} \dim m \ \dim r \ \delta_{s_{23},s_{25}} (-1)^{(3s_{23}+3j_{245}+j_{234})} \\
&\times (-1)^{(m+2r+2s_{12}+2j_{123}+j_{235}+3t_{23}+3j_{125}+j_{124}+1)} \\
&\times \begin{Bmatrix} j_{125} & j_{124} & t_{23} \\ j_{234} & s_{23} & j_{245} \end{Bmatrix} \begin{Bmatrix} j_{124} & j_{125} & t_{23} \\ 1 & r & j_{123} \end{Bmatrix} \begin{Bmatrix} 1 & 1 & 1 \\ m & r & t_{23} \end{Bmatrix} \\
&\times \begin{Bmatrix} j_{125} & m & j_{124} \\ 1 & j_{124} & r \end{Bmatrix} \begin{Bmatrix} 1 & t_{23} & m \\ j_{123} & \frac{1}{2} & \frac{1}{2} \end{Bmatrix} \begin{Bmatrix} \frac{1}{2} & j_{125} & s_{12} \\ j_{124} & j_{123} & m \end{Bmatrix}
\end{aligned}
$$

$A_3 =$ 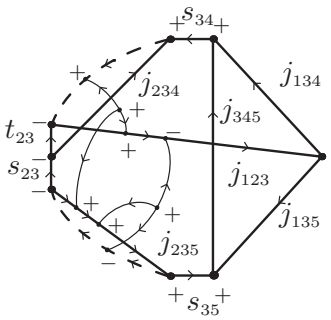

$$
\begin{aligned}
&\textstyle\sum_{n,p,q,v} \dim n\ \dim p\ \dim q\ \dim v\ (-1)^{(j_{135}+j_{345}+s_{34})} \\
&\times(-1)^{(3n+q+v+j_{123}+2j_{234}+2t_{23}+s_{23}+j_{123}+s_{35}+2j_{134}+s_{23})} \\
&\times \begin{Bmatrix} j_{123} & \frac{1}{2} & t_{23} \\ j_{234} & s_{23} & v \end{Bmatrix} \begin{Bmatrix} j_{345} & j_{135} & s_{35} \\ j_{123} & s_{34} & j_{134} \end{Bmatrix} \begin{Bmatrix} s_{35} & j_{123} & s_{34} \\ j_{123} & n & 1 \end{Bmatrix} \\
&\times \begin{Bmatrix} 1 & s_{35} & n \\ j_{235} & \frac{1}{2} & \frac{1}{2} \end{Bmatrix} \begin{Bmatrix} 1 & s_{35} & q \\ j_{235} & \frac{1}{2} & \frac{1}{2} \end{Bmatrix} \begin{Bmatrix} s_{34} & j_{123} & n \\ j_{123} & p & 1 \end{Bmatrix} \\
&\times \begin{Bmatrix} \frac{1}{2} & n & j_{235} \\ 1 & j_{235} & q \end{Bmatrix} \begin{Bmatrix} j_{123} & p & n \\ 1 & s_{23} & v \end{Bmatrix} \begin{Bmatrix} 1 & 1 & 1 \\ v & s_{34} & p \end{Bmatrix} \\
&\times \begin{Bmatrix} \frac{1}{2} & s_{23} & j_{235} \\ 1 & j_{235} & n \end{Bmatrix} \begin{Bmatrix} 1 & \frac{1}{2} & \frac{1}{2} \\ j_{234} & s_{34} & v \end{Bmatrix}
\end{aligned}
$$

$A_4 =$ 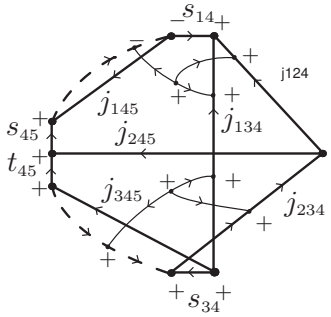

$$
\begin{aligned}
&\textstyle\sum_{a,b,c} \dim a\ \dim b\ \dim c \\
&\times(-1)^{(3a+3b+3c+3s_{34}+j_{234}+j_{145}+j_{345}+\frac{3}{2}+3s_{45}+3j_{134})} \\
&\times \begin{Bmatrix} j_{134} & j_{234} & t_{45} \\ j_{245} & s_{45} & j_{124} \end{Bmatrix} \begin{Bmatrix} j_{134} & j_{234} & t_{45} \\ c & 1 & j_{134} \end{Bmatrix} \begin{Bmatrix} j_{134} & j_{124} & s_{45} \\ b & 1 & j_{134} \end{Bmatrix} \\
&\times \begin{Bmatrix} 1 & 1 & 1 \\ a & t_{45} & c \end{Bmatrix} \begin{Bmatrix} 1 & 1 & 1 \\ s_{14} & b & s_{45} \end{Bmatrix} \begin{Bmatrix} a & j_{134} & j_{234} \\ 1 & j_{234} & c \end{Bmatrix} \\
&\times \begin{Bmatrix} s_{14} & j_{134} & j_{124} \\ j_{124} & 1 & b \end{Bmatrix} \begin{Bmatrix} 1 & s_{14} & s_{45} \\ j_{145} & \frac{1}{2} & \frac{1}{2} \end{Bmatrix} \begin{Bmatrix} j_{234} & \frac{1}{2} & s_{34} \\ j_{345} & j_{134} & a \end{Bmatrix}
\end{aligned}
$$

$A_5 =$ 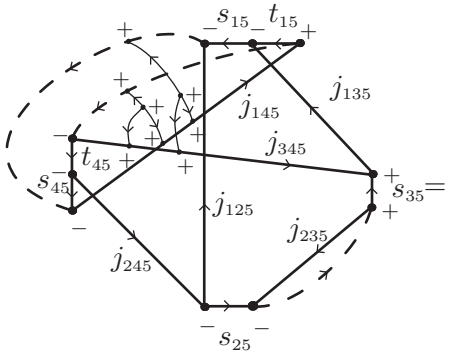

$$
\begin{aligned}
&\textstyle\sum_{a,b,c,d,e,f,g,h,i} \dim a \dim b\ \dim c\ \dim d\ \dim e \\
&\times \dim f\ \dim g\ \dim h\ \dim i\ \delta_{s_{23},s_{25}} (\dim s_{35})^{-1} \\
&\times(-1)^{(3c+2d+2f+2g+3h+3i+12j_{125}+3j_{245}+3s_{25})} \\
&\times(-1)^{(3j_{145}+j_{135}+3j_{345}+3s_{15}+3j_{45}+j_{235}+s_{35})} \\
&\times \begin{Bmatrix} j_{125} & j_{245} & s_{25} \\ j_{345} & j_{135} & i \end{Bmatrix} \begin{Bmatrix} i & j_{345} & j_{24} \\ j_{345} & g & 1 \end{Bmatrix} \begin{Bmatrix} 1 & i & g \\ j_{145} & h & d \end{Bmatrix} \\
&\times \begin{Bmatrix} j_{125} & d & c \\ j_{145} & j_{135} & i \end{Bmatrix} \begin{Bmatrix} h & g & j_{145} \\ j_{145} & 1 & e \end{Bmatrix} \begin{Bmatrix} 1 & 1 & 1 \\ e & d & h \end{Bmatrix} \\
&\times \begin{Bmatrix} a & e & 1 \\ j_{145} & j_{145} & g \end{Bmatrix} \begin{Bmatrix} 1 & 1 & 1 \\ a & e & f \end{Bmatrix} \begin{Bmatrix} e & 1 & a \\ \frac{1}{2} & \frac{1}{2} & \frac{1}{2} \end{Bmatrix} \\
&\times \begin{Bmatrix} d & 1 & e \\ \frac{1}{2} & \frac{1}{2} & \frac{1}{2} \end{Bmatrix} \begin{Bmatrix} j_{125} & \frac{1}{2} & s_{15} \\ \frac{1}{2} & c & d \end{Bmatrix} \begin{Bmatrix} j_{135} & s_{15} & t_{15} \\ \frac{1}{2} & j_{145} & c \end{Bmatrix} \\
&\times \begin{Bmatrix} \frac{1}{2} & j_{345} & t_{45} \\ b & \frac{1}{2} & a \end{Bmatrix} \begin{Bmatrix} t_{45} & j_{245} & s_{45} \\ \frac{1}{2} & j_{145} & b \end{Bmatrix}
\end{aligned}
$$

This completes the evaluation of $A^0_{\Gamma(2,3)}$.

3.3.2 Gauge variant observable: Fermion propagator

For the propagator we calculate one term of the expectation value of $\mathcal{O}_f{}^A_B(2,3) = \psi_2^A\ \bar{\psi}_{3B}$ in a particular gauge. For this observable, the term in the Feynman expansion (3.2.4) that we consider is

$$\begin{aligned}\mathcal{O}_b &= \ldots + (i\alpha)^9 \left(\int_{\mathcal{G}_\mathcal{D}} d\mu(\overline{\psi}_I,\ \psi_I)\right)\ \psi_2^A\ \bar{\psi}_{3B} \\ &\quad \times \overline{\psi}_{1C} D_{12}{}^C_D \psi_2^D\ \overline{\psi}_{2E} D_{21}{}^E_F \psi_1^F\ \overline{\psi}_{1G} D_{15}{}^G_H \psi_5^H\ \overline{\psi}_{5I} D_{51}{}^I_J \psi_1^J\ \overline{\psi}_{2K} D_{23}{}^K_L \psi_3^L \\ &\quad \times \overline{\psi}_{3M} D_{34}{}^M_N \psi_4^N\ \overline{\psi}_{4P} D_{43}{}^P_Q \psi_3^Q\ \overline{\psi}_{4R} D_{45}{}^R_S \psi_5^S\ \overline{\psi}_{5T} D_{54}{}^T_U \psi_4^U\ + \ldots, \end{aligned} \tag{3.3.12}$$

including the factor of 2 coming from the identical contribution of the S^2_{IJ} and S^2_{JI} terms.

Applying the graphical method gives the admissible graph $\Gamma'(2,3)$ corresponding to the above term in the Feynman expansion

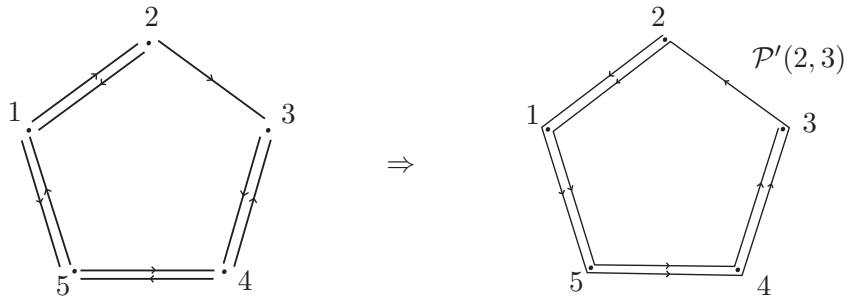

This gives a single path $\mathcal{P}'(2,3)$ of length $E_{\Gamma'(2,3)} = E_{\mathcal{P}'(2,3)} = 9$ passing through the vertices 2154321543. Performing the integration and contracting the indices as before gives the sign factor $\epsilon_{\Gamma(2,3)} = 1$ since there is no closed loop. The amplitude $I_{\Gamma'(2,3)}$ of the graph $\Gamma'(2,3)$ is given by

$$I_{\Gamma'(2,3)}{}^A_B = (i\alpha)^9 \left(D_{21} D_{15} D_{54} D_{43} D_{32} D_{21} D_{15} D_{54} D_{43}\right)^A_B . \tag{3.3.13}$$

This completes the fermionic integration, we can now consider the gravitational integration. As above, we will consider the $c = 0$ configuration $I^0_{\Gamma'(2,3)}$, which is obtained from the above expression by replacing the Dirac matrices D_{IJ} with the quantities $\Sigma_{IJ} U_{IJ}$.

We then choose the maximal gauge fixing tree T on Δ^* given by the set of edges $T = \{21, 15, 54, 43\}$.

We can now apply the graphical methods of section 3.2 to obtain the generating functional

and then the amplitude $A^0_{\Gamma'(2,3)}$ of the graph $\Gamma'(2,3)$ for the tree T. We obtain

$$\begin{aligned} A^0_{\Gamma'(2,3)} &= \left(\frac{\alpha}{4}\right)^9 \prod_{I<J<K} \sum_{j_{IJK}} \dim j_{IJK} (-1)^{2(j_{145}+j_{125}+j_{235}+j_{234}+j_{134})+1} \\ &\times \sum_{s_{23}} \dim s_{23} \\ &\times \Theta^3(j_{123})\Theta^4(j_{125})\Theta^2(j_{134})\Theta^4(j_{145})\Theta^3(j_{234})\Theta^2(j_{345}) \\ &\times A(j_{IJK}, s_{23}), \end{aligned} \tag{3.3.14}$$

where the amplitude $A(j_{IJK}, s_{23}) \in \mathbb{C}$ is obtained by evaluating the spin network diagram displayed below.

$A(j_{IJK}, s_{23}) =$

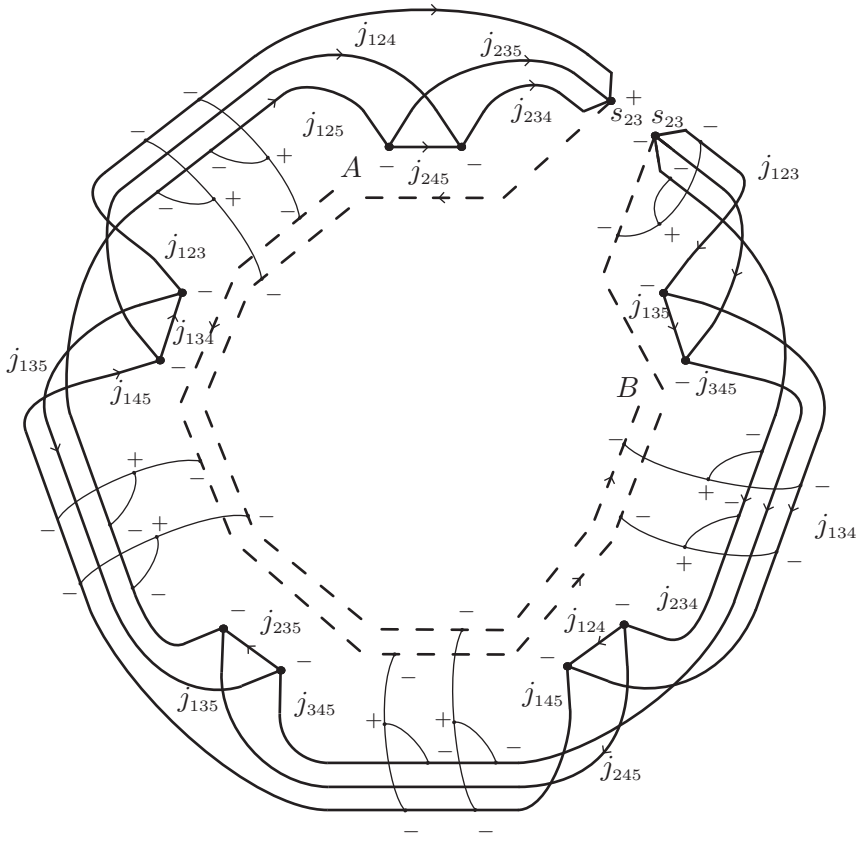

By Schur's Lemma, this will be proportional to the identity map δ^A_B in the fundamental representation multiplied by half the value of the closed spin network evaluation obtained by connecting the two open lines in the $j = 1/2$ representation. The closed diagram can then be recoupled and given as a combination of $6j$ symbols.

3.4 Conclusions

In this chapter, we have constructed spin foam models for various fermionic observables in 3d quantum gravity. The expectation values of the observables are given by a (potentially

large) sum over spin foams with either complex vertex amplitudes or several individual spin network diagrams. This illustrates the difficulties of computing things in theories with local degrees of freedom and is a problem that the 4d models will also face.

One may wonder if it is possible to extend the model to four dimensions. Unfortunately, coupling fermions in even dimensions requires an odd power of the frame field. The current 4d models are constructed by constraining the B field in BF theory to be of the form $B = e \wedge e$ so it is not possible to construct a similar model in 4d without using a constrained formalism [48].

A final remaining issue is the dependence on the triangulation. Unlike the Ponzano-Regge model, the fermionic coupled model is not invariant under Pachner moves. The introduction of local degrees of freedom means the model is no longer topological and something must be done in order to sum over the triangulations in a meaningful way. This which will be discussed for the pure partition function in the next chapter using group field theory.

Chapter 4

Wilson loops, geometric operators and fermions in 3d group field theory

4.1 Introduction

Group field theories (GFTs) provide a method for performing a perturbative sum over 2-complexes with weights that give a particular spin foam partition function evaluated on that 2-complex. In this way, GFTs are a proposal for solving the problem of triangulation dependence in spin foam models and simultaneously provide a method for topology change [4, 20, 49].

The first group field theory was written by Boulatov [50] and was a field theory whose Feynman diagrams were the Ponzano-Regge model evaluated on a 2-complex described by the Feynman graph. This was then extended to 4d BF theory by Ooguri [51]. In this chapter we will be concerned with the construction of a GFT for the spin foam model for 3d gravity coupled to fermions discussed in the last chapter. Other attempts to couple matter to GFTs include the point particles [52] (see also [53]). In an appropriate limit, these amplitudes give a non-commutative field theory [37] which can be cast in the form of a group field theory [54] by perturbing the Boulatov model.

We begin by introducing the Boulatov model and giving a brief overview of the main features of group field theories. To arrive at the fermionic GFT, we first consider Wilson loops and volume operators since these are the building blocks of the model. The Wilson loops require an extra argument in the fields to control the propagation of the loops and the volume operators will require the use of higher spin fields due to the nature of the operators involved. For illustrative purposes, we also include the "quenched" fermion model, which

neglects half of the loop configurations, as this contains all of the main features of the theory without having to include more complicated configurations of loops. We then describe the full GFT for the fermion model and briefly comment on its similarities and differences to the GFT for particles coupled to the Ponzano-Regge model.

4.2 The Boulatov model

A group field theory is constructed by specifying a field on some group manifold and some invariance properties. The pure gravity field [50] is defined as a map from three copies of SU(2) to the complex numbers

$$\phi(g_1, g_2, g_3) : SU(2) \times SU(2) \times SU(2) \to \mathbb{C} \tag{4.2.1}$$

We require that this is invariant under permutations σ of the group variables

$$\phi(g_1, g_2, g_3) = \phi(g_{\sigma(1)}, g_{\sigma(2)}, g_{\sigma(3)}) \tag{4.2.2}$$

and we make the field $SU(2)$ invariant

$$\phi(gg_1, gg_2, gg_3) = \phi(g_1, g_2, g_3) \;\; ; \; g \in \mathrm{SU(2)} \tag{4.2.3}$$

with the projector P_α

$$P_\alpha \phi(g_1, g_2, g_3) = \int_{SU(2)} d\alpha \; \phi(\alpha g_1, \alpha g_2, \alpha g_3) \tag{4.2.4}$$

With the field defined as above, we can write the action S_{GR} for the GFT whose Feynman diagrams produce Ponzano-Regge spin foams.

$$\begin{aligned} S_{\mathrm{GR}}[\phi, \lambda_{\mathrm{GR}}] = \frac{1}{2} \int \prod_{i=1}^{3} dg_i P_{\alpha_1} \phi(g_1, g_2, g_3) P_{\alpha_2} \phi(g_1, g_2, g_3) \\ + \frac{\lambda_{\mathrm{GR}}}{4} \int \prod_{i=1}^{6} dg_i P_{\alpha_1} \phi(g_1, g_2, g_3) P_{\alpha_2} \phi(g_1, g_5, g_6) P_{\alpha_3} \phi(g_2, g_4, g_6) P_{\alpha_4} \phi(g_3, g_4, g_5) \end{aligned}$$

The first term is called the propagator and the second the interaction term as it resembles and behaves like a ϕ^4 scalar field theory. Note that the combinatorics of the group variables in the interaction vertex is the same as for the spins in the 6j symbol. The idea is to construct a path integral weighted by this action and then consider its Feynman diagram expansion. To make the link to the Ponzano-Regge model clearer, we must first Fourier transform the field using the Peter-Weyl theorem.

$$\begin{aligned} P_\alpha \phi(g_1, g_2, g_3) \;\; = \;\; & \sum_{\substack{j_i, m_i, n_i, k_i \\ 1 \le i \le 3}} \int_{SU(2)} d\alpha \phi^{j_1 j_2 j_3}_{m_1 k_1 m_2 k_2 m_3 k_3} \sqrt{d_{j_1} d_{j_2} d_{j_3}} \\ & \times D^{j_1}_{m_1 n_1}(g_1) D^{j_2}_{m_2 n_2}(g_2) D^{j_3}_{m_3 n_3}(g_3) \\ & \times \; D^{j_1}_{n_1 k_1}(\alpha) D^{j_2}_{n_2 k_2}(\alpha) D^{j_3}_{n_3 k_3}(\alpha) \end{aligned}$$

With $m_i, k_i, n_i = -j, ..., j$. Performing the group integrals reduces this to

$$\begin{aligned} P_\alpha \phi(g_1, g_2, g_3) &= \sum_{\substack{j_i, m_i, n_i, k_i \\ 1 \leq i \leq 3}} \psi^{j_1 j_2 j_3}_{m_1 m_2 m_3} \sqrt{d_{j_1} d_{j_2} d_{j_3}} \\ &\quad \times D^{j_1}_{m_1 n_1}(g_1) D^{j_2}_{m_2 n_2}(g_2) D^{j_3}_{m_3 n_3}(g_3) C^{j_1 j_2 j_3}_{n_1 n_2 n_3} \end{aligned} \tag{4.2.5}$$

Where $C^{j_1 j_2 j_3}_{k_1 k_2 k_3}$ is a three-valent $SU(2)$ intertwiner and we have redefined the coefficients as

$$\psi^{j_1 j_2 j_3}_{m_1 m_2 m_3} = \psi^{j_1 j_2 j_3}_{m_1 k_1 m_2 k_2 m_3 k_3} C^{j_1 j_2 j_3}_{k_1 k_2 k_3}. \tag{4.2.6}$$

This can be performed for each of the fields in S_{GR} the results of which are most easily seen graphically.

4.2.1 Feynman amplitudes

We can now consider the partition function for the theory and express it in terms of the Feynman diagram expansion. The expansion will implement a sum over 2-complexes.

$$Z = \int \mathcal{D}\phi e^{-S_{\mathrm{W}}[\phi, \lambda_{\mathrm{GR}}]} = \sum_{\Gamma} \frac{\lambda_{\mathrm{GR}}^{v_{\mathrm{GR}}[\Gamma]}}{\mathrm{sym}(\Gamma)} Z[\Gamma]. \tag{4.2.7}$$

Here Γ denotes a particular Feynman diagram in this sum. The number of vertices in Γ is denoted $v_{\mathrm{GR}}[\Gamma]$ and the symmetry factor of the diagram is written as $\mathrm{sym}(\Gamma)$. Each term $Z[\Gamma]$ in the sum gives the Ponzano-Regge partition function Z_{PR} (as given in chapter 1) evaluated on the 2-complex defined by Γ.

The Feynman rules for the GFT are as follows. The propagator terms gives the following

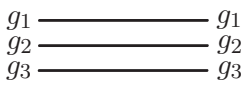

and the interaction vertex

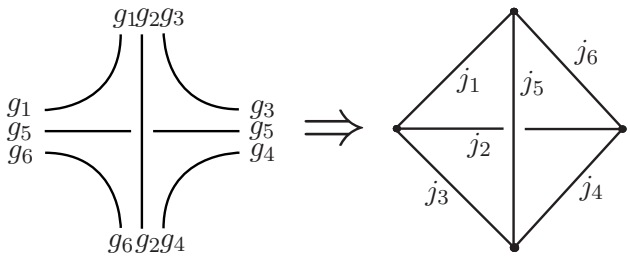

So we see that the Feynman diagram expansion gives a perturbative sum over 2-complexes, there will be some diagrams that give degenerate triangulations. Since the interaction vertex has a 6j symbols associated to it the weight assigned to the whole Feynman diagram is the Ponzano-Regge partition function. As in standard perturbative quantum field theory, the individual Feynman diagrams may require regularisation.

Degenerate contributions

An important consideration is the type of complexes obtained in the Feynman expansion of a GFT. One might wish that the sum would only contain non-degenerate simplicial manifolds (i.e. each tetrahedron can only meet another tetrahedron on a single face) but the GFT obviously includes degenerate contributions. For example the vacuum diagram with two vertices joined together corresponds to the pseudo-triangulation of the 3-sphere with two tetrahedra. The Ponzano-Regge model may still be well defined for all of these diagrams (after regularisation/gauge fixing.)

One way to remove some of these diagrams is to include a colouring of the field [55, 56] which restricts the type of diagrams allowed or to impose that the field is Grassmann valued [55]. This remains an important current issue as for the semiclassical limit of the theory to be correct we should obtain smooth manifolds in some limit.

4.2.2 Current issues in group field theory

Now that we have given a brief overview of the construction of a simple group field theory, there are some other issues and developments in the literature that are worth mentioning. We will not address any of these issues here.

Firstly, it was pointed out in [57] that any local spin foam model, i.e. one whose amplitudes depend only on the simplex it is associated to and any subsimplices, can be expressed as a GFT with an appropriate choice of field and invariance properties. In particular, the Barrett-Crane spin foam model was expressed as a GFT in [58, 59].

The Boulatov model, and most other GFTs, have been considered as functions of a group variable, i.e. the connection. There have been some suggestions on how to include the frame field in the formalism [60, 61](and references therein) or to make the field a function of just the frame field with a suitable transformation.

Recently GFTs have been considered from the point of view of constructive field theory. The scaling properties of the amplitudes with a cutoff were examined in [56, 62]. An earlier attempt to control the convergence of the Boulatov model was the insertion of an additional term in the action [63].

4.3 Wilson loops

We now define a GFT for 3d Euclidean gravity with Wilson loops. The Feynman diagrams of this field theory will give Ponzano-Regge spin foam models with Wilson loop observables

[64]. In fact, the GFT will give all possible Wilson loops in the spin foam so in itself is unlikely to be physically interesting. However, it will be useful for defining the matter coupling. For the Ponzano-Regge model defined on a triangulation Δ, the Wilson loop observable $\mathcal{O}^J_{\mathcal{W}}$ is defined as the trace in the representation J of the holonomy around a closed loop $\mathcal{W}$ in the dual triangulation $\Delta*$

$$\mathcal{O}^J_{\mathcal{W}} = \mathrm{tr}^J(\overrightarrow{\prod_{e\in\mathcal{W}}} g_e). \tag{4.3.1}$$

The expectation value of $\mathcal{O}^J_{\mathcal{W}}$ is then given by

$$\langle \mathcal{O}^J_{\mathcal{W}} \rangle_{\mathrm{PR}}(\Delta) = \int_{SU(2)} \prod_e dg_e \; \mathcal{O}^J_{\mathcal{W}} \; \prod_f \delta\left(G_f\right). \tag{4.3.2}$$

Recall that the group variables g_e represent SU(2) holonomies along dual edges e of Δ, $G_f = \overrightarrow{\prod_{e\in f}} g_e$ is the ordered product of holonomies around a dual face f of Δ. Instead of the usual 6j symbol, the spin network vertex amplitudes for the model will contain an extra edge in the spin J representation at any vertex that is traversed by the Wilson loop.

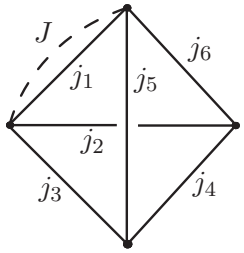

We can now define the GFT for a Wilson loop observable. Since the GFT sums over 2-complexes, we will in fact create all possible Wilson loops at each value of the GFT expansion parameter. This will include disjoint loops so from now on we use $\tilde{\mathcal{W}}$ to denote a configuration of any number of Wilson loops. Unless the loop configuration $\tilde{\mathcal{W}}$ completely saturates the spin foam, we will also require vertex amplitudes for those vertices that are not part of the loop.

To include the Wilson loops, we define an additional field ψ with an extra argument

$$\psi(g_1, g_2, g_3; g) : SU(2) \times SU(2) \times SU(2) \times SU(2) \to \mathbb{C} \tag{4.3.3}$$

This extra variable g will control the way the Wilson loop propagates throughout the 2-complex. We project the additional argument of the field onto the representation J specified by the Wilson loop with the following projector

$$\psi^J(g_1, g_2, g_3; g) = (P^J\psi)(g_1, g_2, g_3; g) = \int_{SU(2)} dh \; d_J \chi^J(gh^{-1})\psi(g_1, g_2, g_3; h) \tag{4.3.4}$$

where $d_J = 2J+1$ is the dimension of the irreducible representation J and χ^J is the character. We also demand that the field is $SU(2)$ invariant by projecting

$$P_\alpha \psi(g_1, g_2, g_3; g) = \int_{SU(2)} d\alpha \; \psi(g_1\alpha, g_2\alpha, g_3\alpha; g\alpha), \tag{4.3.5}$$

this will create the four-valent intertwiners in the Wilson loop vertex amplitudes. Finally, we demand permutation symmetry on the first three arguments.

$$\psi(g_1, g_2, g_3; g) = \psi(g_{\sigma(1)}, g_{\sigma(2)}, g_{\sigma(3)}; g) \tag{4.3.6}$$

We can use the Peter-Weyl theorem to perform a Fourier decomposition of the fields

$$\begin{aligned} P_\alpha \psi^J(g_1, g_2, g_3; g) \;=\; & \sum_{\substack{j_i, m_i, n_i, k_i, a, b \\ 1 \le i \le 4}} \int_{SU(2)} d\alpha \int_{SU(2)} dh \; \psi^{j_1 j_2 j_3 j_4}_{m_1 k_1 m_2 k_2 m_3 k_3 m_4 k_4} \sqrt{d_{j_1} d_{j_2} d_{j_3} d_{j_4}} \\ & \times D^{j_1}_{m_1 n_1}(g_1) D^{j_2}_{m_2 n_2}(g_2) D^{j_3}_{m_3 n_3}(g_3) D^{j_4}_{m_4 n_4}(h) \\ & \times \; D^{j_1}_{n_1 k_1}(\alpha) D^{j_2}_{n_2 k_2}(\alpha) D^{j_3}_{n_3 k_3}(\alpha) D^{j_4}_{n_4 k_4}(\alpha) \\ & \times \; D^J_{ab}(g) D^J_{ba}(h^{-1}) \end{aligned} \tag{4.3.7}$$

Performing the group integrals reduces this to

$$\begin{aligned} P_\alpha \psi^J(g_1, g_2, g_3; g) \;=\; & \sum_{\substack{j_i, m_i, n_i, k_i, s \\ 1 \le i \le 4}} \psi^{j_1 j_2 j_3 J s}_{m_1 m_2 m_3 m_4} \sqrt{d_{j_1} d_{j_2} d_{j_3} d_J} \\ & \times D^{j_1}_{m_1 n_1}(g_1) D^{j_2}_{m_2 n_2}(g_2) D^{j_3}_{m_3 n_3}(g_3) D^J_{m_4 n_4}(g) C^{j_1 j_2 j_3 J s}_{n_1 n_2 n_3 n_4} \end{aligned} \tag{4.3.8}$$

Where $C^{j_1 j_2 j_3 J \; s}_{k_1 k_2 k_3 k_4}$ is a four valent $SU(2)$ intertwiner labelled by s and we have redefined the coefficients as

$$\psi^{j_1 j_2 j_3 J s}_{m_1 m_2 m_3 m_4} = \sum_{k_1, k_2, k_3, k_4} \psi^{j_1 j_2 j_3 J}_{m_1 k_1 m_2 k_2 m_3 k_3 m_4 k_4} C^{j_1 j_2 j_3 J s}_{k_1 k_2 k_3 k_4} \tag{4.3.9}$$

We define the action as a functional of the two fields to be

$$S_{\rm W}[\phi, \psi^J, \lambda_{\rm GR}, \lambda_{\rm W}] = S_{\rm GR}[\phi, \lambda_{\rm GR}] + \frac{1}{2} \int \prod_{i=1}^{3} dg_i P_\alpha \psi^J(g_1, g_2, g_3; g) P_\alpha \psi^J(g_1, g_2, g_3; g)$$

$$+ \frac{\lambda_{\rm W}}{4} \int \prod_{i=1}^{6} dg_i \; dg P_{\alpha_1} \psi^J(g_1, g_2, g_3; g) P_{\alpha_2} \psi^J(g_1, g_5, g_6; g) P_{\alpha_3} \phi(g_2, g_4, g_6) P_{\alpha_4} \phi(g_3, g_4, g_5)$$

With this action we can now compute the propagators and vertex amplitudes of the theory.

4.3.1 Feynman amplitudes

We can now consider the partition function for the theory and express it in terms of the Feynman diagram expansion. The expansion will implement a sum over 2-complexes and

Wilson loop configurations on each 2-complex.

$$Z = \int \mathcal{D}\psi^J \mathcal{D}\phi e^{-S_{\rm W}[\phi,\psi^J,\lambda_{\rm GR},\lambda_{\rm W}]} = \sum_{\Gamma} \frac{\lambda_{\rm GR}^{v_{\rm GR}[\Gamma]} \lambda_{\rm W}^{v_{\rm W}[\Gamma]}}{\rm sym(\Gamma)} Z[\Gamma]. \tag{4.3.10}$$

Here Γ denotes a particular Feynman diagram in this sum. The number of pure gravity vertices in Γ is denoted $v_{\rm GR}[\Gamma]$, the number of Wilson loop vertices is $v_{\rm W}[\Gamma]$ and the symmetry factor of the diagram is written as $\rm sym(\Gamma)$. Each term $Z[\Gamma]$ in the sum gives the spin foam partition function evaluated on the 2-complex defined by Γ.

The Feynman rules for the GFT are as follows. There are two propagators, the pure gravity propagator and one with an extra delta function that determines the path of the Wilson loop.

Similarly, there are two vertex amplitudes corresponding to a vertex that is not intersected by a loop and one that is.

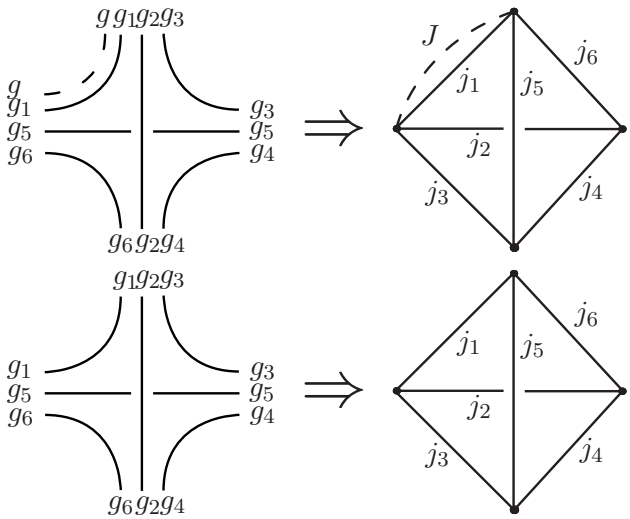

Note that for a fixed $v_{\rm GR}$, $v_{\rm W}$ is the number of dual vertices traversed by the Wilson loops. Special cases include $v_{\rm W} = 0$ which corresponds to a pure partition function without observables and $v_{\rm GR} = 0$ which contains all possible Wilson loops that completely saturate the spin foam.

4.4 Geometric operators

The geometric operators we consider here are constructed from polynomials of the discrete frame field used in the construction of 3d spin foams. Expectation values of these operators

can be computed using the technique of generating functionals [46] and result in so called grasping operators acting on the spin network vertex amplitudes. In particular, we will consider the volume operator although others can be constructed in a similar fashion. There are different ways in which to construct a quantum mechanical volume operator in terms of the frame fields which are equivalent classically. These have been studied in detail in [65]. For a tetrahedron, t, we define the volume operator $\mathcal{V}_t$ to be

$$\mathcal{V}_t = \sum_{w_1,w_2,w_3} \epsilon_{IJK}\, e^I_{w_1} e^J_{w_2} e^K_{w_3}. \tag{4.4.1}$$

The e^I_w are the discrete frame fields associated to each wedge w of Δ^+ and carry an SU(2) Lie algebra index. The summation is over all triples of edges w_1, w_2, w_3 in t that give a non-zero volume. To compute expectation values of this type of observable, one introduces $\mathfrak{su}(2)$ valued sources J_w on each wedge w and defines the generating functional $Z[J_w]$ to be

$$\mathcal{Z}[J_w] = \prod_{\overline{e}} \int_{\mathrm{SU}(2)} dg_{\overline{e}} \prod_w \int_{\mathfrak{su}(2)} de_w \ \exp\left(i \sum_w \mathrm{Tr}\, e_w \left(G_w + J_w\right)\right). \tag{4.4.2}$$

The (unnormalised) expectation value of the volume operator can then be computed using

$$\begin{aligned}\langle \mathcal{V}_t \rangle_{\mathrm{GR}}(\Delta) &= \prod_{\overline{e}} \int_{\mathrm{SU}(2)} dg_{\overline{e}} \prod_w \int_{\mathfrak{su}(2)} de_w \sum_{w_1,w_2,w_3} \epsilon_{IJK} e^I_{w_1} e^J_{w_2} e^K_{w_3} \ \exp\left(i \sum_w \mathrm{Tr}\, e_w G_w \right) \\ &= i \left(\sum_{w_1,w_2,w_3} \epsilon_{IJK} \frac{\delta}{\delta J^I_{w_1}} \frac{\delta}{\delta J^J_{w_2}} \frac{\delta}{\delta J^K_{w_3}} \right) Z[J_w] \Big|_{J_w=0}. \end{aligned} \tag{4.4.3}$$

The source derivations insert Lie algebra generators into the appropriate edges of the 6j symbol which are then contracted with ϵ_{IJK}. Remembering that ϵ_{IJK} is an intertwiner between three vector representations, then, up to some normalisation factors, the resulting spin network vertex amplitudes will be of the form

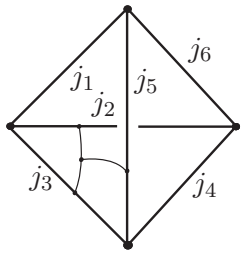

The GFT: We begin by observing that the grasping operation cannot be implemented simply as a projector on the standard Boulatov GFT as the grasping would be non-local in the fields. We resolve this problem by considering vector fields on SU(2). With an appropriate invariance property, this will allow us to construct the graspings by contracting

with the index of the field. We begin by defining a vector field on three copies of SU(2)

$$\phi_a(g_1, g_2, g_3) : \mathrm{SU}(2) \times \mathrm{SU}(2) \times \mathrm{SU}(2) \to \mathbb{V}_1 \tag{4.4.4}$$

Where $\mathbb{V}_1$ is the $j = 1$ SU(2) representation space and a is an index with values $1, 2, 3$. In order to create the necessary intertwiners, we use the following projector on the field

$$\tilde{P}_{\alpha,\beta}\phi_a(g_1, g_2, g_3) = \int_{SU(2)} d\alpha \; d\beta \; D^1_{ab}(\beta)\phi_b(g_1\alpha, g_2\alpha, g_3\beta\alpha^{-1}\beta). \tag{4.4.5}$$

Note that with this projection, the field satisfies the following $SU(2)$ invariance property

$$D^1_{ab}(h)\tilde{P}_{\alpha,\beta}\phi_b(g_1h, g_2h, g_3h) = \tilde{P}_{\alpha,\beta}\phi_a(g_1, g_2, g_3). \tag{4.4.6}$$

We also require the invariance under permutations σ of the group variables by summing over permutations of the field arguments

$$\phi_a(g_1, g_2, g_3) = \sum_\sigma \phi_a(g_{\sigma(1)}, g_{\sigma(2)}, g_{\sigma(3)}). \tag{4.4.7}$$

The mode expansion of this field is then

$$\begin{aligned}\tilde{P}_{\alpha,\beta}\phi_a(g_1, g_2, g_3) = &\sum_{\substack{j_i, m_i, n_i, k_i, p_3, q_3, b \\ 1\le i\le 3}} \phi^{j_1 j_2 j_3}_{m_1 k_1 m_2 k_2 m_3 k_3 b}\sqrt{d_{j_1} d_{j_2} d_{j_3}} D^{j_1}_{m_1 n_1}(g_1) D^{j_2}_{m_2 n_2}(g_2) D^{j_3}_{m_3 n_3}(g_3) \\ &\times \int_{SU(2)} d\alpha \; D^{j_1}_{n_1 k_1}(\alpha) D^{j_2}_{n_2 k_2}(\alpha) D^{j_3}_{p_3 q_3}(\alpha^{-1}) \int_{SU(2)} d\beta \; D^{j_3}_{n_3 p_3}(\beta) D^{j_3}_{q_3 k_3}(\beta) D^1_{ab}(\beta).\end{aligned}$$

Which reduces to

$$\begin{aligned}\tilde{P}_{\alpha,\beta}\phi_a(g_1, g_2, g_3) \;\; = \;\; &\sum_{\substack{j_i, m_i, n_i, q_3, b \\ 1\le i\le 3}} \tilde{\phi}^{j_1 j_2 j_3}_{m_1 m_2 m_3}\sqrt{d_{j_1} d_{j_2} d_{j_3}} C^{j_1 j_2 j_3}_{n_1 n_2 q_3} C^{j_3 j_3 1}_{n_3 q_3 a} \\ &\times D^{j_1}_{m_1 n_1}(g_1) D^{j_2}_{m_2 n_2}(g_2) D^{j_3}_{m_3 n_3}(g_3),\end{aligned} \tag{4.4.8}$$

where the modes have been redefined as

$$\tilde{\phi}^{j_1 j_2 j_3}_{m_1 m_2 m_3} = \sum_{\substack{k_i, p_3, b \\ 1\le i\le 3}} \phi^{j_1 j_2 j_3}_{m_1 k_1 m_2 k_2 m_3 k_3 b} C^{j_1 j_2 j_3}_{k_1 k_2 p_3} C^{j_3 j_3 1}_{p_3 k_3 b} \tag{4.4.9}$$

With this new field, we define the action for the GFT that has a volume grasping on every vertex amplitude.

$$\begin{aligned}S_{\mathrm{VOL}}[\phi, \lambda_{\mathrm{VOL}}] = &\frac{1}{2}\int \prod_{i=1}^{3} dg_i P_{\alpha_1}\phi(g_1, g_2, g_3) P_{\alpha_2}\phi(g_1, g_2, g_3) \\ &+ \frac{1}{2}\int \prod_{i=1}^{3} dg_i \tilde{P}_{\alpha_1,\beta_1}\phi_a(g_1, g_2, g_3)\tilde{P}_{\alpha_2,\beta_2}\phi_b(g_1, g_2, g_3)\delta_{ab} \\ +\frac{\lambda_{\mathrm{VOL}}}{4}\int \prod_{i=1}^{6} dg_i \tilde{P}_{\alpha_1,\beta_1}\phi_a(g_1, g_2, g_3)\tilde{P}_{\alpha_2,\beta_2}\phi_b(g_1, g_5, g_6)\tilde{P}_{\alpha_3,\beta_3}\phi_c(g_2, g_4, g_6) &P_{\alpha_4}\phi(g_3, g_4, g_5)\, \epsilon_{abc}\end{aligned}$$

Feynman rules: The partition function and its Feynman diagram expansion is

$$Z = \int \mathcal{D}\phi_a \mathcal{D}\phi e^{-S_{\text{VOL}}[\phi,\phi_a,\lambda_{\text{VOL}}]} = \sum_{\Gamma} \frac{\lambda_{\text{VOL}}^{v_{\text{VOL}}[\Gamma]}}{\text{sym}(\Gamma)} Z[\Gamma]. \tag{4.4.10}$$

With $v_{\text{VOL}}[\Gamma]$ giving the number of vertices of Γ. There are two propagators for the theory, one for the pure gravity field and one between the grasped fields.

There is a single vertex that is formed by the interaction of three grasping fields with one pure gravity. The dotted lines connect with the vector field propagator while the gravity fields use the usual propagator, note that this means the vector field cannot propagate to the gravity field.

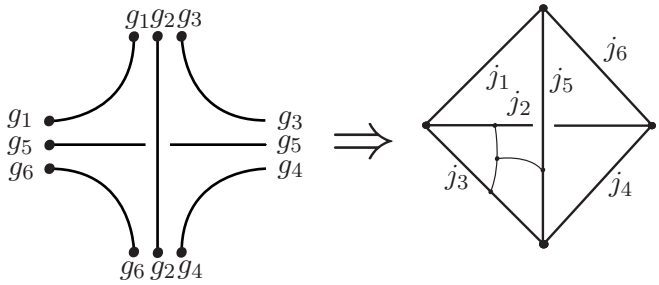

Note that due to the form of the vertex, the Feynman diagram expansion will not produce all 2-complexes but a subset of them. We ignore this issue as we are only considering S_{VOL} as a stepping stone to construction of the fermionic model. However, were we to consider a coloured group field theory, this would not be an issue as the complexes would be the same as the coloured Boulatov model. Since we have imposed the permutation symmetry on the field, we will obtain all possible graspings on the tetrahedral spin network. These different graspings are described in [65].

4.5 Fermions

Using the techniques above, it will now be possible to write the GFT whose Feynman diagrams give fermion fields coupled to 3d spin foam gravity. When one is considering just the partition function, there is an easier way to perform the Berezin integrals that will make constructing the GFT easier. [36]

4.5.1 Massless Fermions in 3d gravity

We will perform the integration over the simplicial fermion fields as in [36], by changing the variables to symplectic Majorana fermions.

We define the new variables as

$$\begin{aligned} \phi_1^A &= \tfrac{1}{2}(\epsilon^{AB}\overline{\psi}_B + i\psi^A), \quad \overline{\phi}_{1A} = \tfrac{1}{2}(-\psi^B\epsilon_{BA} - i\overline{\psi}_A) \\ \phi_2^A &= -\tfrac{i}{2}(\epsilon^{AB}\overline{\psi}_B - i\psi^A), \quad \overline{\phi}_{2A} = \tfrac{i}{2}(-\psi^B\epsilon_{BA} + i\overline{\psi}_A) \end{aligned} \tag{4.5.1}$$

these satisfy the relations

$$\begin{aligned} \phi_1^A &= -\epsilon^{AB}\overline{\phi}_{2B} \\ \phi_2^A &= \epsilon^{AB}\overline{\phi}_{1B}. \end{aligned}$$

The useful property of these variables is that the action splits into two independent components that depend only on one family of Majorana spinors

$$\begin{aligned} S_{\rm D}[\mathbf{e}_w, g_e, \overline{\psi}_v, \psi_v] &= \frac{1}{8}\sum_{or(e)}\sum_e \overline{\psi}_{s(e)A} D_e{}^A{}_B \psi^B_{t(e)} \\ &= -i(S_{\rm M}[\mathbf{e}_w, g_e, \phi_{1v}] + S_{\rm M}[\mathbf{e}_w, g_e, \phi_{2v}]) \end{aligned} \tag{4.5.2}$$

where $S_{\rm M}$ is the action for a single family of Majorana fermions and is given by

$$S_{\rm M} = \frac{1}{8}\sum_{or(e)}\sum_e \phi^A_{s(e)} D_{e\ AB} \phi^B_{s(e)} \tag{4.5.3}$$

This allows the two families to be treated separately and results in two independent loop configurations. The partition function is then given by

$$\mathcal{Z}_{\rm GR\ +D}(\Delta) = \sum_{\mathcal{L}_1,\mathcal{L}_2}\prod_{\overline{e}}\int_{\rm SU(2)} dg_{\overline{e}} \prod_w \int_{\mathfrak{su}(2)} dw_w \left(\prod_{\ell_i\in\mathcal{L}_1}\mathcal{D}_{\ell_i}\right)\left(\prod_{\ell_j\in\mathcal{L}_2}\mathcal{D}_{\ell_j}\right) \exp(S_{\rm GR})$$

In fact, the spin foam model in [36] considered massive fermions and the integration over the Grassmann valued fermion fields was performed by using a hopping parameter expansion in the inverse fermion mass to calculate the Pfaffian of the Dirac matrix defining the action (equation (43) of [36]). The massless case can be obtained directly from the Grassmann integration, i.e. by repeated use of equation (46) of [36] without the volume term, and one obtains the sum over loop configurations given above. Alternatively, using the hopping parameter expansion, if one considers the limit in which the mass parameter is small then the highest order term in the expansion dominates. This is the term Γ_n in equation (50) of [36] which again gives the sum over loop configurations described above. There are two different configurations of loops in the spin foam since it is actually the Pfaffian squared which appears in the path integral.

We will make a simplification to the model before constructing the GFT and neglect the second the second term in D_e, i.e. we will consider only the $c_\Gamma = 0$ configuration. Including the other configurations is not any more difficult but will require many more vertex amplitudes. Up to symmetry, the different vertex amplitudes that we will consider are shown in figure 4.1.

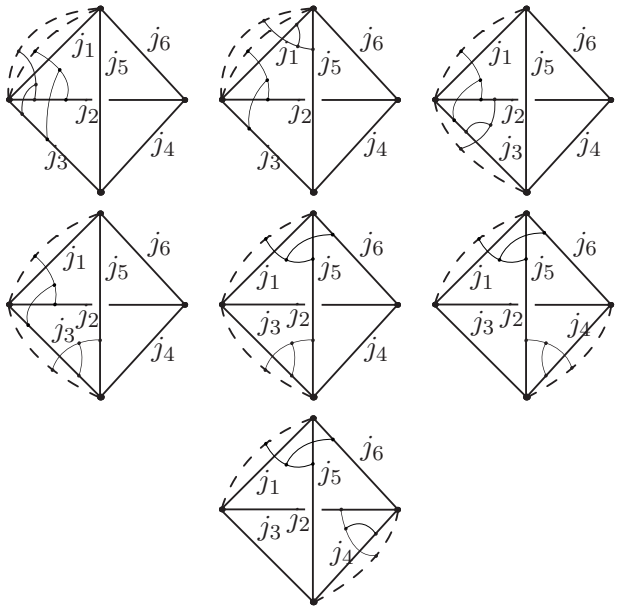

Figure 4.1: Spin network diagrams for the different possible vertex amplitudes for the fermion spin foam model. The dashed lines are in the spin half representation and the curved lines denote the grasping operators in the spin one representation.

The "quenched" model

In the calculation of a fermionic observable, an approximation can be made that neglects one of the fermionic loops, say $\mathcal{L}_2$. This would correspond to considering a single symplectic majorana fermion in [36]. There is then only one type of vertex amplitude

$$\mathcal{A}(\mathcal{L}_1) = \tag{4.5.4}$$

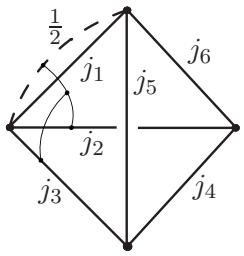

We can understand this as describing a fermion (the spin half line) entering a tetrahedron through one triangle, which is acted on by a grasping operator, then leaving through a different triangle. For clarity we first describe the GFT for this model before moving onto the more complicated configurations possible when there are two fermionic loop configurations involved. We will require three different fields to construct the vertex amplitude:

- The pure gravity field ϕ defined in Section 4.3 and obeying the same symmetries.

$$\phi(g_1, g_2, g_3) : SU(2) \times SU(2) \times SU(2) \to \mathbb{C} \tag{4.5.5}$$

- A Wilson loop field that has been projected to the spin half representation.

$$\psi^{\frac{1}{2}}(g_1,g_2,g_3;g) = (P^{\frac{1}{2}}\psi)(g_1,g_2,g_3;g) : SU(2)\times SU(2)\times SU(2)\times SU(2) \to \mathbb{C} \quad (4.5.6)$$

  This corresponds to the fermion leaving the tetrahedron.

- A final field that contains the grasping operator between the fermion line and the vertex at its source. The field has three free spin one indices

$$\xi_{abc}(g_1,g_2,g_3;g) : SU(2)\times SU(2)\times SU(2)\times SU(2) \to \mathbb{V}_1\otimes\mathbb{V}_1\otimes\mathbb{V}_1, \quad (4.5.7)$$

  the fourth argument of the field is projected to the spin half representation

$$\xi^{\frac{1}{2}}_{abc}(g_1,g_2,g_3;g) = (P^{\frac{1}{2}}\xi_{abc})(g_1,g_2,g_3;g) \quad (4.5.8)$$

  and the following projection will provide the necessary graspings

$$\begin{aligned}(\hat{P}_{\beta_1\beta_2\beta_3\alpha}\xi^{\frac{1}{2}}_{abc})(g_1,g_2,g_3;g) &= \int_{SU(2)}\prod_{i=1}^{3} d\beta_i d\alpha D^1_{ad}(\beta_1)D^1_{be}(\beta_2)D^1_{cf}(\beta_3)\\ &\quad\times\xi^{\frac{1}{2}}_{def}(g_1\alpha, g_2\beta_1\alpha^{-1}\beta_1, g_3\beta_2\alpha^{-1}\beta_2; g\beta_3\alpha^{-1}\beta_3)\end{aligned}$$

  We also allow the field to be unchanged under permutations σ of the first three arguments

$$\xi_{abc}(g_1,g_2,g_3;g) = \xi_{abc}(g_{\sigma(1)},g_{\sigma(2)},g_{\sigma(3)};g) \quad (4.5.9)$$

  This field describes the fermion entering the tetrahedron and grasping the appropriate triangle.

We can see that the action must now be constructed so that the fields appear in the correct configuration to describe a fermion entering and leaving the tetrahedron. The mode expansions for $\phi, \psi^{\frac{1}{2}}$ are given above and the expansion for the quenched fermionic field $\xi^{\frac{1}{2}}_{abc}$ into modes $\left(\xi^{j_1j_2j_3\frac{1}{2}}_{m_1k_1m_2k_2m_3k_3m_4k_4}\right)_{def}$ gives

$$\begin{aligned}(\hat{P}_{\beta_1\beta_2\beta_3\alpha}\xi^{\frac{1}{2}}_{abc})(g_1,g_2,g_3;g) = &\sum_{\substack{j_1,j_2,j_3,m_i,n_i,q_2,q_3,q_4,s\\ 1\le i\le 4}} \xi^{j_1j_2j_3\frac{1}{2}s}_{m_1m_2m_3m_4}\sqrt{d_{j_1}d_{j_2}d_{j_3}d_{\frac{1}{2}}}\\ &\times C^{j_2j_21}_{n_2q_2a}C^{j_3j_31}_{n_3q_3b}C^{\frac{1}{2}\frac{1}{2}1}_{n_4q_4c}C^{j_1j_2j_3\frac{1}{2}s}_{n_1q_2q_3q_4}D^{j_1}_{m_1n_1}(g_1)D^{j_2}_{m_2n_2}(g_2)D^{j_3}_{m_3n_3}(g_3)D^{\frac{1}{2}}_{m_4n_4}(g).\end{aligned}$$

with the following redefinition of the modes

$$\xi^{j_1j_2j_3s\frac{1}{2}}_{m_1m_2m_3m_4} = \sum_{\substack{k_i,p_2,p_3,p_4,d,e,f\\ 1\le i\le 4}}\left(\xi^{j_1j_2j_3\frac{1}{2}}_{m_1k_1m_2k_2m_3k_3m_4k_4}\right)_{def}C^{j_2j_21}_{p_2k_2d}C^{j_3j_31}_{p_3k_3e}C^{\frac{1}{2}\frac{1}{2}1}_{p_4k_4f}C^{j_1j_2j_3\frac{1}{2}s}_{k_1p_2p_3p_4}.$$

The action for the theory is given by

$$S_{\rm Q}[\phi,\psi,\xi,\lambda_{\rm Q}] = \frac{1}{2}\int\prod_{i=1}^{3} dg_i dg\ P_{\alpha_1}\psi^{\frac{1}{2}}(g_1,g_2,g_3;g)\ P_{\alpha_2}\xi^{\frac{1}{2}}_{abc}(g_1,g_2,g_3;g)\ \epsilon_{abc}$$
$$+\frac{1}{2}\int\prod_{i=1}^{3} dg_i P_{\alpha_1}\phi(g_1,g_2,g_3)\ P_{\alpha_2}\phi(g_1,g_2,g_3)$$
$$+\frac{\lambda_{\rm Q}}{4}\int\prod_{i=1}^{6} dg_i dg\ (\hat{P}_{\beta_1\beta_2\beta_3\alpha_1}\xi^{\frac{1}{2}}_{abc})(g_1,g_2,g_3;g)\ P_{\alpha_2}\psi^{\frac{1}{2}}(g_1,g_5,g_6;g)\ P_{\alpha_3}\phi(g_2,g_4,g_6)\ P_{\alpha_4}\phi(g_3,g_4,g_5)\ \epsilon_{abc}$$

Feynman rules: The partition function for the theory is

$$Z = \int \mathcal{D}\psi^{\frac{1}{2}}\mathcal{D}\phi\prod_{a,b,c=1}^{3}\mathcal{D}\xi^{\frac{1}{2}}_{abc}e^{-S_{\rm Q}[\phi,\psi^{\frac{1}{2}},\xi^{\frac{1}{2}}_{abc},\lambda_{\rm Q}]} = \sum_{\Gamma}\frac{\lambda_{\rm Q}^{v_{\rm Q}[\Gamma]}}{\mathrm{sym}(\Gamma)}Z[\Gamma]. \tag{4.5.10}$$

As before, $v_{\rm Q}[\Gamma]$ denotes the number of vertices in the diagram. In this case, the Feynman rules are more specific about the direction of propagation of the fermions throughout the 2-complex. To represent this, we orient the fermion (dashed) lines and demand that the orientation is consistent within each diagram. The propagators are given by

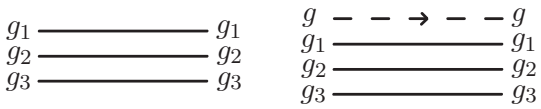

The single vertex and corresponding amplitude of the quenched model is

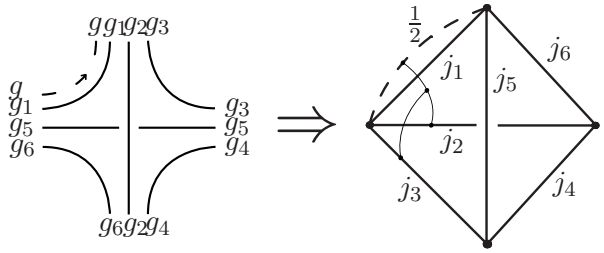

The unquenched model

We now construct the full GFT for massless fermions coupled to 3d gravity. All of the important features of the model are contained in the quenched case, all that remains are the additional complications caused by the inclusion of two independent loop configurations instead of one. As one can see from the fermionic vertex amplitudes illustrated above, we must provide a different interaction vertex for each possible configuration and orientation. We will omit some of the detail as it is essentially the same as the quenched case and the complications involved are unenlightening. We begin by defining the fields

- The pure gravity field ϕ defined in Section 4.3 and obeying the same symmetries.

$$\phi(g_1, g_2, g_3) : SU(2)^3 \to \mathbb{C} \tag{4.5.11}$$

- A Wilson loop field that has been projected to the spin half representation and corresponding to a fermion leaving the tetrahedron through a triangle

$$\psi^{\frac{1}{2}}(g_1, g_2, g_3; g) = (P^{\frac{1}{2}}\psi)(g_1, g_2, g_3; g) : SU(2)^4 \to \mathbb{C} \tag{4.5.12}$$

- A field containing two Wilson loops corresponding to the ends of two fermion lines at a triangle

$$\psi_2(g_1, g_2, g_3; g, f) = SU(2)^5 \to \mathbb{C} \tag{4.5.13}$$

Both Wilson lines are projected to the spin half representation

$$\begin{aligned} \psi_2^{\frac{1}{2},\frac{1}{2}}(g_1, g_2, g_3; g, f) &= \int_{SU(2)} dh_1 \; d_{\frac{1}{2}}\chi^{\frac{1}{2}}(gh_1^{-1}) \int_{SU(2)} dh_2 \; d_{\frac{1}{2}}\chi^{\frac{1}{2}}(fh_2^{-1}) \\ &\quad \times \psi_2(g_1, g_2, g_3; h_1, h_2), \end{aligned} \tag{4.5.14}$$

and the field has the usual invariance property by projection

$$P_\alpha \psi(g_1, g_2, g_3; g, f) = \int_{SU(2)} d\alpha \; \psi(g_1\alpha, g_2\alpha, g_3\alpha; g\alpha, f\alpha) \tag{4.5.15}$$

- The fermion field $\xi_{abc}(g_1, g_2, g_3; g)$ described above which relates to a fermion entering a tetrahedron.

- A tensor field that corresponds to two fermions passing through a triangle, one entering the tetrahedron and one leaving

$$\chi_{abc}(g_1, g_2, g_3; g, f) : SU(2)^5 \to \mathbb{V}_1^{\otimes 3}, \tag{4.5.16}$$

The fourth and final arguments are projected to the spin half representation in the same way as $\psi_2^{\frac{1}{2},\frac{1}{2}}$. There will be a single grasping operation from the fermion entering the tetrahedron that will be provided by

$$\begin{aligned} (\hat{P}_{\beta_i \alpha} \chi_{abc}^{\frac{1}{2},\frac{1}{2}})(g_1, g_2, g_3; g, f) &= \int_{SU(2)} \prod_{i=1}^{3} d\beta_i d\alpha D^1_{ad}(\beta_1) D^1_{be}(\beta_2) D^1_{cf}(\beta_3) \\ &\quad \times \chi_{def}^{\frac{1}{2},\frac{1}{2}}(g_1\alpha, g_2\beta_1\alpha^{-1}\beta_1, g_3\beta_2\alpha^{-1}\beta_2; g\beta_3\alpha^{-1}\beta_3, f\alpha) \end{aligned}$$

- A tensor field that describes two fermions entering the tetrahedron through the same triangle.

$$\tilde{\chi}_{abc,def}(g_1, g_2, g_3; g, f) : SU(2)^5 \to \mathbb{V}_1^{\otimes 6} \tag{4.5.17}$$

Again, the fourth and final arguments are projected to the spin half representation and we create the two grasping operators with

$$
\begin{aligned}
(\tilde{P}_{\beta_i\gamma_i\alpha}\tilde{\chi}^{\frac{1}{2},\frac{1}{2}}_{abc,def})(g_1,g_2,g_3;g,f) = \\
\int_{SU(2)}\prod_{i=1}^{3} d\beta_i d\gamma_i d\alpha D^1_{ap}(\beta_1)D^1_{bq}(\beta_2)D^1_{cr}(\beta_3)D^1_{ds}(\gamma_1)D^1_{et}(\gamma_2)D^1_{fu}(\gamma_3) \\
\times \tilde{\chi}^{\frac{1}{2},\frac{1}{2}}_{pqr,stu}(g_1\gamma_1\alpha^{-1}\gamma_1, g_2\beta_1\alpha^{-1}\beta_1, g_3\gamma_2\beta_2^{-1}\alpha\gamma_2^{-1}\beta_2; g\beta_3\alpha^{-1}\beta_3, f\gamma_3\alpha^{-1}\gamma_3)
\end{aligned}
$$

This projection gives the field the following invariance property

$$
\begin{aligned}
D^1_{ap}(h)D^1_{bq}(h)D^1_{cr}(h)D^1_{ds}(h)D^1_{et}(h)D^1_{fu}(h)(\tilde{P}_{\beta_i\gamma_i\alpha}\tilde{\chi}^{\frac{1}{2},\frac{1}{2}}_{pqr,stu})(g_1h,g_2h,g_3h;gh,fh) \\
= (\tilde{P}_{\beta_i\gamma_i\alpha}\tilde{\chi}^{\frac{1}{2},\frac{1}{2}}_{abc,def})(g_1,g_2,g_3;g,f)
\end{aligned}
$$

All of the new fields defined above are also invariant under permutations of the first three indices. We can now write the action

$$
\begin{aligned}
S_{\rm F} &= S_{\rm F}[\phi, \psi^{\frac{1}{2}}, \psi_2^{\frac{1}{2},\frac{1}{2}}, \xi^{\frac{1}{2}}_{abc}, \chi^{\frac{1}{2},\frac{1}{2}}_{abc}, \tilde{\chi}^{\frac{1}{2},\frac{1}{2}}_{abc,def}, \lambda_{\rm F}] \\
&= \frac{1}{2}\int \prod_{i=1}^{3} dg_i dg \; P_{\alpha_1}\psi^{\frac{1}{2}}(g_1,g_2,g_3;g) \; P_{\alpha_2}\xi^{\frac{1}{2}}_{abc}(g_1,g_2,g_3;g) \; \epsilon_{abc} \\
&\quad + \frac{1}{2}\int \prod_{i=1}^{3} dg_i \; P_{\alpha_1}\phi(g_1,g_2,g_3) \; P_{\alpha_2}\phi(g_1,g_2,g_3) \\
&\quad + \frac{1}{2}\int \prod_{i=1}^{3} dg_i dg dh \; \hat{P}_{\beta_i\alpha_1}\chi^{\frac{1}{2},\frac{1}{2}}_{abc}(g_1,g_2,g_3;g,h) \; \hat{P}_{\beta_i'\alpha_2}\chi^{\frac{1}{2},\frac{1}{2}}_{def}(g_1,g_2,g_3;g,h)\epsilon_{abc}\epsilon_{def} \\
&\quad + \frac{1}{2}\int \prod_{i=1}^{3} dg_i dg dh \; \tilde{P}_{\beta_i\gamma_j\alpha_1}\tilde{\chi}^{\frac{1}{2},\frac{1}{2}}_{abc,def}(g_1,g_2,g_3;g,h) \; P_{\alpha_2}\psi_2^{\frac{1}{2},\frac{1}{2}}(g_1,g_2,g_3;g,h)\epsilon_{abc}\epsilon_{def} \\
&\quad + \frac{\lambda_{\rm F}}{4}\int \prod_{i=1}^{6} dg_i dg dh \; \tilde{P}_{\beta_i\gamma_j\alpha_1}\tilde{\chi}^{\frac{1}{2},\frac{1}{2}}_{abc,def}(g_1,g_2,g_3;g,h) \; P_{\alpha_2}\psi_2^{\frac{1}{2},\frac{1}{2}}(g_1,g_5,g_6;g,h) \\
&\quad \times P_{\alpha_3}\phi(g_2,g_4,g_6) \; P_{\alpha_4}\phi(g_3,g_4,g_5)\epsilon_{abc}\epsilon_{def} \\
&\quad + \frac{\lambda_{\rm F}}{4}\int \prod_{i=1}^{6} dg_i \hat{P}_{\beta_i\alpha_1}\chi^{\frac{1}{2},\frac{1}{2}}_{abc}(g_1,g_2,g_3;g,h) \; \hat{P}_{\beta_j'\alpha_2}\chi^{\frac{1}{2},\frac{1}{2}}_{def}(g_1,g_5,g_6;g,h) \\
&\quad \times P_{\alpha_3}\phi(g_2,g_4,g_6) \; P_{\alpha_4}\phi(g_3,g_4,g_5)\epsilon_{abc}\epsilon_{def} \\
&\quad + \frac{\lambda_{\rm F}}{4}\int \prod_{i=1}^{6} dg_i dg dh \; \tilde{P}_{\beta_i\gamma_j\alpha_1}\tilde{\chi}^{\frac{1}{2},\frac{1}{2}}_{abc,def}(g_1,g_2,g_3;g,h) \; P_{\alpha_2}\psi^{\frac{1}{2}}(g_1,g_5,g_6;g) \\
&\quad \times P_{\alpha_3}\psi^{\frac{1}{2}}(g_3,g_4,g_5;h) \; P_{\alpha_4}\phi(g_2,g_4,g_6)\epsilon_{abc}\epsilon_{def} \\
&\quad + \frac{\lambda_{\rm F}}{4}\int \prod_{i=1}^{6} dg_i dg dh \; \hat{P}_{\beta_i\alpha_1}\chi^{\frac{1}{2},\frac{1}{2}}_{abc}(g_1,g_2,g_3;g,h)\hat{P}_{\alpha_2}\xi^{\frac{1}{2}}_{abc}(g_1,g_5,g_6;g) \\
&\quad \times P_{\alpha_3}\psi^{\frac{1}{2}}(g_3,g_4,g_5;h)P_{\alpha_4}\phi(g_2,g_4,g_6)\epsilon_{abc}\epsilon_{def} \\
&\quad + \frac{\lambda_{\rm F}}{4}\int \prod_{i=1}^{6} dg_i dg dh \; P_{\alpha_1}\psi_2^{\frac{1}{2},\frac{1}{2}}(g_1,g_2,g_3;g,h)\hat{P}_{\alpha_2}\xi^{\frac{1}{2}}_{abc}(g_1,g_5,g_6;g) \\
&\quad \times \hat{P}_{\alpha_3}\xi^{\frac{1}{2}}_{abc}(g_2,g_4,g_6;g)P_{\alpha_4}\phi(g_3,g_4,g_5)\epsilon_{abc}\epsilon_{def} \\
&\quad + \frac{\lambda_{\rm F}}{4}\int \prod_{i=1}^{6} dg_i dg dh \; \hat{P}_{\alpha_1}\xi^{\frac{1}{2}}_{abc}(g_1,g_2,g_3;g)\hat{P}_{\alpha_2}\xi^{\frac{1}{2}}_{abc}(g_1,g_5,g_6;h) \\
&\quad \times P_{\alpha_3}\psi^{\frac{1}{2}}(g_2,g_4,g_6;g)P_{\alpha_4}\psi^{\frac{1}{2}}(g_3,g_4,g_5;h)\epsilon_{abc}\epsilon_{def}
\end{aligned}
\tag{4.5.18}
$$

Feynman rules: The partition function for the theory is

$$
Z = \int \mathcal{D}\phi\mathcal{D}\psi^{\frac{1}{2}}\mathcal{D}\psi_2^{\frac{1}{2},\frac{1}{2}} \prod_{a,\ldots,m=1}^{3} \mathcal{D}\xi^{\frac{1}{2}}_{abc}\mathcal{D}\chi^{\frac{1}{2}\frac{1}{2}}_{def}\mathcal{D}\tilde{\chi}^{\frac{1}{2}\frac{1}{2}}_{ghi,klm} e^{-S_{\rm F}} = \sum_{\Gamma} \frac{\lambda_{\rm F}^{v_{\rm F}[\Gamma]}}{\mathrm{sym}(\Gamma)} Z[\Gamma]. \tag{4.5.19}
$$

The four types of propagator are (in the order given in the action)

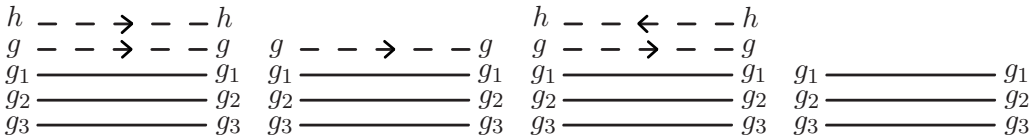

The vertices, listed in the order given in the action, and their corresponding vertex amplitudes are

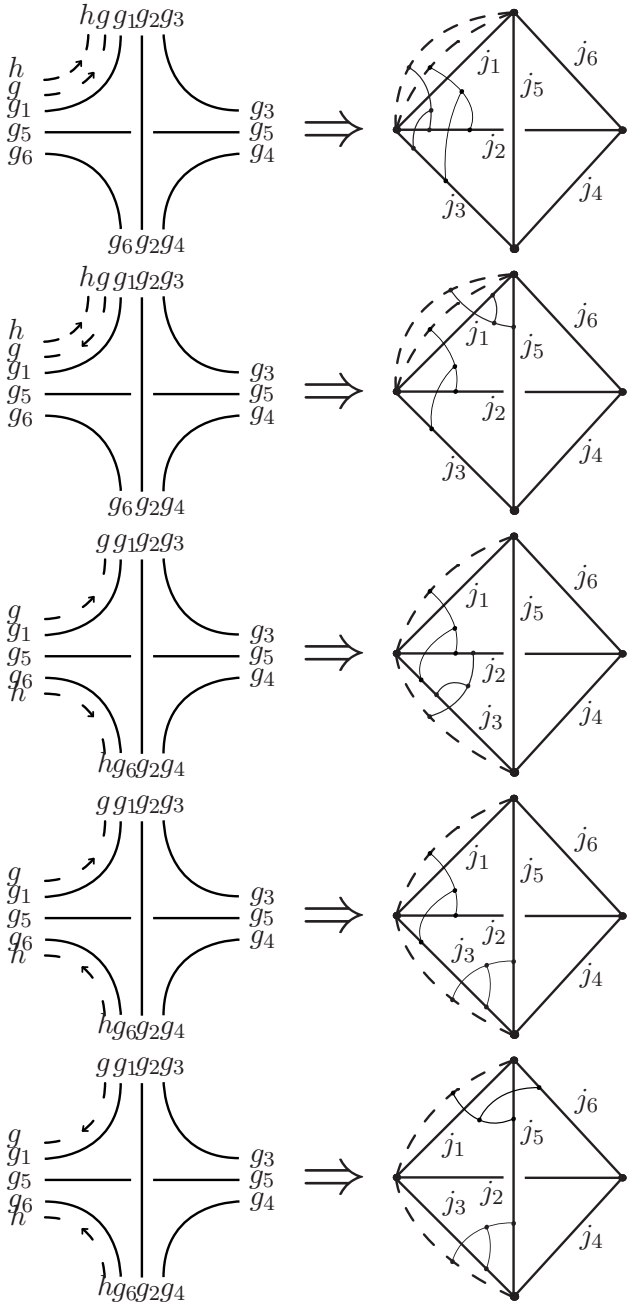

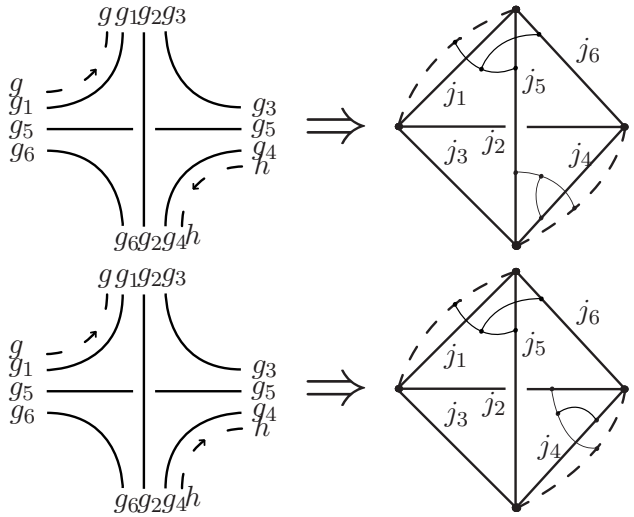

The Feynman diagrams for this GFT reproduce the spin foam model for fermions coupled to 3d gravity defined in [36] with the simplification mentioned previously and the relevant numerical factors absorbed into the coupling coefficient. Note that the fermion spin foam model is only defined on a proper triangulation, not any 2-complex. Some of the Feynman diagrams of the GFT will therefore produce spin foams that do not relate to the original definition of the model. For example, those in which two adjacent tetrahedra are glued on more than one face and the fermions propagate though both of these faces. However, in this particular degenerate example, one can show that the amplitude is zero.

We can also now see that at each value of $v_{\mathrm{F}}[\Gamma]$ we obtain all possible loop configurations that completely saturate the spin foam. Thus the GFT naturally includes the matter diagrams as well as the sum over 2-complexes. This will of course include all matter diagrams on all topologies available for a given value of $v_{\mathrm{F}}[\Gamma]$.

4.6 Conclusions

We have altered the standard GFT for 3d gravity to include observables in the form of Wilson loops, volume operators and fermions. While the physical significance of summing over Wilson loops and volume operators is unclear, they are both essential for constructing the fermionic GFT.

The fermionic GFT gives a way to deal with the triangulation dependence in the spin foam model for fermions, one of the issues mentioned in [36] and, as one would expect, implements the sum over fermionic loops at the same time. We now briefly point out the differences between the fermionic GFT and the GFT for point particles. Firstly, the corresponding spin foam models have very different vertex amplitudes, even for the spinning particle. The particles live on the edges of the spin foam since they have an

associated deficit angle but the fermions propagate along the dual edges as they make use of the SU(2) variables to parallel transport the spinors. Secondly, the particle model allows 3 and 4-valent interaction vertices whereas these are not allowed in the fermionic spin foam due to the Grassmann integration. In the fermionic model, there are two separate configurations of fermionic loops and the loops must necessarily be closed and saturate all of the vertices (again due to the Grassmann variables) whereas there is only a single arbitrary graph in the particle model. Modifications could of course be made to the interaction terms in the particle model to remove some of these differences and considering fermionic observables would change the allowed amplitudes of the fermion model.

It would be desirable to give an alternative GFT for the fermion model which takes several Grassmann variables as its arguments. In this way it may be possible to recreate the model with fewer interaction vertices, however, it would also need to include a dependence on the frame fields in a similar way to [66]. Note that this suggestion is not the same as that in [55] where the fields themselves are Grassmann valued.

Chapter 5

Conclusions

This thesis has discussed various aspects of three dimensional spin foam models for quantum geometry. In the first chapter, we saw how spin networks arise from considering a lattice BF theory path integral and how, with appropriate gauge fixing, they can be used to actually compute transition amplitudes analytically without having to resort to Monte Carlo simulations etc. We arrived at the well known Ponzano-Regge model and discussed some of its properties.

In Chapter 2 we considered the extension of the 6j asymptotic formula, i.e. the Ponzano-Regge amplitude for a single tetrahedron, to a much wider class of triangulations. As expected, we found that the asymptotics were dominated by immersions of the boundary triangulation in Euclidean space weighted by the cosine of the Regge action. It would be interesting to give a better physical interpretation of the determinant of the Hessian that appears in the asymptotic formula. For a single tetrahedron this is proportional to the volume of the tetrahedron cubed as can be seen numerically, however it was not possible to show this analytically.

Chapter 3 and 4 discussed the coupling of fermions to the Ponzano-Regge model and we saw the complications involved in actually computing the relevant amplitudes. Since the number of possible vertex amplitudes of the spin foam model is huge, in this case a numerical method would likely be preferable should one wish to actually perform concrete calculations as there is not a simple formula for the amplitude as for the 6j symbol. The expression in terms of spin networks may prove to be more useful when considering a sum over triangulations such as in the group field theory.

All of this has shown that, although it is only a toy model, 3d gravity still has many interesting problems to consider and will continue to provide insight into constructing theories of quantum geometry in four dimensions. Current four dimensional spin foam models are based on a formulation of GR which can be written as 4d BF theory with

a constraint term. The strategy is then to quantise 4d BF theory as in the 3d case but then attempt to apply this constraint on the quantum theory. The first attempt of this kind was by Barrett and Crane who constructed finite vertex amplitudes for 4d and 3+1d. An analogue of the Ponzano-Regge asymptotic formula was found for these vertex amplitudes (called 10j symbols) which showed that they recovered the Regge action in the semiclassical limit. However, the geometries of adjacent 4-simplices was inconsistent in the Barrett-Crane model and an asymptotic formula for triangulations larger than a single 4-simplex has not been found. This led to some new spin foam models with a better understanding of how the constraints are imposed [16, 67]. The geometry of adjacent 4-simplices do not suffer from the same problems as the Barrett-Crane models and it is possible to include an Immirzi paramater.

The semiclassical limit of the vertex amplitudes of these models was also studied as part of my PhD, see refs [A,B], but this analysis has not been included in this thesis. An alternative version can also be found in [30, 68], in both cases the vertex amplitude was found to contain some function of the Regge action for a flat 4-simplex. While this is a promising result, a study of the semiclassical limit that fully analyses the dynamics of the models is still required before one can conclude that these models have the correct semiclassical limit. For example, non-degenerate, non-flat geometries are certainly included in the quantum theory, but it has not been conclusively shown that the degenerate or flat geometries are not dominant in the semiclassical limit. In the 3d case, the Ponzano-Regge model is an integral over flat SU(2) connections (see [17]) so this is not an issue. We can certainly conclude that geometry emerges from representation theoretic objects in a certain limit for both three and four dimensions. However in 4d, the above issues must be resolved before we can say for certain that general relativity is also present in this limit.

Appendix A

The Peter-Weyl theorem and the Fourier transform of the SU(2) delta function

In this section, we recall the Peter-Weyl theorem and use it to Fourier transform the delta function used in the derivation of the Ponzano-Regge model.

The Peter-Weyl theorem specialised to SU(2) states that the functions

$$\sqrt{2j+1}D^j_{ab}(g), \tag{A.0.1}$$

with $g \in \mathrm{SU}(2)$ and $j \in \mathbb{N}/2$ are the unitary irreducible representations, form an orthonormal basis of $L^2(\mathrm{SU}(2))$. A corollary of this is that any function $u : \mathrm{SU}(2) \to \mathbb{C}$ can be decomposed as

$$u(g) = \sum_{j=0}^{\infty} \sum_{a,b=-j}^{j} c^j_{ab} D^j_{ab}(g), \tag{A.0.2}$$

with the Fourier coefficients given by

$$c^j_{ab} = d_j \int_{\mathrm{SU}(2)} dg u(g) \overline{D^j_{ab}(g)}. \tag{A.0.3}$$

If we project this formula down to class functions, i.e. $u(hgh^{-1}) = u(g)$, then we get

$$\begin{aligned}
\int_{\mathrm{SU}(2)} dh u(hgh^{-1}) &= \sum_{j=0}^{\infty} \sum_{a,b=-j}^{j} \int_{\mathrm{SU}(2)} dh c^j_{ab} D^j_{ab}(hgh^{-1}) \\
&= \sum_{j=0}^{\infty} \sum_{a,b,d,e=-j}^{j} \int_{\mathrm{SU}(2)} dh c^j_{ab} D^j_{ad}(h) D^j_{de}(g) \overline{D^j_{be}(h)} \\
&= \sum_{j=0}^{\infty} \sum_{a,b,d,e=-j}^{j} c^j_{ab} \frac{1}{d_j} \delta_{ab} \delta_{de} D^j_{de}(g) \\
&= \sum_{j=0}^{\infty} \sum_{a=-j}^{j} c^j_{aa} \frac{1}{d_j} \chi^j(g), \qquad \text{(A.0.4)}
\end{aligned}$$

Now we can write the coefficients for the delta function $\delta(g)$

$$\begin{aligned}
c^j_{ab} &= d_j \int_{\mathrm{SU}(2)} dg \delta(g) \overline{D^j_{ab}(g)} \\
&= d_j \overline{D^j_{ab}(1)}. \qquad \text{(A.0.5)}
\end{aligned}$$

Using equation A.0.4 and using $\mathrm{tr}\, D(1) = d_j$, we obtain

$$\begin{aligned}
\delta(g) &= \sum_{j=0}^{\infty} \sum_{a=-j}^{j} d_j \overline{D^j_{aa}(1)} \frac{1}{d_j} \chi^j(g) \\
&= \sum_{j=0}^{\infty} d_j \chi^j(g) \qquad \text{(A.0.6)}
\end{aligned}$$

Appendix B

The stationary phase approximation

To find the asymptotic form of the amplitude, we will use the complex stationary phase formula [26], as in [29]. However we will also require the stationary phase formula for non-isolated critical points. We briefly describe the stationary phase approximation and its generalisation below.

Let D be a closed manifold of dimension n, and let S and a be smooth, complex valued functions on D such that the real part $\mathrm{Re}S \leq 0$. Consider the function

$$f(\lambda) = \int_D dx\, a(x)\, e^{\lambda S(x)}. \tag{B.0.1}$$

The Hessian of S is the $n \times n$ matrix of second derivatives of S denoted H. For now let us assume that the stationary points are isolated, which, by the Morse lemma is a condition equivalent to the statement that the Hessian is non-degenerate at the critical points; $\det H \neq 0$. Such functions are called Morse functions.

In the extended stationary phase, the key role is played by *critical points*, that is, points x_0, which are not only stationary: $\delta S(x_0) = 0$ but for which $\mathrm{Re}S(x_0) = 0$ as well. So to compute the dominant terms in the asymptotics for large spins, we need to find the stationary points of the action S and restrict to those with zero real part. If S has no critical points then for large parameter λ the function f decreases faster that any power of λ^{-1}. In other words, for all $N \geq 1$:

$$f(\lambda) = o(\lambda^{-N}), \tag{B.0.2}$$

If there are isolated critical points, then each critical point contributes to the asymptotics of f by a term of order $\lambda^{-n/2}$. For large λ the asymptotic expansion of the integral yields

for each critical point

$$a(x_0)\left(\frac{2\pi}{\lambda}\right)^{n/2}\frac{1}{\sqrt{\det(-H)}}\,e^{\lambda S(x_0)}\left[1+O(1/\lambda)\right]. \tag{B.0.3}$$

At a critical point, the matrix $-H$ has a positive definite real part, and the square root of the determinant of this matrix is the unique square root which is continuous on matrices with positive definite real part, and positive on real ones. If S admits several isolated critical points with non-degenerate Hessian, we obtain a sum of contributions of the form (B.0.3) from each of them.

B.1 Stationary phase for a manifold of critical points

If the action has degenerate critical points, i.e. the Hessian matrix has zero determinant, care is needed to compute the asymptotics (see eg [69]). Let $\mathcal{C} := \{y \in D \mid \delta S(y) = 0,\ \mathrm{Re}S(y) = 0\}$ denote the set of critical points. Note that we cannot a priori assume $\mathcal{C}$ to be a disjoint union of manifolds, however here we have restricted ourselves to this case so that the following generalized stationary phase theorem applies.

For a smooth function S whose critical set $\mathcal{C}$ is a disjoint union of closed manifolds, each critical manifold $\mathcal{C}_{x_0}$ of dimension p, labelled by some x_0 on the critical manifold, contributes the following to the asymptotic formula [69]:

$$\left(\frac{2\pi}{\lambda}\right)^{(n-p)/2} e^{\lambda S(x_0)}\int_{\mathcal{C}_{x_0}} d\sigma_{\mathcal{C}_{x_0}}(y)\frac{a(y)}{\sqrt{\det(-H^{\top}(y))}}\left[1+O(1/\lambda)\right]. \tag{B.1.1}$$

where $H^{\top}(y)$ is the restriction of the matrix to the directions normal to $\mathcal{C}_{x_0}$ with respect to some Riemannian metric on the domain , and $d\sigma_{\mathcal{C}_{x_0}}$ is the canonical measure induced on the critical submanifold by the same Riemannian measure on the domain space. This extends to the case where $\mathcal{C}$ is a manifold-with-boundary.

Appendix C

Integrals over four and five group elements

Using the angular momentum diagrams, the result for the integration over the tensor product of four group elements is

$$\begin{aligned}
&\int_{\mathrm{SU}(2)} dg\, \pi^i(g)^\alpha{}_\beta\, \pi^j(g)^\gamma{}_\delta \pi^k(g)^\epsilon{}_\zeta \pi^l(g)^\theta{}_\eta = \sum_{m,\kappa,\iota} \sum_{n,\mu,\lambda} \left(\begin{array}{cc|c} \alpha & \gamma & m \\ i & j & \iota \end{array}\right) \left(\begin{array}{cc|c} \kappa & i & j \\ m & \beta & \delta \end{array}\right) \\
&\times \left(\begin{array}{cc|c} \epsilon & \theta & n \\ k & l & \mu \end{array}\right) \left(\begin{array}{cc|c} \lambda & k & l \\ n & \zeta & \eta \end{array}\right) \int_{\mathrm{SU}(2)} dg\, \pi^m(g)^\iota{}_\kappa \pi^n(g)^\mu{}_\lambda \\
= \;& \frac{1}{\dim m} \sum_{m,\kappa,\iota,\mu,\lambda} \left(\begin{array}{cc|c} \alpha & \gamma & m \\ i & j & \iota \end{array}\right) \epsilon^{m\,\iota\mu} \left(\begin{array}{cc|c} \epsilon & \theta & m \\ k & l & \mu \end{array}\right) \left(\begin{array}{cc|c} \kappa & i & j \\ m & \beta & \delta \end{array}\right) \epsilon^m_{\kappa\lambda} \left(\begin{array}{cc|c} \lambda & k & l \\ m & \zeta & \eta \end{array}\right) \\
= \;& \sum_m \left(\begin{array}{cccc} \alpha & \gamma & \epsilon & \theta \\ i & j & k & l \end{array}\right)_m \left(\begin{array}{cccc} i & j & k & l \\ \beta & \delta & \zeta & \eta \end{array}\right)_m ,
\end{aligned} \tag{C.0.1}$$

where the obtained $4j$ symbol is defined as follows

$$\left(\begin{array}{cccc} i & j & k & l \\ \alpha & \beta & \gamma & \delta \end{array}\right)_m = \sum_\kappa \sqrt{\dim m} \left(\begin{array}{ccc} i & j & \kappa \\ \alpha & \beta & m \end{array}\right) \left(\begin{array}{ccc} m & k & l \\ \kappa & \gamma & \delta \end{array}\right). \tag{C.0.2}$$

Using the conjugation (1.5.54), we can also calculate the following integral

$$\int_{\mathrm{SU}(2)} dg\, \pi^i(g)^\alpha{}_\beta\, \pi^j(g)^\gamma{}_\delta \pi^k(g)^\epsilon{}_\zeta \pi^l(g^{-1})^\theta{}_\eta = (-1)^{2l} \sum_m \left(\begin{array}{cccc} \alpha & \gamma & \epsilon & l \\ i & j & k & \eta \end{array}\right)_m \left(\begin{array}{cccc} i & j & k & \theta \\ \beta & \delta & \zeta & l \end{array}\right)_m ,$$

and also

$$\int_{\mathrm{SU}(2)} dg\, \pi^i(g)^\alpha{}_\beta\, \pi^j(g)^\gamma{}_\delta \pi^k(g^{-1})^\epsilon{}_\zeta \pi^l(g^{-1})^\theta{}_\eta = (-1)^{2(k+l)} \sum_m \left(\begin{array}{cccc} \alpha & \gamma & k & l \\ i & j & \zeta & \eta \end{array}\right)_m \left(\begin{array}{cccc} i & j & \epsilon & \theta \\ \beta & \delta & k & l \end{array}\right)_m .$$

This covers all possible four-valent orientations configurations.

Finally, we compute the five-valent integration as follows.

$$\begin{aligned}
&\int_{\mathrm{SU}(2)} dg\, \pi^i(g)^\alpha{}_\beta\, \pi^j(g)^\gamma{}_\delta \pi^k(g)^\epsilon{}_\zeta \pi^l(g)^\theta{}_\eta \pi^m(g)^\iota{}_\kappa = \int_{\mathrm{SU}(2)} dg \sum_{n,\mu,\lambda} \sum_{o,\nu,\xi} \left(\begin{array}{cc|c} \alpha & \gamma & n \\ i & j & \lambda \end{array}\right) \\
&\times \left(\begin{array}{cc|c} \mu & i & j \\ n & \beta & \delta \end{array}\right) \pi^n(g)^\lambda{}_\mu \pi^k(g)^\epsilon{}_\zeta \left(\begin{array}{cc|c} \theta & \iota & o \\ l & m & \nu \end{array}\right) \pi^o(g)^\nu{}_\xi \left(\begin{array}{cc|c} \xi & l & m \\ o & \eta & \kappa \end{array}\right) \\
= &\sum_{n,\mu,\lambda} \sum_{o,\nu,\xi} \sum_{p,\rho,\sigma} \left(\begin{array}{cc|c} \alpha & \gamma & n \\ i & j & \lambda \end{array}\right) \left(\begin{array}{cc|c} \mu & i & j \\ n & \beta & \delta \end{array}\right) \left(\begin{array}{cc|c} \lambda & \epsilon & p \\ n & k & \rho \end{array}\right) \\
&\times \left(\begin{array}{cc|c} \sigma & n & k \\ p & \mu & \zeta \end{array}\right) \left(\begin{array}{cc|c} \theta & \iota & o \\ l & m & \nu \end{array}\right) \left(\begin{array}{cc|c} \xi & l & m \\ o & \eta & \kappa \end{array}\right) \int_{\mathrm{SU}(2)} dg\, \pi^p(g)^\rho{}_\sigma \pi^o(g)^\nu{}_\xi \\
= &\sum_{n,o} \left(\begin{array}{ccccc} \alpha & \gamma & \epsilon & \theta & \iota \\ i & j & k & l & m \end{array}\right)_{n,o} \left(\begin{array}{ccccc} i & j & k & l & m \\ \beta & \delta & \zeta & \eta & \kappa \end{array}\right)_{n,o},
\end{aligned} \tag{C.0.3}$$

where the $5j$ symbol is given by the following expression

$$\left(\begin{array}{ccccc} i & j & k & l & m \\ \beta & \delta & \zeta & \eta & \kappa \end{array}\right)_{n,o} = \sum_{\mu,\sigma} \sqrt{\dim n \dim o} \left(\begin{array}{ccc} i & j & \mu \\ \beta & \delta & n \end{array}\right) \left(\begin{array}{ccc} n & k & \sigma \\ \mu & \zeta & o \end{array}\right) \left(\begin{array}{ccc} o & l & m \\ \sigma & \eta & \kappa \end{array}\right). \tag{C.0.4}$$

Again, from the above, it is immediate to obtain that

$$\begin{aligned}
&\int_{\mathrm{SU}(2)} dg\, \pi^i(g)^\alpha{}_\beta\, \pi^j(g)^\gamma{}_\delta \pi^k(g)^\epsilon{}_\zeta \pi^l(g)^\theta{}_\eta \pi^m(g^{-1})^\iota{}_\kappa \\
&= (-1)^{2m} \sum_{n,o} \left(\begin{array}{ccccc} \alpha & \gamma & \epsilon & \theta & m \\ i & j & k & l & \kappa \end{array}\right)_{n,o} \left(\begin{array}{ccccc} i & j & k & l & \iota \\ \beta & \delta & \zeta & \eta & m \end{array}\right)_{n,o},
\end{aligned}$$

and that

$$\begin{aligned}
&\int_{\mathrm{SU}(2)} dg\, \pi^i(g)^\alpha{}_\beta\, \pi^j(g)^\gamma{}_\delta \pi^k(g)^\epsilon{}_\zeta \pi^l(g^{-1})^\theta{}_\eta \pi^m(g^{-1})^\iota{}_\kappa \\
&= (-1)^{2(l+m)} \sum_{n,o} \left(\begin{array}{ccccc} \alpha & \gamma & \epsilon & l & m \\ i & j & k & \eta & \kappa \end{array}\right)_{n,o} \left(\begin{array}{ccccc} i & j & k & \theta & \iota \\ \beta & \delta & \zeta & l & m \end{array}\right)_{n,o}.
\end{aligned}$$

This covers all possible group integrals that can appear in the fermionic model.

References

[1] G. Ponzano and T. Regge. Semiclassical limit of racah coefficients. In F. Block, editor, *Spectroscopy and group theoretical methods in physics*, pages 1–58. North Holland, 1968.

[2] Laurent Freidel and David Louapre. Ponzano-Regge model revisited. I: Gauge fixing, observables and interacting spinning particles. *Class. Quant. Grav.*, 21:5685–5726, 2004. doi: 10.1088/0264-9381/21/24/002.

[3] Joseph D. Romano. Geometrodynamics versus connection dynamics (in the context of (2+1) and (3+1) gravity. *Gen. Rel. Grav.*, 25:759–854, 1993. doi: 10.1007/BF00758384.

[4] C. Rovelli. *Quantum Gravity.* Cambridge University Press, 2004.

[5] John Baez and Javier Muniain. *Gauge fields knots and gravity.* World Scientific, 1994.

[6] Robert M. Wald. *General Relativity.* Chicago, Usa: Univ. Pr. (1984) 491p.

[7] Steven Giddings, James Abbott, and Karel Kuchar. Einstein's theory in a three-dimensional space-time. *Gen. Rel. Grav.*, 16:751–775, 1984. doi: 10.1007/BF00762914.

[8] Etera R. Livine and James P. Ryan. A Note on B-observables in Ponzano-Regge 3d Quantum Gravity. *Class. Quant. Grav.*, 26:035013, 2009. doi: 10.1088/0264-9381/26/3/035013.

[9] L. H. Kauffman and S. L. Lins. *Temperley-Lieb recoupling theory and invariants of 3-manifolds.* Princeton University Press, 1994.

[10] P. E.S. Wormer and J. Paldus. Angular momentum diagrams. *Adv. Quant. Chem.*, 51:59–124, 2006.

[11] Louis Kauffman. *Knots and Physics.* World Scientific, 2001.

[12] Seth A. Major. A spin network primer. *Am. J. Phys.*, 67:972–980, 1999. doi: 10.1119/1.19175.

[13] D.A. Varshalovich, A.N. Mokalev, and V.K. Khersonskii. *Quantum theory of angular momentum*. World Scientific, 1988.

[14] R. Oeckl. *Discrete gauge theory - from lattices to TQFT*. Imperial College Press, 2005.

[15] Emanuele Alesci and Carlo Rovelli. The complete LQG propagator: I. Difficulties with the Barrett-Crane vertex. *Phys. Rev.*, D76:104012, 2007. doi: 10.1103/PhysRevD.76.104012.

[16] Laurent Freidel and Kirill Krasnov. A New Spin Foam Model for 4d Gravity. *Class. Quant. Grav.*, 25:125018, 2008. doi: 10.1088/0264-9381/25/12/125018.

[17] John W. Barrett and Ileana Naish-Guzman. The Ponzano-Regge model. *Class. Quant. Grav.*, 26:155014, 2009. doi: 10.1088/0264-9381/26/15/155014.

[18] V.G. Turaev and O.Y. Viro. State sum invariants of 3-manifolds and quantum 6-j symbols. *Topology*, 31:865, 1992.

[19] Hirosi Ooguri and Naoki Sasakura. Discrete and continuum approaches to three-dimensional quantum gravity. *Mod. Phys. Lett.*, A6:3591–3600, 1991. doi: 10.1142/S0217732391004140.

[20] Laurent Freidel. Group field theory: An overview. *Int. J. Theor. Phys.*, 44:1769–1783, 2005. doi: 10.1007/s10773-005-8894-1.

[21] J. Moussouris. *Quantum models of space-time based on recoupling theory*. PhD thesis, St. Cross College, Oxford, 1983.

[22] Mikio Nakahara. *Geometry, Topology and Physics*. Taylor and Francis, 2003.

[23] Justin Roberts. Classical 6j-symbols and the tetrahedron. *GEOM.TOPOL.*, 3:21, 1999.

[24] Razvan Gurau. The Ponzano-Regge asymptotic of the 6j symbol: an elementary proof, 2008.

[25] Maite Dupuis and Etera R. Livine. Pushing Further the Asymptotics of the 6j-symbol. *Phys. Rev.*, D80:024035, 2009. doi: 10.1103/PhysRevD.80.024035.

[26] L. Hormander. *The analysis of linear partial differential operators I*. Springer-Verlag, 1983.

[27] Etera R. Livine and Simone Speziale. A new spinfoam vertex for quantum gravity. *Phys. Rev.*, D76:084028, 2007. doi: 10.1103/PhysRevD.76.084028.

[28] A. Perelomov. *Generalized coherent states and their applications*. Springer-Verlag, 1986.

[29] John W. Barrett, R. J. Dowdall, Winston J. Fairbairn, Henrique Gomes, and Frank Hellmann. Asymptotic analysis of the EPRL four-simplex amplitude. *J. Math. Phys.*, 50:112504, 2009. doi: 10.1063/1.3244218.

[30] Florian Conrady and Laurent Freidel. Quantum geometry from phase space reduction. *J. Math. Phys.*, 50:123510, 2009. doi: 10.1063/1.3257109.

[31] K. Steffen. A symmetric flexible Connelly sphere with only nine vertices. See: http://demonstrations.wolfram.com/SteffensFlexiblePolyhedron/ for Mathematica code.

[32] Herman Gluck. Almost all simply connected surfaces are rigid. In *Lecture notes in mathematics 438: Geometric Topology*. Springer-Verlag, 1975.

[33] Carlo Rovelli. Graviton propagator from background-independent quantum gravity. *Phys. Rev. Lett.*, 97:151301, 2006. doi: 10.1103/PhysRevLett.97.151301.

[34] Simone Speziale. Towards the graviton from spinfoams: The 3d toy model. *JHEP*, 05:039, 2006.

[35] Eugenio Bianchi, Elena Magliaro, and Claudio Perini. LQG propagator from the new spin foams. *Nucl. Phys.*, B822:245–269, 2009. doi: 10.1016/j.nuclphysb.2009.07.016.

[36] Winston J. Fairbairn. Fermions in three-dimensional spinfoam quantum gravity. *Gen. Rel. Grav.*, 39:427–476, 2007. doi: 10.1007/s10714-006-0395-x.

[37] Laurent Freidel and Etera R. Livine. Ponzano-Regge model revisited. III: Feynman diagrams and effective field theory. *Class. Quant. Grav.*, 23:2021–2062, 2006. doi: 10.1088/0264-9381/23/6/012.

[38] Simone Speziale. Coupling gauge theory to spinfoam 3d quantum gravity. *Class. Quant. Grav.*, 24:5139–5160, 2007. doi: 10.1088/0264-9381/24/20/014.

[39] Peng Xu and Yongge Ma. Geometry vs. Matter: The emergence of scalar matter from modified 3D spinfoam model. *Phys. Rev.*, D80:104024, 2009. doi: 10.1103/PhysRevD.80.104024.

[40] Winston J. Fairbairn and Alejandro Perez. Extended matter coupled to BF theory. *Phys. Rev.*, D78:024013, 2008. doi: 10.1103/PhysRevD.78.024013.

[41] Valentin Bonzom and Etera R. Livine. A Immirzi-like parameter for 3d quantum gravity. *Class. Quant. Grav.*, 25:195024, 2008. doi: 10.1088/0264-9381/25/19/195024.

[42] Heinz J. Rothe. *Lattice Gauge Theories: An Introduction*. World Scientific, 2005.

[43] S. Elitzur. Impossibility of spontaneously breaking local symmetries. *Phys. Rev. D*, 12(12):3978–3982, Dec 1975. doi: 10.1103/PhysRevD.12.3978.

[44] Stefano Fachin and Claudio Parrinello. Global gauge fixing in lattice gauge theories. *Phys. Rev. D*, 44(8):2558–2564, Oct 1991. doi: 10.1103/PhysRevD.44.2558.

[45] L. Giusti, M. L. Paciello, C. Parrinello, S. Petrarca, and B. Taglienti. Problems on lattice gauge fixing. *Int. J. Mod. Phys.*, A16:3487–3534, 2001. doi: 10.1142/S0217751X01004281.

[46] Laurent Freidel and Kirill Krasnov. Spin foam models and the classical action principle. *Adv. Theor. Math. Phys.*, 2:1183–1247, 1999.

[47] Florian Girelli, Robert Oeckl, and Alejandro Perez. Spin foam diagrammatics and topological invariance. *Class. Quant. Grav.*, 19:1093–1108, 2002. doi: 10.1088/0264-9381/19/6/305.

[48] R. Capovilla, T. Jacobson, J. Dell, and L. Mason. Selfdual two forms and gravity. *Class. Quant. Grav.*, 8:41–57, 1991. doi: 10.1088/0264-9381/8/1/009.

[49] Daniele Oriti. The group field theory approach to quantum gravity. 2006.

[50] D. V. Boulatov. A Model of three-dimensional lattice gravity. *Mod. Phys. Lett.*, A7: 1629–1646, 1992. doi: 10.1142/S0217732392001324.

[51] Hirosi Ooguri. Topological lattice models in four-dimensions. *Mod. Phys. Lett.*, A7: 2799–2810, 1992. doi: 10.1142/S0217732392004171.

[52] Daniele Oriti and James Ryan. Group field theory formulation of 3d quantum gravity coupled to matter fields. *Class. Quant. Grav.*, 23:6543–6576, 2006. doi: 10.1088/0264-9381/23/22/027.

[53] Kirill Krasnov. Quantum gravity with matter via group field theory. *Class. Quant. Grav.*, 24:981–1022, 2007. doi: 10.1088/0264-9381/24/4/016.

[54] Winston J. Fairbairn and Etera R. Livine. 3d spinfoam quantum gravity: Matter as a phase of the group field theory. *Class. Quant. Grav.*, 24:5277–5297, 2007. doi: 10.1088/0264-9381/24/20/021.

[55] Razvan Gurau. Colored Group Field Theory. 2009.

[56] Joseph Ben Geloun, Jacques Magnen, and Vincent Rivasseau. Bosonic Colored Group Field Theory. 2009.

[57] Michael Reisenberger and Carlo Rovelli. Spin foams as Feynman diagrams. 2000.

[58] Roberto De Pietri, Laurent Freidel, Kirill Krasnov, and Carlo Rovelli. Barrett-Crane model from a Boulatov-Ooguri field theory over a homogeneous space. *Nucl. Phys.*, B574:785–806, 2000. doi: 10.1016/S0550-3213(00)00005-5.

[59] Alejandro Perez and Carlo Rovelli. 3+1 spinfoam model of quantum gravity with spacelike and timelike components. *Phys. Rev.*, D64:064002, 2001. doi: 10.1103/PhysRevD.64.064002.

[60] Daniele Oriti and Tamer Tlas. Encoding simplicial quantum geometry in group field theories. *Class. Quant. Grav.*, 27:135018, 2010. doi: 10.1088/0264-9381/27/13/135018.

[61] Daniele Oriti. Group field theory and simplicial quantum gravity. *Class. Quant. Grav.*, 27:145017, 2010. doi: 10.1088/0264-9381/27/14/145017.

[62] Laurent Freidel, Razvan Gurau, and Daniele Oriti. Group field theory renormalization - the 3d case: power counting of divergences. *Phys. Rev.*, D80:044007, 2009. doi: 10.1103/PhysRevD.80.044007.

[63] Laurent Freidel and David Louapre. Non-perturbative summation over 3D discrete topologies. *Phys. Rev.*, D68:104004, 2003. doi: 10.1103/PhysRevD.68.104004.

[64] Laurent Freidel and David Louapre. Ponzano-Regge model revisited. II: Equivalence with Chern- Simons. 2004.

[65] Jonathan Hackett and Simone Speziale. Grasping rules and semiclassical limit of the geometry in the Ponzano-Regge model. *Class. Quant. Grav.*, 24:1525–1546, 2007. doi: 10.1088/0264-9381/24/6/010.

[66] Daniele Oriti and Tamer Tlas. A New Class of Group Field Theories for 1st Order Discrete Quantum Gravity. *Class. Quant. Grav.*, 25:085011, 2008. doi: 10.1088/0264-9381/25/8/085011.

[67] Jonathan Engle, Etera Livine, Roberto Pereira, and Carlo Rovelli. LQG vertex with finite Immirzi parameter. *Nucl. Phys.*, B799:136–149, 2008. doi: 10.1016/j.nuclphysb.2008.02.018.

[68] Florian Conrady and Laurent Freidel. On the semiclassical limit of 4d spin foam models. *Phys. Rev.*, D78:104023, 2008. doi: 10.1103/PhysRevD.78.104023.

[69] Pablo Ramacher. Singular equivariant asymptotics and the moment map i. 2009.